Aus dem Physik-Departement
Universität Freiburg (Schweiz)

Microscopic characterization of electron field emission from carbon nanotubes and carbon thin-film electron emitters

Inaugural-Dissertation

zur Erlangung der Würde eines *Doctor rerum naturalium*
der Mathematisch-Naturwissenschaftlichen Fakultät
der Universität Freiburg in der Schweiz

vorgelegt von

Lars-Ola Nilsson

Älmhult, Schweden

Dissertation Nr. 1337

Druckerei Saint-Paul Freiburg
2001

Von der Mathematisch-Naturwissenschaftlichen Fakultät der Universität Freiburg in der Schweiz angenommen, auf Antrag der Herren

Prof. Dr. Louis Schlapbach, Universität Freiburg (Präsident der Jury)
Prof. Dr. André Châtelain, EPFL, Lausanne (Referent)
Dr. Pierangelo Gröning, Universität Freiburg (Koreferent)

Freiburg, den 19. Juni 2001

Der Leiter der Dissertation	Der Dekan
Prof. Dr. Louis Schlapbach	Prof. Dr. Alex von Zelewsky

Abstract

The developement of electronic devices based on micron-sized vacuum electron sources during the last decades [1] have triggered intense research on highly efficient carbon based thin film electron emitters [2].

We developed a new vacuum field emission apparatus composed of a field emission microscope (FEM) and a scanning anode field emission microscope (SAFEM), in order to investigate the low threshold electron field emission from carbon based thin films and carbon nanotubes. The unique design enabled us to characterize different chemical vapor deposited diamond, diamond-like carbon and carbon nanotube (CNT) thin films with the SAFEM and individual carbon nanotube emitters with the FEM. The first part (chapter 2) of this thesis provides a technologically relevant description of carbon cold cathode electron emission, whereas more fundamental physical aspects with regard to emission anisotropy and short term instability are discussed in the second part (chapter 3).

The emission from carbon thin films is explained by Fowler-Nordheim tunneling [3] of electrons from tip-like structures in the micro- and the nanometer range, which locally amplify the applied field [4] by the field enhancement factor β. From the investigations accomplished with the SAFEM it became clear that the emission properties of thin film emitters are best characterized by the spatial distribution of their field enhancement β(x,y). The β(x,y) maps can be used to describe the emitted current density and emission site density (ESD) of thin film emitters. Our measurements clearly show that a high density of field enhancing structures (FES) in a narrow field enhancement range is advantageous in order to obtain a high ESD but the emitter density must not surpass an upper critical limit. If the inter-FES separation becomes comparable with the typical size of the FES, electrostatic screening will reduce the emitted current density.

The SAFEM investigations have also shown that deviations from the Fowler-Nordheim characteristics and emission degradation occur above a critical (for our samples > 300 nA) emission current and is ascribed to the resistivity of the conduction path between the emitter and the substrate. It seems that the emission degradation is induced by joule heating at the emitter-substrate interface.

From the FEM investigations of single CNTs we have gained better insight into the phenomena occurring at the tip apex of the CNTs during field emission. It seems that the observed FEM patterns are representing the molecular orbitals of the CNT tip apex. Such orbitals can be modified by impinging atoms or molecules coming from the gas phase or more probable from the outgassing phosphor screen. If the impinging species are adsorbed to the CNT tip apex it is possible that enhanced resonant tunneling states are created.

Zusammenfassung

Die Entwicklung elektronischer Geräte, deren Funktionsweise auf Mikrometer grossen Elektronenquellen beruht [1], haben im letzen Dezenium intensive Forschungsaktivitäten auf dem Gebiet von dünnen, Elektronenemittierenden Filmen aus Kohlenstoff ausgelöst [2].

Zur Untersuchung der Elektronen-Feldemission dieser Filme und von Kohlenstoff Nanoröhrchen, haben wir eine neue Feldemissions Anlage im Ultrahochvakuum gebaut. Diese besteht aus einem Feldemissions Mikroskop (FEM) und einem Raster Anoden Feldemissions Mikroskop (SAFEM). Elektronenemitter aus Filmen verschiedener Kohlenstoffmodifikationen wurden analysiert, insbesondere in der Gasphase abgeschiedene Diamant- und diamantähnlichen Filme, sowie Filme von direkt auf Substraten aufgewachsenen Nanorörchen. Der erste Teil (Kapitel 2) dieser Dissertation beschreibt vor allem die technologische Relevanz der kalten Elektronenemission von Kohlenstoff, während fundamentale physikalische Aspekte, z.B. Anisotropie und Instabilität der Emission im zweiten Teil (Kapitel 3) behandelt werden.

Die Elektronenemission von Kohlenstoffschichten kann durch Fowler-Nordheim Tunneln aus scharfen Spitzen [3], die bis einige Mikrometer hoch sein können, beschrieben werden. Solche Strukturen können das angelegte Feld erheblich vergrössern (um dem Faktor β) [4]. Durch SAFEM Untersuchungen konnten wir zeigen, dass die Emissionseigenschaften von dünnen emittierenden Filmen am besten durch die räumliche Feldüberhöhung β(x,y) beschrieben werden. Sowohl die feldemittierte Stromdichte wie auch die Emitterdichte (ESD) kann mit β(x,y) charakterisiert werden. Unsere Messungen zeigen klar, dass eine hohe Emitterdichte in einem möglichst engen Feldüberhöhungsintervall für eine hohe ESD vorteilhaft ist. Die Dichte darf allerdings einen kritischen Schwellenwert nicht überschreiten. Oberhalb eines kritischen Wertes des Verhältnis zwischen Emitterhöhe und Emitterabstand wird die Emission durch elektrostatische Abschirmung abschwächt.

Die SAFEM Untersuchungen haben weiter gezeigt, dass oberhalb einer kritischen Stromlimite (für unsere Proben > 300 nA) Abweichungen von der Fowler-Nordheim Charakteristik und Emissiondegradation eintritt. Dieses Verhalten wird der Resistivität des Strompfades zum Emitter zugeschrieben. Es scheint als ob die Emissionsdegradation durch Joulesches Erwärmen am Emitter-Substrat verursacht ist.

Aus den Untersuchungen einzelner CNT's mit dem FEM haben wir ein besseres Verständnis für die Phänomene an der Emitter-Spitze während der Feldemission erworben. Die gemessenen FEM-Muster sind wahrscheinlich als Abbildung molekularer Orbitale zu interpretieren. Sie können Fremdatomen adsorbiert an der gekrümmten CNT-Haube entsprechen. Es scheint, das der Phosphorschirm die verantwortliche Quelle solcher Atome oder Moleküle ist.

Contents

Preface

This thesis is based on research carried out at the *Physics Department of the University of Fribourg, Switzerland* during the period 1997 - 2001. It consists of three chapters: 1) An introduction to electron emission with emphasis on carbon based cathodes, 2) a presentation of scanning anode field emission microscopy on carbon thin film electron emitters and 3) a discussion of the phenomena leading to emission current instabilities at single emitting sites.

The chapter 2 consist of five articles which are intended to elucidate the emitting properties and similarities of different types of carbon thin film electron emitters. The main aim has been to determine and experimentally verify a general description of the electron emission in terms of the thin film physical properties. The scanning anode field mission microscope (SAFEM) and the field emission microscope (FEM) are therefore presented first. Optimization and suggestions of improved carbon cold cathode designs are presented at the end of chapter 2.

The last chapter 3 consists of two articles treating the *environmental stability* of carbon nanotubes and starts with a general description of FEM measurements on carbon nanotubes.

The published or submitted articles included in this thesis are*:

Microscopic characterization of electron field emission
L. Nilsson, O. Groening, O. Kuettel P. Groening and L. Schlapbach
Submitted to JVST B (2001) 41

Scanning field emission from patterned carbon nanotube films
L. Nilsson, O. Groening, C. Emmenegger, O. Kuettel, E. Schaller, L. Schlapbach, H. Kind, J.-M. Bonard and K. Kern
Appl. Phys. Lett. **76**, *2071 (1999)* 73

Characterization of thin film electron emitters by scanning anode field emission microscopy
L. Nilsson, O. Groening, P. Groening, O. Kuettel and L. Schlapbach

---

*Please note that the references for the publications are placed at the end of the respective paper!

List of abbreviations

a-C	amorphous carbon
AMLCD	active matrix liquid crystal display
β	field enhancement factor
BN	boron-nitride
CNT	carbon nanotube
CRT	cathode ray tube
CVD	chemical vapor deposition
DLC	diamond like carbon
E_a	applied electric field
E_F	Fermi energy
E_s, E_{site}	local electric field at emission site
ESD	Emission Site Density
E_{thr}	electric threshold field
E_{Vac}	vacuum energy level
ϕ	work function
$f(\beta)$	field enhancement distribution
FE	field emission
FEA	field emitter array
FED	field emission display
FEM	field emission microscopy
FES	field enhancing structure
F-N, FN	Fowler Nordheim
FPD	flat panel display
ITO	indium tin oxide
MWNT	multiwalled carbon nanotube
NEA	negative electron affinity
SAFEM	Scanning anode field emission microscopy
SEM	Scanning electron microscopy
Spindt-tip	μm-sized field enhancing metal tip
SWNT	Singlewalled carbon nanotube
VMED	vacuum microelectronic devices

Chapter 1

Introduction

1.1 Electron emission sources in vacuum microelectronic devices

Several daily used electronic devices are based on electron sources. Some of the more familiar examples of such devices are cathode ray tubes (CRT) in television sets, X-ray generators and microwave amplifiers. Many of the electron sources in these devices have relied upon thermionic electron emission for several decades. The operating principle here is based upon heating (> 1000 °C) of filaments by currents whereby electrons gain enough thermal energy to be ejected from the solid (i.e. the filament) into vacuum. The free electrons in the vacuum can then be accelerated by means of electric fields to produce an image on a phosphor screen of a CRT or X-rays, microwaves etc. Albeit rather inexpensive and delivering high current densities thermionic emitters have a number of significant drawbacks: The large heat dissipation causes rather large energy consumption and most important of all, the thermionic electron sources cannot be made very small and cannot be turned on and off at high frequencies. The term ”small” here refers to length scales on the order of one micrometer. A device design based on a large number of parallel operated micron-sized electron sources can in some cases offer technological advantages over a single bulky electron source, e.g. in the screen of a portable computer or a mobile phone. The thermionic emitter might therefore not offer a good solution in some devices where size and energy dissipation of the electron source is crucial.

Fortunately field emission (FE) from solids has opened the door to the miniaturization of electron sources. In field emission electrons are ejected from solids under the action of intense electric fields and has been known since 1897 [5]. However it was not until two decades ago that improvements in micro fabrication techniques triggered much progress in the manufacturing of devices with miniaturized electron sources. These devices are commonly called vacuum microelectronic devices (VMED) and make use of a large number of micron-sized field emitting electron sources, also called field emitters. The field emitting sources in the VMED are built to nanoscale tolerances. The generation of electrons by field emission is however not the only criteria of functionality in the VMED. The field emitted electrons have also to be transported by means of electric fields in vacuum in order to fulfill some useful task, e.g. generate light on phosphor screens in television sets by cathodoluminescence. The VMED therefore depend for their operation on collision-free ballistic motion of electrons in vacuum [1]. The motion is called ballistic since in contrast to conventional solid state microelectronics, the field induced transport of the free electrons in vacuum is not subjected to scattering or collisions. The major advantage of the ballistic motion in vacuum resides in the fact that the energy dissipation and the energy spread is very low and the time of flight is short as compared to the collision dominated solid state transport in a typical semiconductor such as silicon.

There are three critical aspects to vacuum microelectronics [1]:

- Extracting the electrons from the metal or semiconducting material in which they are stored and emitting them into the vacuum in sufficient quantities and with a sufficiently narrow energy spread to enable a device to operate as designed.
- Fabrication of a device structure to the necessary dimensions and tolerances, including deposition of thin layers of material with the physical properties necessary for device operation.
- Stable device operation in the vacuum enclosure as designed without generating unwanted discharges and environmental changes.

The high brilliance of field emitter devices can be exploited in scientific instruments like the scanning electron microscope (SEM), where the resolution and performance can be enhanced if the thermionic electron source is replaced by a field emission source. Low energy dissipation and short switching time (short time of flight) make VMED interesting for several other important applications like high high power radio frequency amplifiers, electron guns for klystrons or traveling wave tubes and data storage (studied by Hewlett Packard) where field emitted electron beams are used to read and to write bits of data into a storing medium. However the first large scale commercial application of micro field emission sources is likely to be for arrays of miniature, cold cathodes, which are required for thin matrix addressable cathodoluminescent display devices called field emission flat panel displays (FED).

It has become evident during the last decade that the fabrication process (see point two above) of such matrix addressable cold cathodes is highly critical and cost intense. One has therefore sought to find less expensive and less critical fabrication techniques of the cathodes in e.g. FEDs. Several reports on highly efficient electron emission from carbon based compounds so called carbon *thin film electron emitters* have therefore triggered much interest and research efforts [6–10]. The main reason to this is that the carbon thin films are relatively easy to produce over large area substrates without high cost or highly critical processes. The carbon based electron sources are further expected to give a number of other important advantages over the more traditional FE electron sources, like lower power consumption and cheaper driving electronic circuitry. The reason for this is that the operating voltage (20-50 Volts) of the carbon electron sources are expected to be lower than for other electron sources (80-100 Volts).

Whereas most of the research activities on the electron emission from carbon compounds during the last decade have been focused on the emission mechanism(s) (workfunction versus field enhancement), the main emphasis of the research in this PhD thesis has been put upon a description of the global emission behavior of carbon thin films in terms of their microscopic field emission properties. A better understanding of the overall electron emission from a large carbon thin film surface in terms of the local emission properties at the individual, single emission sites, will facilitate the improvement of the cold cathode performance. Such a description will in addition help a manufacturer to estimate the technological difficulty of the production of carbon thin film emitters as compared to conventional electron emission concepts in the VMED design.

1.2 Electron field emission

Electron emission from a single emitter

The energy required to extract an electron from the Fermi level E_F of a neutral solid to a rest position in the vacuum not too far away from the surface is termed the work function ϕ, and is usually given in electron volts (eV) [11]. The work function has values 2-5 eV for metals and arises from two effects. The first, or inner potential, is the intrinsic partial free energy of ”solution” of electrons in the metal and is the difference between the chemical potential (Fermi level) of the electron in the metal and that at a very large distance from it in a field free vacuum. The second component arises from electrostatic effects due to spill-out of electrons at the surface and decays slowly with distance. This spill-out causes an electron deficiency on the metal side of the solid-vacuum interface and gives rise to a condensor or dipol layer, with the negative end outermost. If the surface is rough there is a second spill-over in addition with electrons flowing into the concave portions of steps and produces an opposite dipol with the positive end outward. The surface structure is therefore responsible for the crystallographic anisotropy in ϕ. Similar effects can occur for adsorbed molecules on the surface.

In thermionic emission and photoemission electrons are given sufficient energy to overcome the potential step of ϕ at the surface of a solid. In field emission (FE) on the other hand, the step is deformed into a potential barrier so that the unexcited electrons can leak or tunnel out *through* it. This situation is depicted in Fig. 1.1.

When a field E_s is applied to the surface, electrons close to the Fermi level E_F will see a barrier height ϕ and thickness $x = \phi/eE_s$ (to a first approximation). If this is thin (< 2 nm) enough, the electrons of the conducting material will have a finite probability of tunneling. However the electron cloud does not terminate sharply at the interface so the triangular potential barrier is only a first approximation to the shape of V(x) at the surface. Besides the potential V(x) near the surface is decreased by an image term $1/(4\pi\varepsilon_0)\cdot e^2/4x$ which lowers the effective potential barrier. The typical distribution of the field emitted electrons as a function of the normal energy is indicated in Fig. 1.1. The intensity of the FE electrons is higher close to E_F as a result of the increased thickness of the barrier for energies below E_F.

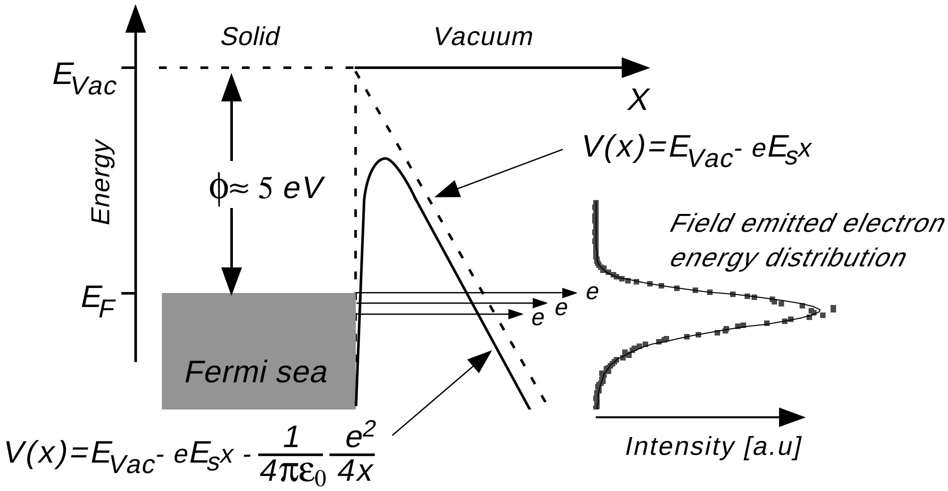

Figure 1.1: Tunneling of electrons from the Fermi sea of electrons through the potential barrier at the surface of a conducting solid into vacuum. The size of the local field at the emission site E_s as well as the workfunction ϕ and field enhancement β can be determined from the intensity and shape of the field emitted electron energy distribution. Half width at full maximum is about 0.25 eV for the energy distribution shown here (not drawn to scale).

The Fowler-Nordheim equation [3] relates the emitted current density J to the electric field E_s normal to the surface at zero temperature by

$$J = \frac{1.56 \cdot 10^{-6}}{\phi t^2(y)} E_s^2 \exp\left(\frac{-6.83 \cdot 10^7 \phi^{1.5}}{E_s} \cdot v(y)\right) \tag{1.1}$$

with

$$y = \sqrt{\frac{e^3 E_s}{4\pi\varepsilon_0 \phi^2}}$$

J is the emission current density in [A/cm^2]. ϕ [eV] the emitter work function and E_s [Vcm^{-1}] the local field at the emission site. The expressions t(y) and v(y) are the Nordheim elliptic functions, which can be approximated by $t^2(y) \simeq 1.1$ and $v(y) \simeq 0.95 - y^2$ [1].

In order to describe the emission current I of a single metal-like emitter over a wide range of electric fields the simplified FN-formula as proposed by Spindt et al. [1], where the elliptic functions v(y) and t(y) are approximated, can be used:

$$I = A \cdot \frac{1.5 \cdot 10^{-6}}{\phi} E_s^2 \exp(\frac{10.4}{\sqrt{\phi}}) \exp(\frac{-6.44 \cdot 10^7 \phi^{1.5}}{E_s}) \tag{1.2}$$

In order to account for experimentally observed emission currents of carbon thin film emitters, A takes values of 10^{-11}- 10^{-9} cm^2. Though A has the dimension of an area and theoretically only takes account of the emitting area in the F-N theory, in experiment the pre-exponential factor A will also depend on the bandstructure of the emitter.

From the intensity of the FE electrons and the exponentially decaying slope of the FE distribution towards low electron energies, Dr. Gröning was able to determine the local field E$_s$ and the workfunction ϕ independently for several carbon based emitters. He found that the local field at the emission site E$_s$ is on the order of 4000 V/μm for an emission current around 50 nA and that the workfunction is close to 5.0 eV [4, 12] for several carbon compounds like CVD nanodiamond, multiwalled CNTs and discharge activated DLC. Furthermore it seems reasonable to assume that the sp^2 phase in graphite-like compounds is responsible for the low threshold electron emission from carbon thin film emitters. The graphite-like compounds like multiwalled CNTs possesses a high density of electron states in the vicinity of the fermi level and can hence be treated as conductors. Due to the metal-like conductivity and relatively high workfunction around 5 eV the electron emission of graphite-like compounds can therefore to a good approximation be treated according to the classical Fowler Nordheim theory with tunneling through a potential barrier like in Fig. 1.1. By putting A= 10^{-9} and ϕ= 5.0 eV in expression 1.2 we obtain a relation for the emission current of a single emitter, which depends only on the local field E$_s$ at the emission site.

Since the applied field E$_a$ in a typical diode type FE experiment is several orders of magnitude lower than E$_s$, the applied field must be amplified by means of field enhancement at the emission site. It is well known that such field enhancement can be achieved with sharp protruding structures/asperities on the cathode surface like metal or silicon tips in the (sub-) micrometer range, Fig. 1.4(b). Carbon or more correctly graphite-like carbon compounds like CNTs are also known to form these sharp field enhancing structures (FES), Fig. 1.5. In order to understand how the applied field is amplified let us imagine a small conductive sphere hovering at a distance h above the cathode in a diode type electrode gap. The sphere is electrically connected to the cathode. The field E_s at the surface of the free sphere of radius r and potential V is E_s= V/r according to electrostatics. At the surface of an actual tip the field is reduced from this value by the presence of the conical shank, but is given to a good approximation by E_s= V/αr, where $\alpha \sim 5$ near the tip apex and increases with polar angle [11]. The value of α is reduced to a value close to 1 for a very thin structure like a carbon nanotube. The electric potential V(x=h) at height h above the negative electrode in an electrode gap of the type depicted in Fig. 1.4(a), is given by V(h)= E_a·h. The field enhancing property of a tip is therefore to a good approximation given by

$$E_s = \frac{V(h)}{\alpha r} = \frac{h}{\alpha r} E_a = \beta \cdot E_a \qquad (1.3)$$

where the factor h/αr is called the β or field enhancement factor. If we insert E_s of equation 1.3 into 1.2, we obtain an expression which is dominantly dependent on the field enhancement β. This because the workfunction is relatively stable around a high value of approximately 5 eV and the emission current is only weakly dependent on the pre-exponential factor A in the range 10^{-11}-10^{-9} cm^2. We can therefore to a good approximation describe the emission current of a single emitter in terms of the local electric field E_s or the local field enhancement β if we put A= 10^{-9} and ϕ= 5.0 eV in expression 1.2. From field emission microscopy (FEM) it can be realized that the emission of a single CNT not occurs homogeneously over the whole active emission area on the CNT cap but in time varying lobed patterns (see Chapter 3). Such emission variations can be explained by anisotropic local changes in the workfunction on the emission site tip apex. However since the variation of the local emission intensity within a lobed pattern in general is on the order of one order of magnitude, it can be shown that the effects of the workfunction anisotropy are negligible in comparison with changes in the field enhancement (see paragraph 2.4.2). We therefore conclude that the emission current from a single emitter to a good approximation is given by expression 1.2, which dominantly depends on the local field E_s and the field enhancement β at the emission site.

The thin film electron emitter

The previous description of the electron emission is restricted to a single emission source. These are rarely encountered in real device technology, except possibly for the scanning electron microscope. Instead it is often desirable to operate a large number of electron emitting sources in parallel. With a high density of miniaturized emission sources large current densities and high resolution vacuum microelectronic devices like flat panel displays can be realized. We like to think of these bundled and large number of parallel emitting sources as *emitter ensembles* or as *thin film electron emitters* and would like to treat them in "units" or "packages". For an efficient device operation, the units have to fulfill several quality criteria or requirements regarding emission homogeneity, density of emission sources, current density, emission long- and short term stability etc. within the units as well as between several parallel operated units. In order to fulfill these requirements we need a realistic description of the emission from each of the units. This will help to understand why the emitting site density is different for different types of thin film emitters as shown in Fig. 1.5. With a realistic description of the thin film emission the requirements of quality can be understood in physical meaningful entities, which can be modified in order to optimize the emission not only from one emitter but from the entire thin film emitter ensemble.

1.3 The field emission flat panel display

Without doubt the FED has been the most important technological driving force to the interest and progress in vacuum microelectronic devices in recent years. The world wide annual revenues in the flat panel display (FPD) market are expected to increase to more than US$ 80 billion [13] in the next three to four years [14]. The FPDs are attractive for consumer electronics like portable computers, cellular phones, car navigation systems and almost every thinkable electronic device with a communication interface between the user and the device. The image on the screen of a cathode ray tube (CRT) is produced by an electron beam which is scanned across the phosphor coated screen. The electron beam is generated by a thermionic source which together with the beam deflection system and the limited deflection angle make the CRT bulky. In contrast to the CRT a FED makes use of up to several hundred electron sources for every pixel. Since every pixel is made up of separate electron sources the FED design can be made very compact and some like to call the FED a thin CRT. The electrons in the FED are produced by electron field emission. In order to get appreciable FE currents rather high electric fields up to 5000 V/μm are needed [11]. Such high fields can not be realized on flat surfaces wherefore micron-sized tip-like structures are used for field amplification (also called field enhancement). The micron-sized tips of traditional FEDs are made up of matrix addressable evaporated metal or etched silicon tips which are arranged in arrays of hundreds of tips [15]. An example of such field emission arrays (FEA) of micron-sized tips is shown in Fig. 1.2.

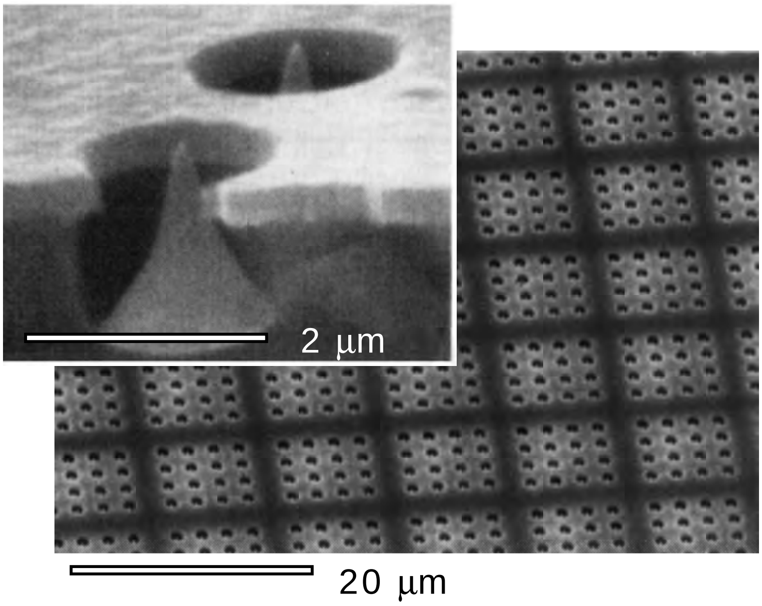

Figure 1.2: Field emitter arrays (FEA) of evaporated metal tips, also called Spindt-tips [16].

The voltage applied between the tips and the gate is usually less than 100 Volts, which means that "of the shelf" integrated circuits can be used to control the column-row addressing of individual pixels. Nevertheless it is desirable to reduce the operating voltage in order to reduce the cost for the drivers. Current densities in excess of several hundreds Acm^{-2} can be achieved with a packing density of 10^7 tips/cm^2 and gate-cathode voltages of 100V [1]. The system of the FEAs and the gate is separated from the phosphor coated transparent faceplate by a vacuum gap typically some millimeters wide, also depicted in Fig. 1.3(a). Sometimes some kind of focusing electrode system is additionally used between the FEA and the faceplate to improve the quality of the image. The electrons which are field emitted from the FEA into the vacuum gap are accelerated towards the screen due to a high voltage applied to the screen and the display image results from cathodoluminescence of the phosphor material, which serves as anode. Depending on the phosphor efficiency one distinguishes between low- and high-voltage displays where the former is in the range of <2 kV and the latter >5 kV. To achieve full color images stripes of red, green and blue (RGB) phosphors are deposited on a conductive transparent layer (typically Indium Tin Oxide, ITO) covering the whole anode plate. Each phosphor strip is associated with a specific FEA in the cathode and in each pixel the three primary colors can be simultaneously excited. The intensity of light produced by the subpixel within the RGB triad is adjusted relative to one another, and the human eye is then relied upon for integrating the spatially separated RGB dots into a perceived color image. The number of column drivers is therefore increased in comparison with a monochrome display for the same number of pixels.

1.4 Competing flat panel display technologies

The FED is one of several competing alternatives to the by now well established state of the art active matrix liquid crystal display (AMLCD). Recent development in organic light emitting diodes (OLED) [17], light emitting polymers (LEP) [18], read and rewritable electronic paper [19, 20] and heavily improved performance of the traditional AMLCD over the last years has made the battle for the FED on the market tougher. Some of the main FED advantages [21] like low power consumption ($\sim$57 W/m^2), wide viewing angle (±80 °), wide operating temperature range (-5 to +85 °C), fast pixel response time ($\sim$10 μs) and high brightness ($>$ 600 cd/m^2 for high voltage phosphors) are qualities which still make the FED very interesting for portable electronics, car navigation system subjected to direct sun light, large area electronic billboards etc. The large number of micro tips per pixel make a FED less vulnerable to pixel defects as the emitter failure of some tips does not critically affect the operation of the display. The AMLCD in contrast, where each color component is controlled by two transitors, lacks the FED redundancy and the failure of one or more transitors will cause visible defects and therefore higher costs since part of the AMLCD production have to discarded. Of the same reason is the cost of an AMLCD higher than the proportionality to the size of the screen would suggest. Nevertheless the AMLCD industry has managed to improve production yield and lower the cost per unit during the last years. The AMLCD pixel switching time has also been improved to deal with streaming media, real time video etc.

The improved AMLCD performance combined with the ongoing research on competitive flat panel display technologies makes it necessary to more carefully correlate the product quality, product price and costumer needs. As an example the new generation of the american armored vehicle Abrams will make use of high resolution monochrome FEDs delivered by the french based company PixTech [22]. Obviously a price of US$ 2000 or even 5000 for a display is a small price to pay compared to a US$ 10 million armored vehicle. The client is in this case willing to pay the relative large difference in price between a FED and an AMLCD for a relatively small increase in quality and performance. However the same cannot necessarily be said for a car, or even less for consumer electronics. To reach the wide market of consumer electronic the FED price per unit must be drastically reduced compared to today. The process of fabricating arrays of microtips requires expensive processes like lithographic patterning, mask aligners, evaporators and clean rooms. In this respect one would like to see cheaper and easier manufacturing techniques of the cathodes in FEDs. The question of the future success of commercialized FEDs is therefore clearly related to the application, the desired quality, price and future technological progress of not only the FEDs but also competing FPD technologies.

1.5 The hope for the flat thin film electron emitter

At the beginning of the last decade several reports [6, 7] were given, showing highly efficient electron emission at low electric fields on the order of some volts per micrometer from what was believed to be perfectly flat surfaces without surface protrusions or tips [23]. These cathodes are referred to as flat thin film electron emitters and were, or possible still are to some scientists, thought to provide the solution to several of the technological difficulties associated with the cathode design in FEDs. The reason for this stems from the fact that a surface which emits electrons more or less homogeneously at fields as low as some few volts per micrometer due to a low workfunction or negative electron affinity requires less expensive patterning processes and much simpler device design. In contrast to the micrometer-sized design of FEA tips, the ideal flat electron emitter could be homogeneously deposited, by e.g. chemical vapor deposition, over rather large areas of substrates with much lower spatial tolerance and hence lower cost. Instead of defining hundreds of FEA microtips as electron sources for a pixel of typically ~ 100 μm width, the whole FEA sub-element could be replaced by a electron emitting flat thin film. The basic difference and advantage over the FEA design is illustrated in Fig. 1.3(b), where however the gate not has been sketched around the flat thin film emitter.

Carbon based materials like diamond, diamondlike carbon (DLC) or different compounds of graphite and diamond containing small amounts of hydrogen or nitrogen were thought to deliver these flat homogeneously electron emitting films [2]. The fact is that appreciable electron emission currents were measured from these carbon compounds at very low applied fields E_a on the order of some few volts per micrometer in diode type emission set-ups of the type illustrated in Fig. 1.4(a).

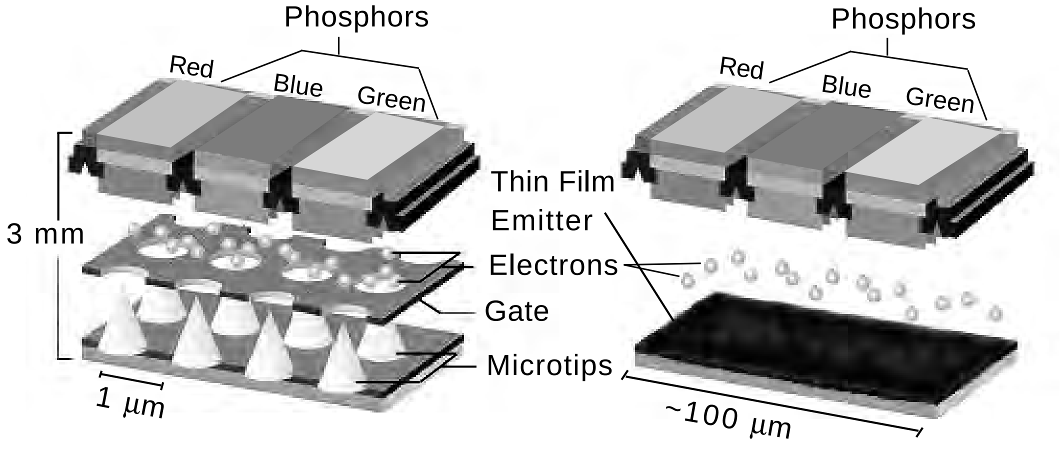

(a) Metal tip array emitter

(b) Ideal flat thin film emitter

Figure 1.3: The principal design of a flat field emission display (FED) in the case of (a) metal tip arrays [22] and (b) an ideal flat thin film emitter without surface asperities or tips.

Several explanations have been forwarded to explain the low threshold electron emission of the presumably flat carbon films. They are generally based upon diamond seen as a wide band gap semiconductor with negative electron affinity (NEA). NEA means that the conduction band of diamond is energetically higher than the vacuum energy level E_{Vac} [24–27]. The electrons were thought to tunnel into the conduction band of the diamond due to strong band bending at the back contact-diamond interface. The strong band bending would result from field penetration into the insulating diamond matrix. The injected electrons would be transported from the back contact to the diamond surface due to the internal electric field. This transport would take place either ballistically or as hopping from defects or dopants. Due to the NEA the electrons would be emitted into the vacuum without further barriers or restraints [23]. One would therefore expect exceptionally low workfunctions (~ 0.1 eV) of these materials [28, 29].

Since most of these results were based on diode type experiments like in Fig. 1.4(a), where the cathode surface was assumed flat, the calculations from the so called Fowler-Nordheim formula (see section 1.2) yielded extremely low workfunctions of tens of meV. However already in the ninties several scientists were skeptical to such low workfunctions [30, 31]. The electron emission was spatially imaged using both scanning anode techniques and phosphor screens and was clearly not homogeneous, which of course not exclude the emission models above. The once much promising diamondlike carbon never fulfilled the high expectations, since the density of emission sites for most applied fields was low and normally came from just some few isolated spots on a surface of typically 1 cm^2. In addition there were other intriguing questions to answer about the electron injection, the field penetration and the surface charge accumulation.

Surface asperities and field enhancement

Careful investigations of the field emission from carbon thin film emitters have shown that the low threshold emission at isolated sites is due asperities or structures at the surface or maybe inside of the carbon films [12, 31]. Such asperities can be very sharp wherefore they can exhibit a field enhancing effect. The applied field can therefore be amplified several hundred, possibly up to thousand times. The field enhancement effect of a conducting tip or asperity is illustrated in Fig. 1.4(b).

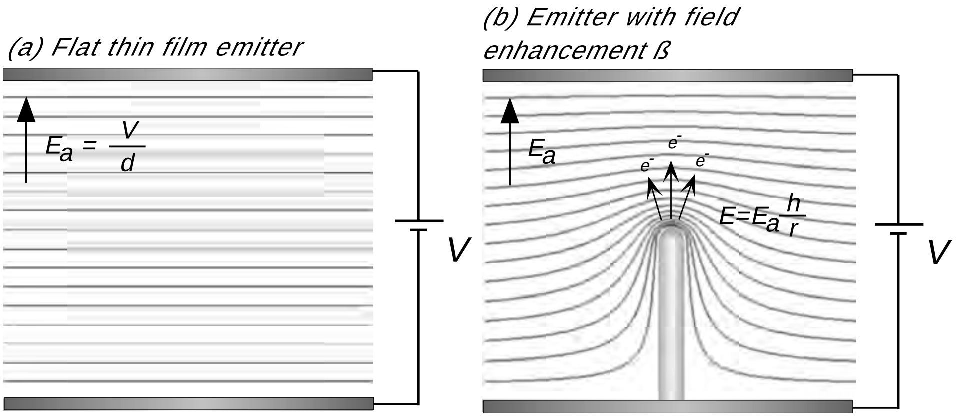

Figure 1.4: The local field at the surface of the ideal flat thin film emitter (a) is thought to be up to three orders of magnitude lower than for the tip like emitter with field enhancement β (b). The surface area of emission is several orders of magnitude higher in the case of (a), which makes the surface less sensitive to sputter erosion of impinging ions.

The equipotential lines are concentrated around the tip apex, where the amplification of the applied field E_a is of the order of the aspect ratio h/r, where h is the height and r is the radius of curvature of the structure. The field amplification is mostly called field enhancement and is designated the greek letter β. Some examples of different emitting structures on carbon containing thin film electron emitters are shown in the scanning electron micrographs of Fig. 1.5. These films are typically grown from the gasphase (chemical vapor deposition, CVD) of different carbon containing gases like methane or acetylene on silicon or quartz substrates under the influence of low pressure plasmas [2, 32].

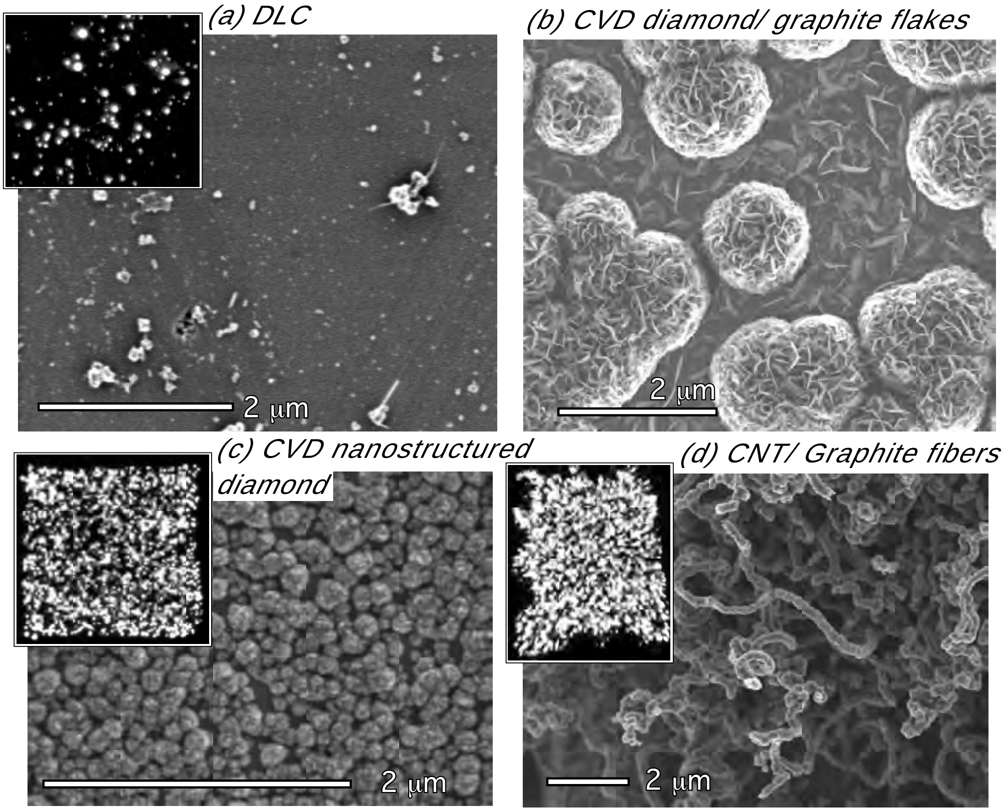

Figure 1.5: Various examples of electron emitting thin films. (a) Diamond like carbon; inset (15×15 mm^2) depicts electron emission on a phosphor screen for an applied field ∼ 7 V/μm. (b) Chemical vapor deposited (CVD) nanocrystalline diamond with a large fraction of sp^2, grown at 1020 °C. (c) CVD nanocrystalline diamond; inset (7×7 mm^2) depicts electron emission on a phosphor screen for an applied field ∼ 10 V/μm. (d) multiwalled carbon nanotubes and graphite fibers emit very well. Inset (4×5 mm^2) depicts electron emission on a phosphor screen for an applied field ∼ 12 V/μm.

In order to introduce defects and influence the electronic properties of the grown films, small amounts of gaseous nitrogen or boron can be added during the growth process. Depending on growth parameters like pressure, temperature and gas composition films with a wide range of different properties like sp^2/sp^3 ratio, (graphite/diamond), crystallinity, amounts of defects, conductivity and of course surface roughness can result. One of the reasons for which the surface roughness not was seriously taken into account during the early emission experiments on diamondlike carbon (DLC) films, was that DLC normally is considered a very smooth film. Nevertheless some DLC films contain asperities that can act as field enhancing structures. Even if these are few they will contribute to the emission in diode type experiments. However as indicated by the three insets of spatially resolved emission on the phosphor screens in Fig. 1.5, different types of films and structures appear to be better or worse electron emitters. Whereas the DLC films in general have a low emitting site density (ESD), the carbon nanotube film in (d) can show an ESD up to 10^4 sites per cm^2 for applied fields of 1 to 10 $V/\mu m$. Various compositions of CVD nanostructured diamond and graphite, (b) and (c) have been reported to show equally high ESD.

We thus realize that the emission from carbon based films is analogous to the metal tip emission from a physical point of view. The simple picture of the flat thin film electron emitter as it is sketched in Fig. 1.4(a) is therefore wrong and must be replaced by geometrical field enhancement due to tip like structures as in (b). This is unfortunate from a technological point of view, since the major incentive to the interest in the carbon based emission was due to the flat thin film emitter depicted in Fig. 1.3(b) and 1.4(a). To replace the metal tip FEA advantageously by the carbon based thin film emitter, the following requirements must be placed upon the cathode and the emitting structures [1]:

- The emitting carbon field enhancing structures (FES) must be capable of being fabricated to submicron tolerances to that the emitting area is precisely defined and does not change during its operating lifetime. For application in a high resolution FED an emitting site density of at least 10^7 per cm^2 is recommended.

- The emission characteristics must be scalable and reproducible over large area substrates from one emitting source to another.

- Cathode manufacturing should be inexpensive and possible over large area substrates like quartz at low temperatures (< 500 °C), without highly critical processes and adaptable to a wide variety of applications.

- The emission current must be voltage controllable, preferably with drive voltages lower than 50 V, with integrated circuits from "off the shelf".

- Depending on the application the source must be capable of emitting sufficiently large current densities. A current of one microampere from one μm^2 area requires a current density of 100 A/cm^2. One mA/cm^2 can be regarded as a lower limit for a source to reach wide applications in VMED.

- The energy density that must be supplied from the external source must be manageable.

- The energy spread of the field emitted electron must be small for applications where highly mono energetic electron beams are desired, e.g. in high resolution electron microscopy.

- The (long-term) emission must be stable during its device operational time of life (tens of thousands of hours).

- The (short-term) emission fluctuations (noise) must be kept small enough not to limit device performance.

- The cathode must be resistant to unwanted occurrences in the vacuum tube environment, such as ion bombardment, reaction with residual gases, temperature extremes and arcing.

In order to satisfy the three first requirements we need a good quantitative description of the emission, not only from one but from many parallel operated emission sources of the thin film emitter ensemble (chapter 2). The importance the spatial distribution of the field enhancement β(x,y) of thin film emitters has for the ESD and the consequences this has for the homogeneity of the emission has to be clarified. These answers will explain the origin of the different field dependent ESDs in the insets of Fig. 1.5.

1.6 Carbon allotropes

Graphite and Diamond

Carbon compounds are unique in several ways. One distinction relates to the wide variety of allotropic forms these materials can assume, see Fig. 1.6. Under ambient conditions and in bulk form, the **graphite** phase with strong in-plane trigonal sp^2 bonding is the thermodynamically stable phase [33]. At high temperature and pressure a thermodynamic equilibrium transformation to the **diamond** [34] structure with tetrahedral sp^3 bonding takes place [35, 36]. Using non-equilibrium methods, diamond films can also be prepared at low pressures by chemical vapor deposition methods [37–39]. The structure of the graphite phase is highly anisotropic with metallic behavior in the basal plane and poor electrical conductivity perpendicular to the graphene layers. In contrast, diamond is an isotropic, fcc-cubic, wide band-gap semiconductor. In terms of the mechanical properties, graphite is the stiffest material in nature (highest in-plane elastic modulus), while diamond is the hardest material. Although both graphite and diamond are formed from the same element of the periodic table, they exhibit pronounced differences with regard to the structure and electronic properties.

Atomic carbon has a $1s^2 2s^2 2p^2$ electronic state configuration. The reason for the wide variety of properties resides in the fact that the energies of the 2s and 2p states are very close in carbon molecules [43]. When forming solids or molecules carbon can therefore form linear combinations called *hybridizations* of the 2s and 2p orbitals if the resulting binding energy of the carbon molecule is lower than the energy of the orbitals of the free atoms. In graphite strong covalent in-plane

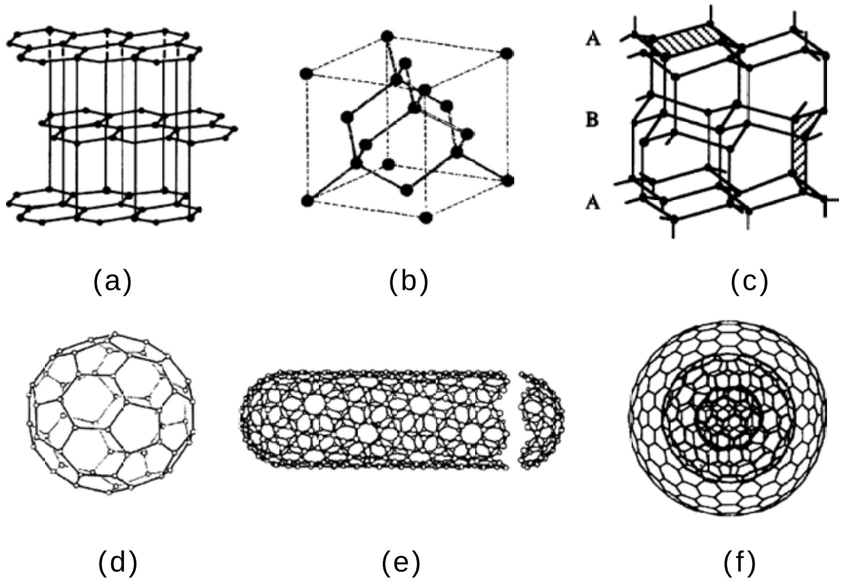

(a) (b) (c)

(d) (e) (f)

Figure 1.6: Allotropic stable forms of carbon (a) graphite [40], (b) diamond [41], (c) lonsdaelite [40], (d) fullerene C_{60} [42], (e) single-walled nanotube (SWNT) [42], (f) onion C_{540}.

bonds are formed between a carbon atom and its three nearest neighbors from 2s, $2p_x$ and $2p_y$ atomic orbitals. Since each in-plane hybrid orbital is a linear combination of $\frac{1}{3}$s and $\frac{2}{3}$p atomic orbitals this bonding arrangement is called sp^2 hybridization. The remaining electron in a pure p_z orbital is only weakly localized and provides weak interplanar bonding (van der Waals) between the graphene sheets and semimetallic conduction behavior parallel to the graphene layers. If in contrast the four electrons belonging to the 2s, $2p_x$, $2p_y$ and $2p_z$ are mixed in four sp^3 hybrid orbitals (linear combinations of $\frac{1}{4}$s and $\frac{3}{4}$p orbitals), the tetrahedral bonded structure of diamond is obtained. With a gap of 5.5 eV between the filled valence band and the empty conduction band diamond therefore is an insulator in the absence of dopants. In view of the high charge carrier mobility diamond can possess semiconducting properties. Acceptor levels can be introduced by substitutional boron with p-type activation levels of 370 meV and n-type (phosphor) donor levels with 500 meV activation energies [44]. The properties of graphite and diamond are summarized in table 1.1 [45].

Amorphous Carbon

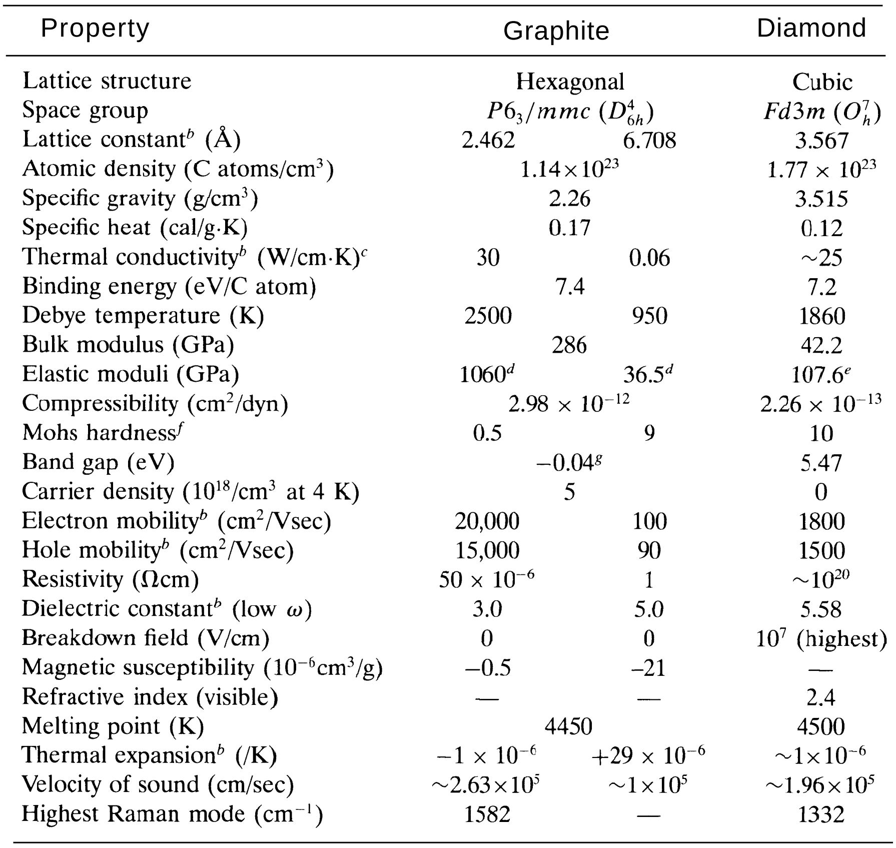

Property	Graphite		Diamond
Lattice structure	Hexagonal		Cubic
Space group	$P6_3/mmc$ (D_{6h}^4)		$Fd3m$ (O_h^7)
Lattice constant[b] (Å)	2.462	6.708	3.567
Atomic density (C atoms/cm^3)	1.14×10^{23}		1.77×10^{23}
Specific gravity (g/cm^3)	2.26		3.515
Specific heat (cal/g·K)	0.17		0.12
Thermal conductivity[b] (W/cm·K)[c]	30	0.06	~25
Binding energy (eV/C atom)	7.4		7.2
Debye temperature (K)	2500	950	1860
Bulk modulus (GPa)	286		42.2
Elastic moduli (GPa)	1060[d]	36.5[d]	107.6[e]
Compressibility (cm^2/dyn)	2.98×10^{-12}		2.26×10^{-13}
Mohs hardness[f]	0.5	9	10
Band gap (eV)	−0.04[g]		5.47
Carrier density (10^{18}/cm^3 at 4 K)	5		0
Electron mobility[b] (cm^2/Vsec)	20,000	100	1800
Hole mobility[b] (cm^2/Vsec)	15,000	90	1500
Resistivity (Ωcm)	50×10^{-6}	1	$\sim 10^{20}$
Dielectric constant[b] (low ω)	3.0	5.0	5.58
Breakdown field (V/cm)	0	0	10^7 (highest)
Magnetic susceptibility (10^{-6}cm^3/g)	−0.5	−21	—
Refractive index (visible)	—	—	2.4
Melting point (K)	4450		4500
Thermal expansion[b] (/K)	-1×10^{-6}	$+29 \times 10^{-6}$	$\sim 1 \times 10^{-6}$
Velocity of sound (cm/sec)	$\sim 2.63 \times 10^5$	$\sim 1 \times 10^5$	$\sim 1.96 \times 10^5$
Highest Raman mode (cm^{-1})	1582	—	1332

Table 1.1: Properties of graphite (left column in-plane values and right column values perpendicular to the graphene sheets) and diamond [45].

When sp^2-graphitic- and sp^3-diamond-like bonds are mixed a highly disordered network of predominately sp^2 bonded carbon with almost no sp^1 bonds is formed [46–48]. This form of carbon is often referred to as **amorphous carbon** (a-C). a-C has no long range order but exhibit short range order (length scale of $\sim$ 10 $\mathring{A}$) which varies significantly from one preparation method to another. The ratio of sp^2 to sp^3 bonds and the hydrogen content is therefore most influential in characterizing the short range order.

A perfectly sp^2 ordered graphene sheet is a zero-gap semiconductor. The introduction of disorder and sp^3 defects creates a semiconductor with localized states near the Fermi level and an effective band gap between mobile filled valence band states and empty conduction states. The greater the disorder and the greater the concentration of sp^3 bonds, the larger is the band gap.

The **tetrahedral a-C** and the **hydrogenated tetrahedral a-C** are often called **diamondlike carbon (DLC)** as they can be both opaque, smooth and exhibit a hardness close to diamond. Thin films of DLC were regarded as very promising candidates for cold cathode applications during the middle of the last decade.

Fullerenes and Carbon Nanotubes

A **fullerene** is best viewed upon as a closed sp^2-bonded carbon cage. The radius of the cap curvature is obtained if pentagons are introduced into the hexagonal sp^2 bonding network of a graphene sheet [45,49]. The best known example of this family of carbon allotropes (and most stable) is the icosahedral C_{60} molecule, where the almost spherical shape is created by 20 hexagons and 12 pentagons, see Fig. 1.6(d). The bonding between the carbon atoms is predominately sp^2 as in graphite, but because of the curvature some sp^3 bonding is also admixed to the carbon wave functions. If two or more carbon cages with different radii are enclosed into each other an onion-like fullerene, Fig. 1.6(f), is obtained.

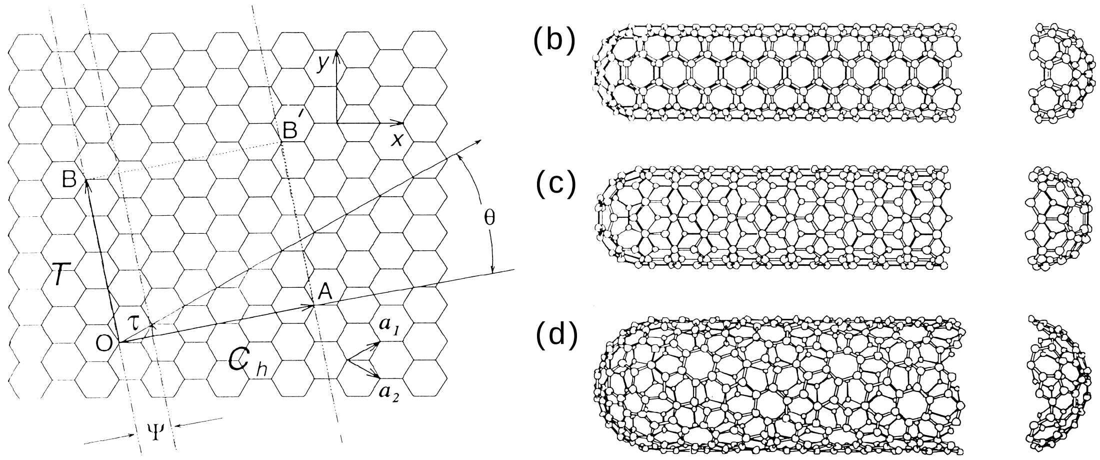

Figure 1.7: The 2D graphene sheet is shown in (a) along with the chiral vector $\mathbf{C}_h = n\mathbf{a}_1 + m\mathbf{a}_2$, which specifies the chirality of the nanotube [50]. $\mathbf{C}_h$ is defined by the integers (n,m), the chiral angle Θ and the unit vectors $\mathbf{a}_1$ and $\mathbf{a}_2$ on the honeycomb lattice. By rolling up the graphene sheet in the direction of $\mathbf{C}_h$ for $\Theta = 30°$ an "armchair" SWNT tubule (b) is obtained. The $\Theta = 0°$ direction gives a "zigzag" tubule (c) and a general direction with $0 < |\Theta| < 30°$ a "chiral" (d) tubule. (n,m) in the figure corresponds to (b): (5,5), (c): (9,0) and (d): (10,5).

One may conceptualize **carbon nanotubes** (CNT) as cylinders rolled from a graphene sheet and capped at both ends by hemispheres of fullerenes [33,50,51], see Fig. 1.7. The high curvature of the graphene sheets (defined as a simple layer of the graphite structure) increases the total energy of the tubules per carbon atom, but this is more than compensated by a lowering of the energy because of the absence of dangling bonds at the edges of the graphene sheets. CNTs which have been rolled up from a single graphene sheet are called singlewalled nanotubes (SWNT) and tubes consisting of several or many concentric layers are called multiwalled nanotubes (MWNT). The diameter of MWNTs ranges from 10 to 50 nm with lengths up to more than 10 μm, whereas the SWNT are much thinner with typical diameters from 0.7 to 1.8 nm. Though much smaller in diameter, carbon nanotubes are often grown concurrently to vapor grown carbon fibers, see Fig. 1.8. The high length to diameter ratio is of decisive importance to the field emission properties.

The chirality of a SWNT, which expresses in which direction the graphene sheet is rolled up, can be of three basic types: chiral, zigzag and armchair SWNT. Depending on the chirality the SWNT can be either metallic or semiconducting. All armchair tubes are metallic, whereas 2/3 of the zigzag tubes are semiconducting. Bandstructure calculations show that MWNTs are of semimetallic nature [52].

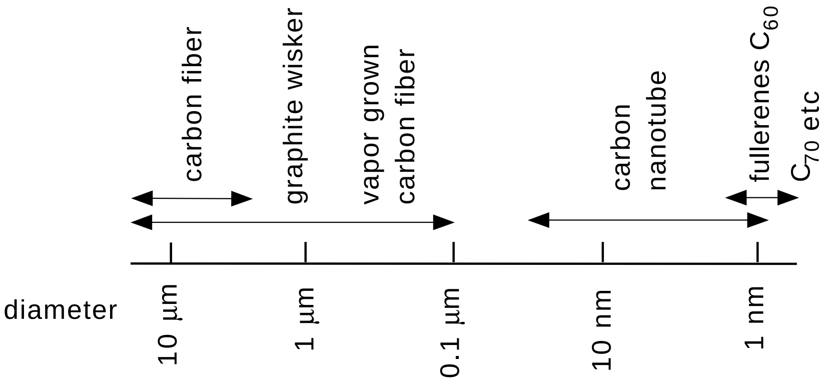

Figure 1.8: The size dependence of different graphite-based carbon types which can form high aspect ratio field enhancing structures (FES).

Synthesis of Carbon Nanotubes

Both fullerenes, MWNTs and SWNTs can be synthesized by *laser ablation* of a graphite target [32]. Especially high yields of SWNTs have been obtained by this method. Another method by which MWNTs and SWNTs can be produced is the *electric arc discharge* where a large arc-electric current of about 80 A is ignited between two carbon electrodes (gap $\sim$ 1 mm) in an atmosphere of typically 300 Torr He [32]. If metal catalysts are co-evaporated in the arc-discharge small yields of SWNT can be obtained. Finally in the *catalytic decomposition of hydrocarbons* methode, MWNT are catalytically synthesized on Fe, Ni or Co clusters in the presence of carbon-hydrogen containing gases like benzene, methane or acetylene. Contrary to the arc-discharge method the MWNTs thereby produced are not straight. Crucial point in this method lies in controlled production of MWNT with regard to length, diameter and alignment for application as field emitters. Li et al. have reported a method for producing aligned CNTs grown on silicates by using Co particles in meso-porous silica [53].

Why use carbon as field emitter ?

Curved structures with high aspect ratio are not only limited to carbon nanotubes but perhaps the most known examples of tubelike structures with diameters in the nanometer range are formed by asbestos minerals e.g. chrysotil, whose fibrous characteristics are determined by the tube structure of tetrahedron and octahedron layers [54]. However being silicates they are insulators. Layered compounds seem to be necessary for the formation of nanotube structures and in general all compounds possessing graphite-analogue layered structures should be able to form nanotubes or fullerene-type structures. MoS_2, WS_2 and their analogues of transition metal chalcogenides are the counterparts to graphite and C_{60} in carbon chemistry. This similarity can be easily understood based on their crystal structures. The Group 6 chalcogenides are layered materials with hexagonal symmetry similar to graphite and they possess the typical honeycomb structure of graphite. Other examples of layered compounds include vanadium oxide tubes [55] and boron-nitride (BN) nanotubes. Whereas silicates and BN tubes [57] are documented insulators, MoS_2, WS_2 [56] are expected to show a weak ionic conductivity along the tube axis. It is likely that the in-plane bonding of a two-atom type honeycomb lattice has a pronounced ionic character with localized electrons and poor in-plane conductivity. The strong sp^2 in-plane bonds of graphite with weakly localized p_z electrons provides an ideal compromise of conductivity, high chemical and mechanical stability which a two-atom type honeycomb lattice cannot provide.

We therefore summarize the unique properties which has made the graphite phase the ideal emitter material:

- The layered structure of graphite provides perfect building blocks for high aspect ratio structures like MWNT or graphite whiskers, which are necessary to create the high fields required to obtain low threshold electron emission.

- The graphite whiskers have the potential to be grown or deposited in a parallel process at low cost over large area substrates.

- Graphite has high or sufficiently high in-plane conductivity as a consequence of non-localized electrons. Carbon nanotubes have been reported to be able to carry currents up to 3 mA [58, 59].

- High mechanical and chemical stability. The strong covalent in-plane bonding network guarantees a structure which is less sensible to disruption due to ion bombardment and deformation due to migration of atoms during high field conditions.

References for chapter 1

[1] I. Brodie, C. Spindt, Advances in electronics and electron physics **83**, 1 (1992).

[2] J.E. Jaskie, MRS Bulletin **21**, 59 (1996).

[3] R.H. Fowler, L.W. Nordheim, Proc. Roy. Soc. London **A119**, 173 (1928).

[4] O. Gröning, "Field emission properties of carbon thin films and carbon nanotubes", Inaugural-Dissertation no **1258**, University of Fribourg (1999).

[5] R.W. Wood, Phys. Rev. Ser. I, **5**, 1 (1897).

[6] M.W. Geis, N.M. Elfremov, J.D. Woodhouse, M.D. McAleese, M. Marywka, D.G. Socker, J.F. Hochedez, IEEE Trans. ED. Lett. **12**, 456 (1991).

[7] C.Wang, A.Garcia, D.C. Ingram, M. Lake, M.E. Kordesch, Electron. Lett. **27**, 1459 (1991).

[8] Heer W.A, Châtelain A., Ugarte D., Science, **270**, 1179 (1995).

[9] Yu.V. Gulyaev, L.A. Chernozatonskii, Z.Ja. Kosakovskaja, N.I. Sinitsyn, G.V. Torgashov, Yu. F. Zakharchenko, J. Vac. Sci. technol. B, **13(2)**, 435 (1995).

[10] J.-M. Bonard, J.P. Salvetat, T. Stöckli, W.A de Heer, L. Forró, A. Châtelain, Appl. Phys. Lett. **73**, 918 (1996).

[11] R. Gomer, Field emission and field ionization American Institute of Physics (1993).

[12] O.Gröning, O.M. Küttel, P.Gröning and L.Schlapbach, J. Vac. Sci. Techol. **B17**, 1064 (1999).

[13] R.L. Fink, Z. Tolt, Z. Yaniv, Surface and Coatings **108-109**, 570 (1998).

[14] www.stanfordresources.com

[15] D. Temple, Mater. Sci. Eng. **R24**, 185 (1999).

[16] P.R. Schwoebl, I. Brodie, J. Vac. Sci. Technol. **B13**, 4, 1391 (1995).

[17] A. Dino, E. Ghassan, E. Jabbour, N. Peyghambarian, Advanced Materials **12**, 1249 (2000).

[18] M. T. Bernius, M. Inbasekaran, J. O'brien, W. Wu, Advanced Materials **12**, 1737 (2000).

[19] B. Cominskey, J.D. Albert, H. Yoshizawa, J. Jacobson, Nature **394**, 253 (1998).

[20] www.eink.com

[21] B. R. Chalamala, Yi Wei, B. E. Gnade, IEEE Spectrum **April**, 43 (1998).

[22] www.pixtech.com

[23] M.W. Geis, J.C.Twichell and T.M. Lyszcyarz, J. Vac. Sci. Technol. **B14**, 2060 (1996).

[24] J. van der Weide, Z. Zhang, P.K. Baumann, M.G. Wensell, J. Bernholc, R.J. Nemanich, Phys. Rev. B, **50**, 5803 (1994).

[25] L. Diederich, Negative electron affinity of hydrogen-terminated diamond surfaces studied by photoelectron spectroscopy, Thesis no **1210**, University of Fribourg (1998).

[26] R.L.Bell, Negative electron affinity devices, Clarendon press, Oxford (1973).

[27] F.J. Himpsel, J.A. Knapp, J.A. VanFechte, D.E. Eastman, Phys. Rev. B **20**, 624 (1979).

[28] J. Robertson, Mat. Res. Soc. Symp. Proc. Vol. **509**, 83 (1998).

[29] S.P. Bozeman, P.K. Baumann, B.L. Ward, M.J. Powers, J.J. Cuomo, R.J. Nemanich, D.L. Dreifuss, Diamond and Rel. Mat. **5**, 802 (1996).

[30] O.Gröning, O.M. Küttel, P.Gröning and L.Schlapbach, Appl. Surf. Sci. **111** 135 (1997).

[31] F.Lacher, C.Wild, D.Behr, P.Koidl, Diamond and Rel. Mat.**6**, 1111 (1997).

[32] K. Tanaka, T. Yamabe, K. Fukui, The Science and Technology of Carbon Nanotubes, Elsevier (1999).

[33] Carbon Nanotubes preparation and properties, Ed. T.W. Ebbesen, CRC Press (1997).

[34] B.B Pate, Surface Science **165**, 83-142 (1986).

[35] P.W. Bridgeman, Scientific American, November, **42** (1955).

[36] F.P. Bundy, H.P. Bovenkerk, H.M. Strong, R.H. Wentorf, Journ. of Chem. Phys. **35**, 383 (1961).

[37] E. Maillard-Schaller, Study of the interface between highly oriented diamond and silicon, Thesis no **1145**, University of Fribourg (1996).

[38] N. Setka, J. Mater. Res. **4**, 664 (1989).

[39] N. Othake, M. Yoshikawa, J. Electrochem. Soc. **137**, 717 (1990).

[40] K.E. Spear, J. Am. Ceram. Soc. **72**, 171 (1989).

[41] C. Kittel, *Physique de l'Etat Solide*, 5e Edition, ed. Dunod (1983).

[42] J.H. Weaver, D.M. Poirier in *Solid State Physics, Advances in Research and Applications*, ed. H. Ehrenreich and F. Spaepen, Academic Press, 2 (1994).

[43] A. Beiser, Atome, Moleküle, Festkörper, Vieweg (1983).

[44] S. Koizumi, M. Kamo, Y. Saito, S. Mita, A. Sawabe, C. Uzan-Saguy, A. Reznik, R. Kalish, Diam. Rel. Mat., **7**, 540 (1998).

[45] M.S. Dresselhaus, G. Dresselhaus, P.C. Eklund, Science of Fullerenes and Carbon Nanotubes, Academic Press (1995).

[46] S.Aisenberg, R.Chabot, Jour. Appl. Phys. **42**, 2953 (1971).

[47] D.R.McKenzie, Rep. Prog. Phys. **59**, 1611 (1996).

[48] *Amorphous Carbon: State of the Art*, Ed. S.R.P. Silva, J. Robertsson, W. I. Milne, G.A.J. Amaratunga, World Scientific (1997).

[49] H.W. Kroto, J.R Heath, S.C.O'Brien, R.F. Curl, R.E. Smally, Nature **318**, 162 (1985).

[50] M. Endo, S. Iijima, M.S. Dresselhaus, *Carbon Nanotubes*, Pergamon (1996).

[51] T.W.Ebbesen, P.M. Ajayan, Nature **358**, 220 (1992).

[52] J.C. Charlier, J.P. Michenaud, Phys. Rev. Lett. **70**, 1858 (1993).

[53] J.Li, C. Papadopoulos, J. M. Xu, M. Moskovits, Appl. Phys. Lett. **75**, 367 (1999).

[54] W. Tremel, Angew. Chem. Int. Ed. **15**, 2175 (1999).

[55] P.M. Ajayan, O. Stephan, Ph. Redlich, C. Colliex, Nature **375**, 564 (1995).

[56] G.L. Frey, S. Elani, M. Homoyonfer, Y. Feldman, R. Tenne, Phys. Rev. B **57**, 6666 (1998).

[57] X. Blase, A. Rubio, S.G. Louie, M.L. Cohen, Europhysics Lett. **28**, 335 (1994)

[58] P.J. de Pablo, E. Graugnard, B. Walsh, R.P. Andres, S. Datta, R. Reifenberger, Appl. Phys. Lett. **74**, 323 (1999).

[59] S. Frank, P. Poncharal, Z.L. Wang, W.A. de Heer, Science **280**, 1744 (1998).

Chapter 2

The carbon thin film electron emitter

2.1 Properties of the carbon thin film electron emitter

Description of the emission from an emitter ensemble

Whereas a single carbon emitter can be said to be completely characterized in terms of its workfunction (ϕ), pre-exponential factor (A), contact resistance (R), local field (E_s) and field enhancement (β) according to equation 1.2 and 1.3, the description of the overall emission behavior from a thin film emitter ensemble requires a statistical approach. The number of degrees of freedom with regard to geometrical alignment, orientation and inter-emitter distances within the thin film emitter ensemble is much larger than for the single site emitter. It can also be expected that R, ϕ and A exhibit some variation. Electrostatic screening have to be taken into account for a thin film emitter, since the presence of a large number of emitters may affect the local electric field E_s at the emission sites (electrostatic screening), see section 2.3. The emission properties can therefore vary considerably from one position to another within the emitter ensemble.

An example of a thin film emitter with a large scatter in the spatial emission current I(x,y) is shown in Fig 2.1(a), where parts of the surface show no emission at all. The scatter in geometrical field enhancement, workfunction, pre-exponential factor A, contact resistances R and electrostatic screening effects are here responsible for the variation. The scatter in the I(x,y) map is highly undesirable, because the device performance with regard to brightness homogeneity is largely reduced. In order to understand and improve the emission homogeneity a quantitative description of the I(x,y) map in terms of β, R, ϕ and A is needed.

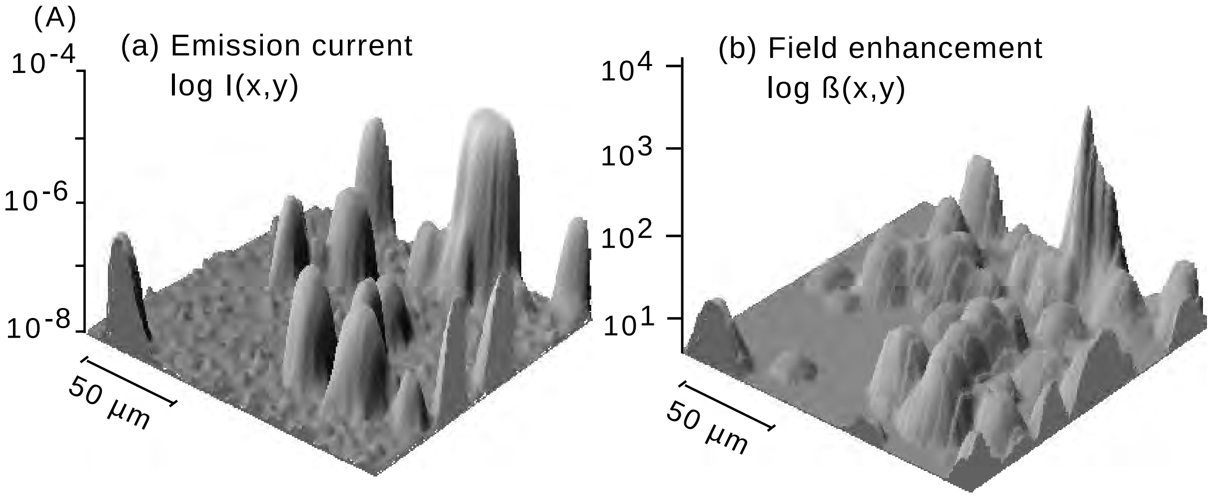

Figure 2.1: The spatial variation (a) of the emission current I(x,y) under a constant applied voltage of 320 Volts (tip-cathode distance ~ 7 μm) can be explained by the local variation (b) of the spatial field enhancement β(x,y). The I(x,y) and the β(x,y) maps were determined by two independent field emission scans, were the β(x,y) map was deduced from the voltage V(x,y) map according equation 2.1 under the constant emission current 50 nA.

As will be seen in Chapter 3 a small time dependent local anisotropy of ϕ is expected on each emitter, but this variation plays a minor role for the overall thin film emission, see paragraph 2.4.2. Based on the observations of the field emitted electron energy distributions from several carbon based compounds it seems safe to assume a constant workfunction ϕ, approximately 5 eV for every emitting site [1].

Since every emitter is made of the same material, preferably the sp^2 phase, it can be safely assumed that the pre-exponential factor A does not show a large scatter but can be assigned a constant value in the range 10^{-11}-10^{-9} cm^2 for all sites of the emitter ensemble. The contact resistances R between each emitter and the thin film substrate can show a large scatter. For a quantitative description of the emission current we are however forced to assume a constant value of R. It should be pointed out that the effect of R upon the emitted current is negligible for low emission currents. By setting A, ϕ and R constant, the emission current from each site of the emitter ensemble is determined by the local field enhancement β according to the modified Fowler-Nordheim equation 1.2 and equation 1.3. It thus appears that the emitting properties I(x,y) to a good approximation can be described in terms of the local field enhancement. If we therefore assign the spatial co-ordinates (x_i,y_i) to emitter number i with local field enhancement β_i, the spatial field enhancement can be written as $\beta_i(x_i, y_i)$. Normally we omit the subscript and simply write β(x,y). This means that the description of the local emission current I(x,y) theoretically can be reduced to the measurement of h(x,y), r(x,y) and α(x,y) according to equation 1.3. Even if one could assume constant values of r(x,y)= r and α(x,y)= α, the exact measurement of large aspect ratio asperities h(x,y) is very difficult.

Fortunately the spatial distribution of the field enhancement β(x,y) can be directly determined by using *in-situ* scanning anode FE measurements where the emission current is maintained on a constant level. Such a β(x,y) map corresponding to the same thin film emitter area where the I(x,y) emission current map was recorded, is shown in Fig. 2.1(b). Even if the borders of the two independently determined emission maps do not exactly coincide, one immediately realizes the current spatial dependency upon the local field enhancement. Locally large emission currents are correlated to large local field enhancement and vice versa. The characterization of the thin film electron emitter must thus include a determination of the spatial field enhancement β(x,y) and the single site emission properties.

Thin film electron emitters are however often characterized in terms of a "threshold" field E_{thr} required to produce a "threshold" current density in a typical large anode diode type FE experiment. Such characterizations can be misleading since a cathode with a spatial extension in the mm^2-range may contain a small number, sometimes only one, of strong emitters with exceptionally high field enhancement and thus can have a low E_{thr}. These strong emitters appear very seldom on most thin film emitter surfaces and can only with a great deal of luck be pin-pointed in a 200×200 μm^2 window. An example of a such a strong ($\beta \sim 1500$) accidentally spotted emitter is seen in the right upper part of Fig. 2.1(b). In analogy to the single site emitter one may therefore be lead to think that a low E_{thr} is the premium quality of a thin film emitter. A low E_{thr} is advantageous but is no guarantee that the thin film emission is homogeneous as indicated in Fig. 2.1(a). Other standards to describe a "good" thin film emitter are thus needed. In contrast to E_{thr}, $\beta(x,y)$ offers a unique description of the thin film emitting properties under a wide variety of experimental conditions. Such a description is indispensable in order to optimize the cold cathode device performance.

Scanning anode field emission microscopy

In order to investigate the thin film emission properties with high lateral resolution a scanning anode field emission microscope (SAFEM) was developed, see Fig. 2.2. The SAFEM is the method of choice for FE investigations in contrast to non-microscopic techniques like photoelectron spectroscopy which do not take a variation in the properties of the individual emitters into account.

Figure 2.2: The scanning anode field emission microscope (SAFEM) is part of a vacuum field emission apparatus which incorporates a field emission microscope (FEM).

The SAFEM is based on a micrometer-sized tip which serves as an anode. By recording the emission as a function of the spatial position of the tip above the thin film emitter, FE maps (or scans) with micrometer resolution can be obtained. Such maps are normally extending from 100×100 μm^2 up to 1000×1000

μm^2.

The SAFEM can be operated in one of two possible modes. In the first mode the emission current is recorded for a constant applied voltage. This mode is called the constant voltage mode (CVM). The I(x,y) map obtained in the CVM is the analogue to the electron emission on a phosphor screen, albeit with higher resolution. The term CVM is therefore also used for electron emission with phosphor screens.

In the second mode of operation the emission current is maintained on a constant level for every tip position along the FE scan and the voltage applied to the tip must therefore be adjusted according to the individual emitter efficiency. Since the spatially recorded emission voltage V(x,y) is determined for a constant emission current this mode is called the constant current mode (CCM). The CCM opens interesting possibilities to describe the spatially resolved field enhancement β(x,y). If the potential distribution between the tip and the cathode is assumed homogeneous, the spatial field enhancement can be approximately determined using equation 1.3 for a constant emission current according to

$$\beta(x,y) = \frac{d \cdot E_s}{V(x,y)} \tag{2.1}$$

where E$_s$ [Vμm^{-1}] is the local electric field at the emission site for a constant emission current and d [μm] is the typical tip-cathode distance. Energy resolved FE measurements from thin emitting films have shown, that an emission current of 50 nA approximately corresponds to an electric field E$_s$= 4000 Vμm^{-1} at the tip apex of the emitting structure [1]. The β(x,y) map in Fig. 2.1(b) was derived using equation 2.1 with E$_s$= 4000 Vμm^{-1}.

The β-distribution

It is natural to assume that the field enhancing landscape β(x,y) may vary from one type of thin film emitter sample to another. Different samples can be more or less rough. In addition it seems logical that if the roughness is determined in a small window on a sample, there is no immediate reason to expect the same roughness in an equally sized window chosen elsewhere on the same sample surface. This underlines the need for a statistical approach in the treatment of the thin film emitter characteristics. We therefore define a distribution f(β) of the field enhancement

$$dN = f(\beta)d\beta \qquad\qquad f(\beta): \quad \beta - distribution \qquad (2.2)$$

where dN is the number of emitting sites with field enhancement β in the small range β to β+dβ per unit area of the sample surface. f(β) can be seen as a probability distribution since the number of sites dN is proportional to their probability of existence on a unit area. Clearly, since the β-distribution f(β) is defined per unit area [cm^{-2}], the probability of encountering an emission site with a high field enhancement value is approximately proportional to the sample area up to a critical area limit. This means that the measurement of the electric threshold field E$_{thr}$ at which a threshold current density limit is reached, depends both on the spatial position as well as the size of the anode, as long as the anode size not is larger than the critical area limit. In contrast to the threshold field, f(β) is an unequivocal figure of merit for every thin film electron emitter. f(β) defines not only E$_{thr}$ statistically through the sites of the highest field enhancement but more importantly the emission homogeneity and current density. The emitting site density (ESD) is calculated from f(β) according to

$$ESD(E_a) = \int_{\beta_{min}=\frac{E_t}{E_a}}^{\infty} f(\beta)\, d\beta \qquad\qquad [cm^{-2}] \qquad (2.3)$$

E$_t$ is the local field at an emission site required to produce a minimum recordable emission current I$_t$. On a phosphor screen I$_t$ corresponds to the minimum emission site current, required for the eye to observe the emission spot. β_{min} corresponds to the lowest field enhancement value which can be detected at an applied field E$_a$, with regard to I$_t$.

The emission current density is calculated in a similar manner

$$J(E_a) = \int_0^{\infty} f(\beta) \cdot I(\beta, E_a)\, d\beta \qquad\qquad [A/cm^{-2}] \qquad (2.4)$$

I(β, E$_a$) is the emission current from the sites in the range β to β+dβ when the applied field is E$_a$.

We conclude that any standards of characterization of thin film electron emitters must include the β-distribution and knowledge of the spatial emitting properties. f(β) and β(x,y) can be said to give a complete description of the collective emitting behavior of thin electron emitting films. The following sections will therefore focus on how to measure f(β) and β(x,y) using mainly scanning anode field emission microscopy.

References for 2.1

[1] O. Gröning, "Field emission properties of carbon thin films and carbon nanotubes", Inaugural-Dissertation no **1258**, University of Fribourg (1999).

2.2 Microscopic characterization of electron field emission

L. Nilsson, O. Groening, O. Kuettel P. Groening and L. Schlapbach
Institute of Physics, University of Fribourg, Pérolles, CH-1700 Fribourg, Switzerland

Submitted to Journal of Vacuum Science and Technology B (2001)

Abstract

We report on the functional capabilities of a scanning anode field emission microscope (SAFEM) which combined with a phosphor screen is used to investigate and correlate individual electron emission site characteristics of low threshold thin film electron emitters in the μm regime. Spatially recorded extraction voltage V(x,y) maps under constant emission current or emission current I(x,y) maps under constant anode voltage reveal spatially divergent emission properties on thin film emitters. The V(x,y) maps are used to derive the field enhancement β(x,y) maps which gives a better description of the thin film emission properties as compared to electric threshold fields which depends on anode-cathode geometry. Individual emission site current stability of thin film emitters can be investigated with the SAFEM, and a high resolution field emission microscope to investigate the environmental stability of single carbon nanotubes mounted on filaments as a function of partial gas pressures and temperature.

2.2.1 Introduction

Higher demands for low power portable electronic equipment has been a driving force during the last 20 years for extensive research efforts in the field of vacuum microelectronic devices [1]. Such devices make use of miniaturized electron field emission (FE) sources (also called cold cathodes) [2,3]. Contrary to conventional thermionic cathodes, traditional field emission cathodes make use of very high electric fields ($\sim 2{-}3000 V/\mu$m), in order to extract the electrons from a solid into the vacuum [4]. Due to the high electric field, the surface potential step which confines the electrons to the solid, is lowered and becomes a triangular shaped potential barrier. As the width of the surface potential barrier approaches 2 nm, electrons will tunnel from the highest occupied states in the solid into vacuum. This process is also referred to as Fowler-Nordheim (F-N) tunneling. In order to create fields sufficiently high, tip-like structures in the μm range are used to enhance the applied field, wherefore these are called field enhancing structures (FES). To a first approximation the FES amplify the applied field by a factor β of the order h/r, where h is the height of the tip and r the radius of curvature of the tip apex.

The production of such μm-sized tips requires expensive lithographic processes. The metal tips can suffer from emission degradation due to current runaway caused by sputter erosion and chemical contamination and hence require a high vacuum environment for operation [1]. There is thus a strong incentive to simplify both the design and production of the μm sized electron emitters over large areas in vacuum microelectronics.

During the last decade different forms of chemical vapor deposited (CVD) diamond, diamond like carbon (DLC), tetrahedral amorphous carbon (ta-C) etc. emerged as possible cold cathode candidates due to reports of extraordinary low electric threshold FE properties [5, 6, 8, 9]. It was believed that the reason for the enhanced FE was connected with the electronic properties rather than the FES of the films [10].

A thin film emitter which has not to rely on FES, with spatially homogeneous emission at applied fields below 10 V/μm could mean completely sputter insensitive, efficient and low cost cold cathodes. From a technological point of view this was very promising due to the fact that the incorporation of such materials in gated structures like FEAs, could be done easily over large areas at low cost using standard CVD techniques. As a consequence several attempts have been made and are underway to replace conventional metal microtips with a wide range of different carbon thin film cathodes, including carbon nanotube (CNT) thin film emitters [11]. Whereas the electron emission from CNTs clearly is governed by geometric field enhancement, the emission mechanism of DLC and CVD diamond films is still under dispute. An important reason for that resides in the lack of experimental standards and general descriptions of the emission from thin film emitters under a wide range of experimental conditions. It is well known from experiments with phosphor screens that the low-threshold carbon thin-film emission in fact not is homogeneous but originate from isolated spots. This sole fact indicates the need to investigate the FE on a microscopic level, and consequently several groups have chosen to adopt some kind of scanning tunneling (STM) or atomic force microscopy (AFM) in field emission mode. STM and AFM seem in the first place well adapted for FE investigations but there are some fundamental problems. In order to obtain FE, tip-like structures on the surface are needed to create field enhancement. For the principle of field amplification to work the distance between the anode and the FES must not be smaller than the typical size of the FES. We believe that the emitting regions on the DLC films in fact are not perfectly smooth on a sub-μm level, which in analogy to the CNT films would explain why it is hard to distinguish between contact and emission currents in close range AFM/STM "FE" measurements of emitting regions on DLC films.

In order to measure low threshold emission, we therefore have to ascertain that the typical electrostatic conditions with high field enhancement at the emission site are fulfilled and that the minimum anode-cathode distance is larger than the typical size of the FES. In the case of a CNT thin film this would mean a anode-cathode distance of at least several μm as given by the topography. As a consequence we developed a scanning anode field emission microscope (SAFEM) with a typical anode-cathode separation of several μm. We thereby can measure individual emission site current-voltage (I-V) or current-time (I-t) characteristics and obtain statistical data on the spatially or time dependent FE behavior of thin film emitters. Combined with FE measurements done with a phosphor screen the SAFEM gives a better characterization of thin film emitters as compared to FE measurements from large cathode areas.

With regard to the size of the anode and the typical anode-cathode distance we differentiate between microscopically and macroscopically recorded FE data, where the former is recorded on a μm length scale with a μm-sized anode and the latter on a mm-sized (or more) length scale with a mm-sized (or more) anode. We also call macroscopically recorded FE, integrated FE since the integral behavior of a large number of emission sites on a thin film are measured in parallel. This paper is a report on the performance and technical characteristics of the SAFEM and FEM systems illustrated with some selected measurement examples.

2.2.2 Three stages of FE investigations

In order to work efficiently and without loss of time the field emission characterization can be done in three partly independent stages:

- *Rapid sampling of the thin film emitter with the phosphor screen.*

  (This gives an early and fast indication of the overall emitting properties.)

- *High resolution SAFEM characterization.*

  (Detailed information about single emitting sites on a thin-film emitter can be obtained at micrometer resolution.)

- *FEM characterization of individual emitters.*

  (Investigations of emitter environmental stability.)

- *Rapid sampling of the thin film emitter with the phosphor screen*

In the first stage stage we perform rapid sampling of the thin film emitter using a phosphor screen. This gives fast and first qualitative information about the emitting site density (ESD), which is an important criteria of quality for a thin film emitter. Based on these preliminary investigations it can be judged whether a sample is worth further investigations or not. We are of natural reasons mainly interested in films with a high density which emit homogeneously at low applied fields. The rapid sampling with the phosphor screen is however limited by the resolution. For an ESD over 10^4 cm^{-2} the emission spots on the screen starts to overlap. Furthermore the current from the strongest sites may rise several orders above the weakest sites which can lead to emitter disruptions and arcing. Due to these limitations we normally proceed to the second stage with the more time consuming SAFEM characterizations (if the thin film sample has a high ESD and a low electric threshold).

- *High resolution SAFEM characterization*

The SAFEM enhances the spatial resolution as compared to the phosphor screen. The ESD can be measured at higher fields but again emitter disruption is a problem. This problem can easily be solved using a constant emission current mode during FE scanning. The voltage is thereby adjusted as a function of tip position in order to maintain a constant level of the emission current. Such measurements allows a determination of the spatially resolved field enhancement β(x,y) and single site emitter disruption current levels. Furthermore the emission current of single sites can be correlated to the respectively field enhancement factors. A wide spectrum of single site emission characterizations is open with the analytical capabilities of the SAFEM. The resolution of the SAFEM is however insufficient for investigations of certain events taking place at the emitter tip apex. Higher spatial resolution and magnification is therefore provided by field emission microscopy performed on single CNTs.

- *FEM characterization of individual emitters*

FEM patterns are used to investigate the spatial density of states at the CNT emitter tip apex at high almost atomic resolution. Such investigations can be used to investigate the origin of the emission current instabilities and the effects of adsorbates. The emission current environmental stability can be investigated as a function of different gases in the vacuum chamber background and of the emitter temperature.

2.2.3 Experimental equipment

The three stages of FE investigations can be accomplished in three measurement set-up's integrated into one a ultra-high vacuum chamber which consists of two independent measurement stations.

The first measurement station contains a phosphor screen which can be used either to investigate emission from thin film emitters or from single CNTs pasted to a heating filament. The latter is the field emission microscope (FEM). Through a view window images of the phosphor screen can be taken at different magnification using a charge coupled device (CCD) camera.

The second measurement station contains the scanning anode field emission microscope SAFEM with which spatially resolved FE characterization of thin film electron emitters is performed. The measurement stations are moved in and out of the chamber from below via two parallel sliding rails ensuring easy and fast action of sample changing/manipulation. For thin film emitter investigations with either the phosphor screen or the SAFEM a base pressure in the range of 10^{-8} mbar is sufficient and we then use viton sealings for rapid look-in/out of the samples. When the *environmental stability* of single CNTs is investigated in the FEM, copper sealings must be used to reach a pressure of 10^{-10} mbar. The whole system of fourway crosses, pump, measurement stations and CCD camera is suspended with rubber bearings to reduce the effects of vibrations.

The first measurement station hosts two experimental set-up's using cathodoluminescent screens to monitor the FE behavior of single or thin film electron emitters (Fig. 2.3). We usually use phosphor coated screens (1), but have also tried YAG and Indium Tin Oxide (ITO) screens, were the latter is well suited for samples which require high applied fields. The emission patterns on the screens are recorded with a CCD camera and a zoom-lens and the images are transferred to the PC with a framegrabber card. The sample (2) is mounted onto a table (3) which is movable in the z direction and connected via a piston (8) through a feedthrough to a micrometer screw. The distance d between the sample and the screen can therefore be adjusted with about 10 μm resolution without spacers. This is advantageous because artifacts due to spacer leakage currents can be avoided. The ESD can also be recorded as a function of the applied field E_a using a constant driving voltage. The voltage dependent sensitivity of the phosphor screen does therefore not influence the ESD. However care has to be taken to ensure a backlash-free motion of the table. We have solved this by using stainless steel springs (7).

In order to ascertain that the screen and the thin film emitter surface are parallel over a cm-sized area, the screen can be tilted using three screws (5). The

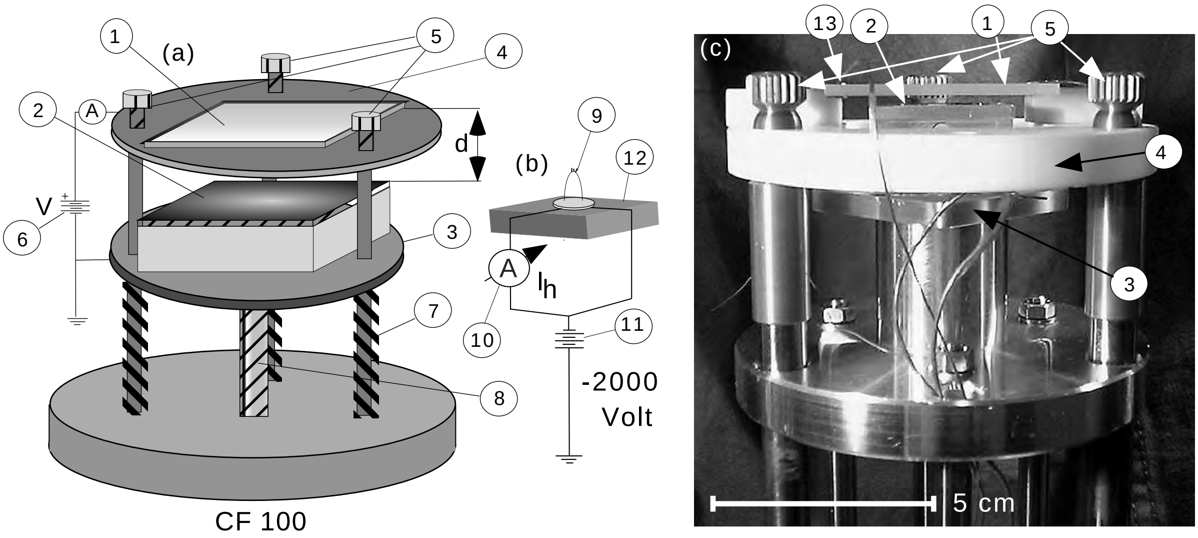

Figure 2.3: (a) Schematic sketch of the FE equipment for integral measurements using a phosphor screen with a thin film emitter mounted to the sample holder. (b) Sample holder with heating filament for field emission microscopy. (c) Close-up of the screen and the thin film sample holder. (1) phosphor screen (2) thin film emitter (3) table for the sample holder (4) insulating teflon support for the screen (5) adjustment screws to tilt the screen in order to make the screen and sample parallel (6) high voltage supply (7) stainless steel spring (8) micrometer screw (9) carbon nanotubes pasted to filament (10) transformator and current meter (11) high voltage supply (12) teflon support (13) electric connector to the screen.

sample is grounded in the case of a thin film emitter and the voltage (typically 2-3 kV) is applied with a high voltage (6) supply to the screen which is suspended with a teflon insulation (4).

Fig. 2.3(b) shows schematically the set-up for the FEM experiment. When FEM is performed the screen is grounded and a negative voltage of 2000 V is applied to the filament (9) delivered by AGAR Scientific Ltd. (type A054). The source-measure unit Keithley 237 is connected to the screen (13) to record emission current fluctuations. An insulated AC-voltage source (10) enables us to run currents I_h up to 3 A through the filament and observe FEM images of CNTs, pasted to the filament with conductive carbon cement, in-situ during heating. The CNTs are usually heated up to 1200 K. We can additionally perform FEM in the presence of different partial gas pressures like O_2, H_2O, H_2 etc.

The second measurement station contains the scanning anode field emission

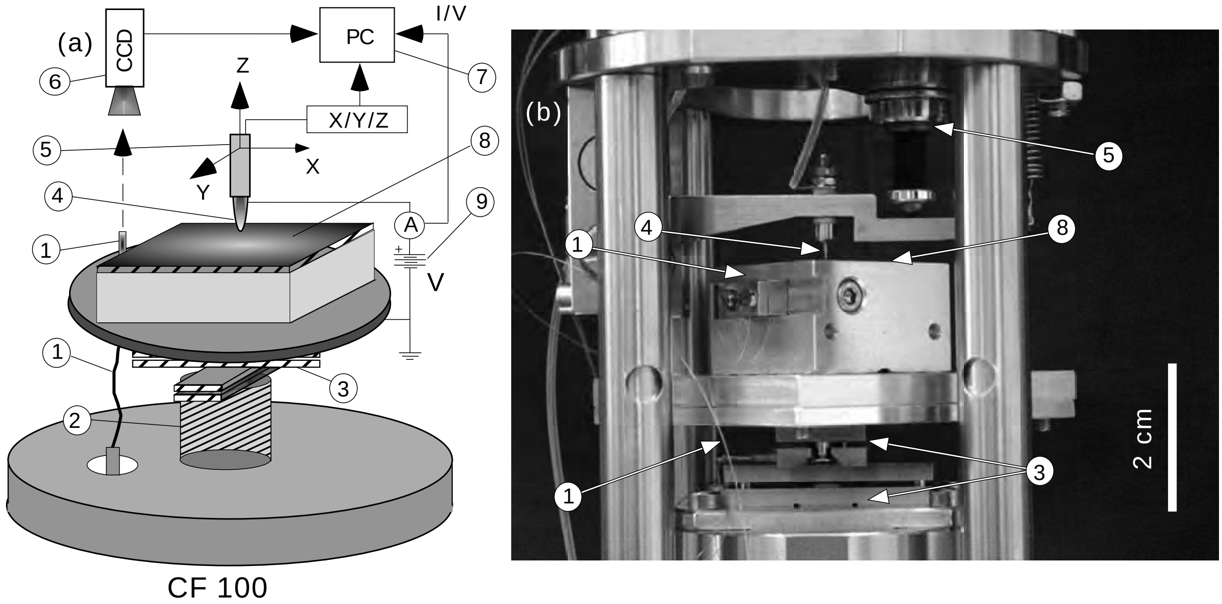

Figure 2.4: (a) Schematic sketch of the scanning anode field emission microscope. (b) Close-up of the sample holder and the micro positioner. (1) optic fiber (2) coarse adjustment screw to approach the sample to the anode (3) x/y micro positioner MS5 (4) Pt/Ir anode tip (5) z pico motor (6) CCD camera to monitor x/y translation (7) computer control with LabView (8) thin film sample (9) Keithley source measure unit

microscope (SAFEM) and consists essentially of the following parts (Fig. 2.4). The x-y motion of the sample is realized using two UHV compatible ”piezo” (3) micro positioner (micro slides MS 5 from Omicron). The MS 5 is a linear step motor driven by piezo elements with step sizes between 40 to 400 nm and with 5 mm maximum travel. The thin film emitter is mounted onto a grounded sample holder (8) attached on top of the MS 5 motors. The position of the sample is measured by tracking a light source (1) created by an optic fiber (1) which is feed into the chamber through a home-made feedthrough. The tracking is done by a 8 bit gray-scale CCD camera (6) with sub-μm resolution in x and y direction. The FE current I under constant applied voltage (Constant Voltage Mode - CVM) or the extraction voltage V under constant emission current (Constant Current Mode - CCM) can then be recorded as a function of anode tip (4) position for thin film areas up to 5×5 mm^2 with sub-μm re-positioning resolution. We usually work with voltages in the range 60 - 500 Volts in the CVM and typical emission currents in the range 10 - 50 nA per emission site in the CCM. The distance d takes generally a value between 5 to 15 μm depending on the size of the scanned area. The emission is recorded with a Keithley 237 source measure unit (9) where the level of noise is lower than 1 nA.

The absolute position measurement enables us to re-find an arbitrary emitting site and to correlate several current I(x,y) or voltage V(x,y) maps. The size of the FE maps is generally between 200×200 μm^2 to 800×800 μm^2. We use a Pt/Ir anode tip (4) from DME (type 1744) which is originally intended for use in scanning tunneling microscopy (STM) and has a radius of curvature less than 1 μm. The typical radius of curvature is however about 1 μm after a number of FE scans, since the tip is gently moved into electrical contact (z step size about 50 nm) with the sample surface to check anode-sample distance d. The anode-sample distance d is held constant during FE scanning (not STM mode) and is controlled by a backlash free single axis UHV picomotor (5), model NFUHV from Surface Interface Inc. The resolution of the FE maps is limited to about the anode-cathode separation due to the convolution of the sample topography, sample-anode distance d and anode radius of curvature.

2.2.4 Rapid sampling of the thin film emitter with the phosphor screen

For accurate measurements of the emission current density as a function of the applied field the screen can be replaced by a guard ring anode. The 2 mm cylindric anode with a guard ring is shown in the inset (c) of Fig. 2.5. The inset (c) also shows an electrostatic simulation of the equipotential lines created by the system of the central anode and the surrounding guard ring. The same voltage V is applied to the outer and inner anode of area A [cm^2]. The current density J= I/A can then be recorded for a homogeneous applied field E= V/d, where d= 50 μm is the anode-cathode distance and I is the current of the inner anode, without disturbing electrostatic effects from the edges of the central anode (inhomogeneous applied field).

The resulting J-E curve is shown in (a) and inset (b) clearly shows the typical Fowler-Nordheim behavior in the low emission current region. This kind of measurement yields only limited characterization of the FE properties. J-E or I-V characteristics give no information about the ESD and we therefore need to

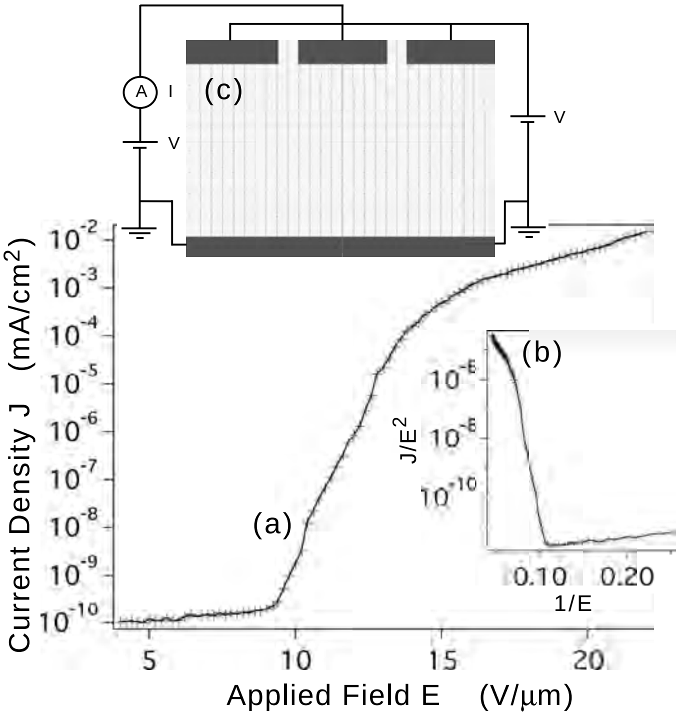

Figure 2.5: (a) Current density J as a function of the applied field E for a carbon based thin film emitter. (b) The corresponding Fowler-Nordheim plot. (c) The geometry with a center anode (for which the current was recorded) and the surrounding guard ring to obtain a homogeneous applied field.

---

monitor the spatial distribution and the ESD of the electron emission.

In the *first stage* of the FE characterization the phosphor screen gives fast and valuable information about the spatial distribution of emission from the thin film emitter. Thereby attention should be paid to the calibration of the screen sensitivity. The sensitivity of the screen is voltage dependent and may vary between different types of cathodoluminescent coatings. The cathodoluminescence depends also on the emitted current density, wherefore the ESD is a function of the emitted current per site and the driving voltage. As a consequence it can be advantageous to use different types of screens depending on the electron emission efficiency of a particular thin film emitter sample. The dependence of the ESD as a function of the driving voltage is shown in Fig. 2.6 for a constant applied field. Some thin film emitters may sometimes require high fields for electron emission and Indium Tin Oxide (ITO) screens can be a better option than phosphor screens in these cases, since too high electron energies soon degrades the performance of the phosphor. Hence during ESD experiments attention has to be paid to use a voltage range well adapted to the screen sensitivity. A driving voltage higher than 1 kV seems reasonable for our high voltage phosphor screen, as indicated by the saturation of the ESD in Fig. 2.6(a).

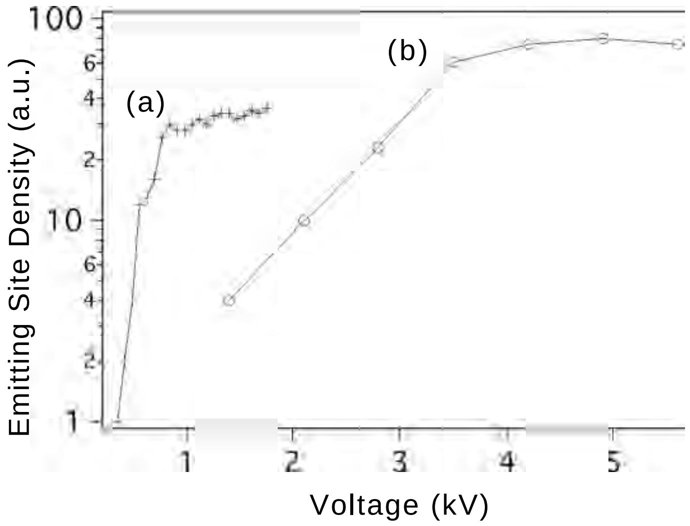

Figure 2.6: The ESD measured as a function of the voltage applied to the phosphor (a) screen and to the ITO screen (b) for constant applied fields. The thin film emitter used in (b) requires a higher field (7 V/μm) than the film (2.8 V/μm) used in (a) in order to record an ESD.

After a careful calibration of the screen, where the operating voltage is determined, the ESD can be recorded as a function of the applied field E for a constant driving voltage. An example of how the screen can look like during typical FE conditions is shown in the inset of Fig. 2.25. The screen shows the typical spot-wise electron emission from a carbon nanotube (CNT) film, catalytically grown in a methane/hydrogen atmosphere. The ESD as a function of the applied field E is shown in the upper right inset of Fig. 2.7.

We have investigated a numerous types of films like chemical vapor deposited (CVD) diamond, dimondlike carbon (DLC) and tetrahedral amorphous carbon (ta-C) with various contents of defects and dopant levels of hydrogen and nitrogen. In all cases so far observed the emission always originated from isolated spots similar to the inset of Fig. 2.7 but in general with a lower density. The emission sometimes only consisted of some few (1-10) irregular distributed spots for a cm^2-sized thin film emitter area (typically for DLC or ta-C films). Whereas the emission mechanism of DLC and ta-C still is under dispute, the emission from CNT films clearly is governed by geometric field enhancement β. The CNTs obey a statistical variation with regard to positions and field enhancement on the sample surface. The variation in the field enhancement is responsible for the variation in the ESD from thin electron emitting films.

If dN= f(β)·dβ is the number of emitting sites in the field enhancement range [β, β+dβ] per unit area where f(β) is the so called β-distribution, we can calculate f(β) from the ESD-E characteristics [12]. We note that f(β) gives a better description of the emitting properties of a thin film than turn-on fields or I-V characteristics, since these in general depends on how the measurement is done, the size of the measured area etc. A detailed discussion about f(β) is beyond the scope of this paper and the interested reader is referenced to [12].

In order to investigate ESDs higher than 10^4 emitters/cm^2 and f(β) in the low field enhancement regime (in this case below 400), scanning anode field emission microscopy has to be performed.

2.2.5 High resolution SAFEM characterization

2.2.5.1 Considerations on the sample position

During FE scanning the sample is moved in x and y directions. The absolute position measurement is done by tracking the light source attached to the sample holder using a CCD camera. The x and y axis are thus defined by the CCD camera pixel array and have to be aligned with the directions of the piezo step motors. The x/y scanning system has therefore to be calibrated to avoid lateral run-out or deviation $\triangle Y_{tot}$ perpendicular to the x-direction of translation. $\triangle Y_{tot}$ is usually less than 1 μm per 200 μm travel in x direction.

The lens is set to the highest magnification in order to have the best possible resolution per CCD pixel. We pay attention to adjust the diaphragm of the lens for the recorded light source to have a well defined circular shape without fringe- or "star-like-shape" effects. With the framegrabber software we set the intensity inside the recorded light spot be saturated on the CCD pixel array (maximum=

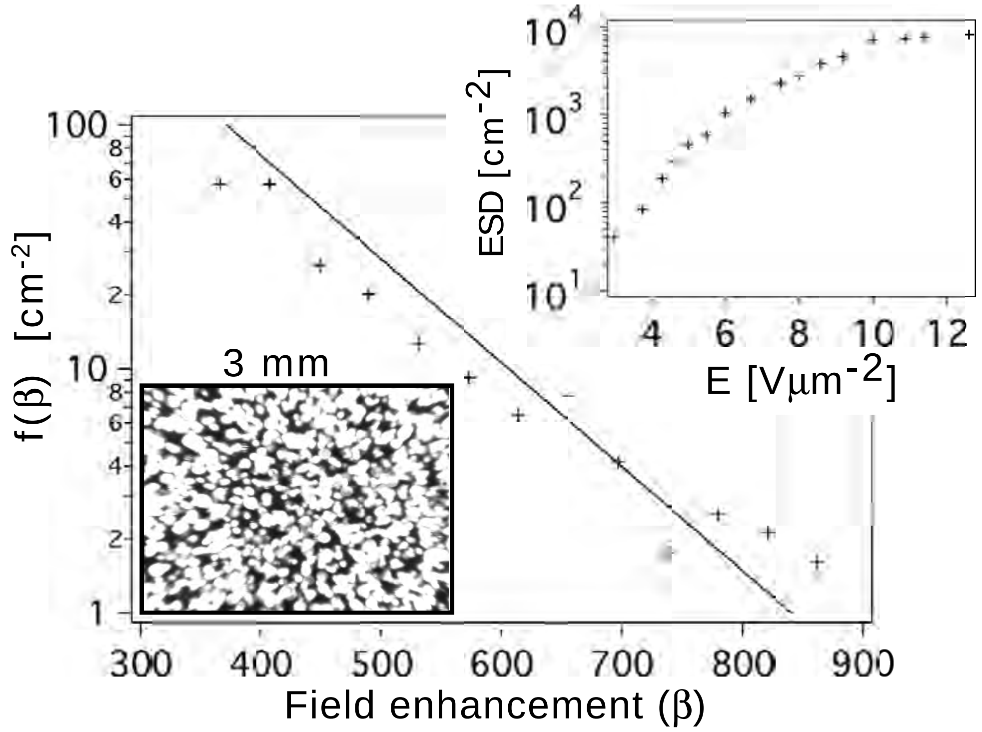

Figure 2.7: The β-distribution function f(β) is calculated from the the ESD shown in the upper inset. The ESD was measured as a function of the applied field for a CNT thin film emitter shown in the lower inset at 11.4 V/μm.

255/pixel). This is important since the position is calculated as the center of gravity of the spot according:

$$X_g = \frac{\sum_i^n x_i \cdot \triangle I_i}{\sum_i^n \triangle I_i} \tag{1a}$$

$$Y_g = \frac{\sum_i^n y_i \cdot \triangle I_i}{\sum_i^n \triangle I_i} \tag{1b}$$

The summation is taken over the pixel (x_i, y_i) with the light intensity $\triangle I_i$, where i=1 to n is the index of pixel in a $\sqrt{n} \times \sqrt{n}$ CCD frame of n pixel, which is cut out around the center of gravity from the main frame or CCD image. If the intensity is not maximized to 255/pixel inside the recorded light spot, small intensity variations inside the light spot between different positions (x_i,y_i) may cause the calculation (1) to be incorrect. Such intensity variations can be induced by dust particles on the CF100 view window or by reflexes between the view window and the lens.

Thereafter the anode is approached to the sample into a suitable distance at which a FE scan can be performed. An applied voltage of less than 100 V means in general for the case of a CNT film, that the tip-sample distance is less than 5 μm. In order to check and avoid possible contact currents during the FE scan the sample is translated several hundred micrometers in both x and y directions with a small voltage (< 1 V) applied to the anode.

Before starting FE scanning the x micro positioner has to be run back and forth 5-10 times in order to avoid strong initial oscillations with regard to the micro positioner step length.

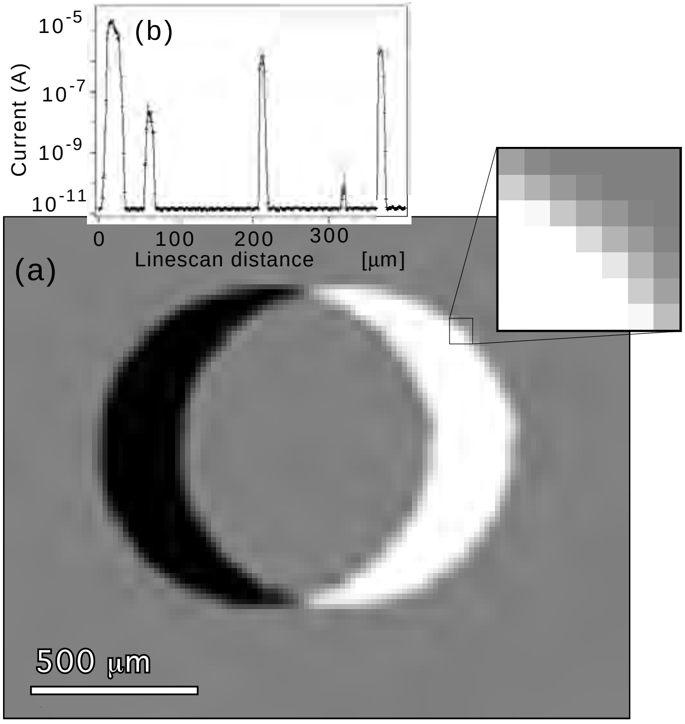

Figure 2.8: The difference between the two superimposed CCD images (a) (corresponding to start and end of a linescan) where the light source has been translated 15.7 pixel in x direction, is used to calculate the sample translation. The inset (b) shows an example of a linescan where the current has been recorded 100 times as a function of position in x direction. The inset shows the transition from saturated CCD pixel (white) to zero CCD intensity outside the light spot.

A FE scan consists of a number N_y, typically 100, of what we call linescans.

A linescan is N_x consecutive equidistant translation steps in x direction where the current (CVM) or the voltage (CCM) is recorded for each step. Such a CVM linescan is shown in the inset (b) of Fig. 2.8. In general N_x=N_y but not always. We sometimes like to change the emission parameters like the emission current in CCM, between adjacent scans. This can be useful in order to investigate the collective emission degradation behavior of thin film emitters. The position of the x/y sample holder is determined for the start (X^s, Y^s) and endpositions (X^e, Y^e) of each linescan. Two CCD frames corresponding to (X^s, Y^s) and (X^e, Y^e) for a single linescan are superimposed in the image of Fig. 2.8(a). The start- and endpositions allows to find the position of an arbitrary emitter anywhere on the sample surface. The emitting sites of several sequential FE maps can therefore be correlated which allows to compare individual emission currents with the corresponding field enhancement and vice versa.

2.2.5.2 Sample position calculation errors and translation precision

In order to obtain a spatially resolved FE image of the thin film emitter, which we throughout this text refer to as a FE scan or FE map, several sequentially and adjacent linescans with well defined steps in x and y directions must be recorded. This is a problem of technical relevance since the precision with which the sample position (X_g, Y_g) is recorded according to (1) and with which the sample is transported by the MS5 micro positioner strongly affects the resolution and precision of the FE scan. We therefore like to investigate how accurate the calculation (1) is and with which precision we can define the length of the steps in x and y directions and re-positioning of the micro positioner.

Fig. 2.29(b) shows the spatial fluctuations dy and dx around the normalized center of gravity (X_g= 0.0, Y_g= 0.0) for 1000 calculations according to (1) for a 34 pixel large light spot. The CCD images were sequentially recorded with the micro positioner at rest (no intermediate translation). The spatial fluctuations are induced by discretization errors in the intensity of the pixel at the fringe between subsequent light spots. The fringe of the light spot is about 3-4 pixel broad and is seen in the magnified inset of Fig. 2.8. The pixel intensity is 255 inside of the spot and 0 at 4 pixel distance from the inner fringe. The intensity per pixel varies between 255 and 0 within the fringe, and variations in the discretization levels of pixel between two CCD frames (e.g. from 122

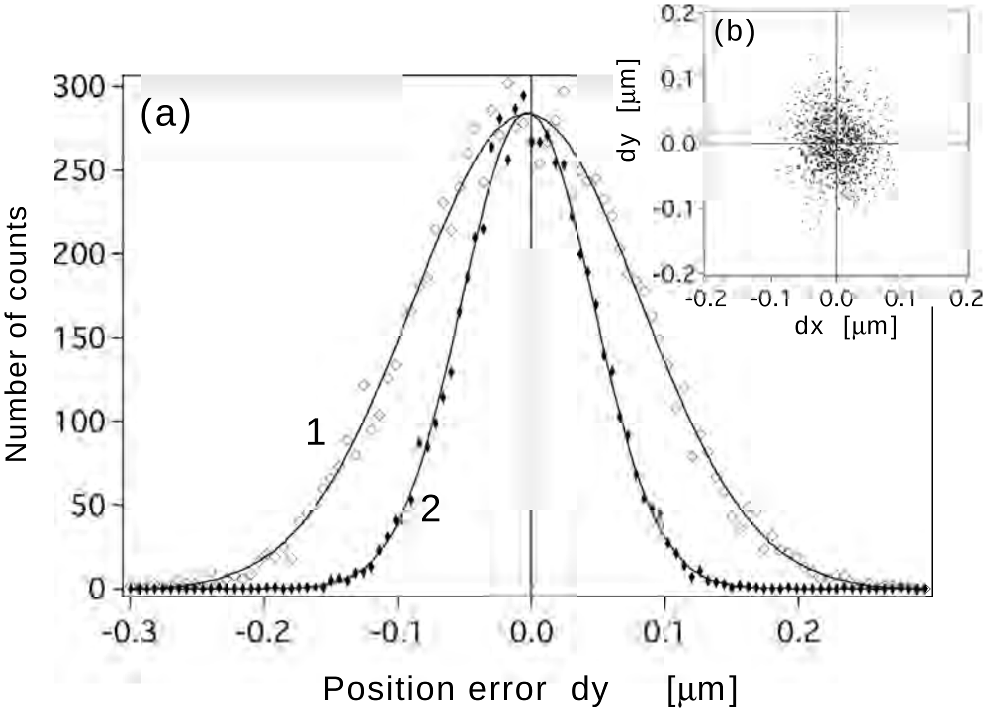

Figure 2.9: (a) Histogram of the deviation dy=(y_i-ŷ) for 10^4 recordings (ŷ is the average of all CCD images), where each recording was obtained from a single CCD image (1) or from an average of five CCD images (2). (b) Inset shows the spatial variation dx/dy of 1000 calculations of the center of gravity for a light source at rest.

---

to 123 etc.) cause X_g and Y_g to fluctuate on a sub-μm scale as indicated in Fig. 2.9(b). We made 10^4 subsequent recordings of the spatial variation (dx, dy) around the center of gravity (X_g= 0.0, Y_g= 0.0) where each recording was calculated as an average of five images. For comparison 10^4 additional recordings with only one image per recorded (dx, dy) data point were obtained. The two histograms we obtained from the recordings are depicted in Fig. 2.9(a) for dy (dx looks similar) and fitted with gaussian distributions. Fit 2 coincides with the 5×10^4 data points and has been normalized to the fit 1, which coincides with the 10^4 data points of the additional comparative recordings. Full width at half maximum (FWHM) is 0.059 μm for fit 2 and 0.102 μm for fit 1. When we calculate X_g and Y_g for the start and end points of the linescans we most often average five frames and can thus be confident that the position error (dx, dy) induced by the calculation (1) generally is less than 0.1 μm. This value is better than required for the resolution of most of our FE scans, which is limited by sample topography, anode radius and anode-sample distance to approximately 5 μm.

An accurate sample position calculation is an absolute but not sufficient requirement in order to obtain a FE map. We also need a precise control of the translation and re-positioning of the x and y micro positioner, since the MS5 motors experience a kind of oscillating behavior with regard to the linescan length (Fig. 2.10). After the first linescan (which can be twice the length of the second or third linescan), Fig. 2.10 shows how the linescan length stabilizes towards an average value after a maximum, indicated 1, is passed. A weak oscillation cannot be avoided (see numbers 2-4 in Fig. 2.10(a)-(c)). (a)-(c) depict the evolution of the linescan lengths for 100 consecutive linescans of three subsequent 100×100 pixel FE maps over the same CNT thin film emitter area. Between the scans, the sample has to be repositioned at the starting point, wherefore the initialization procedure of 5-10 translations in x direction (to filter the strongest oscillations) is repeated.

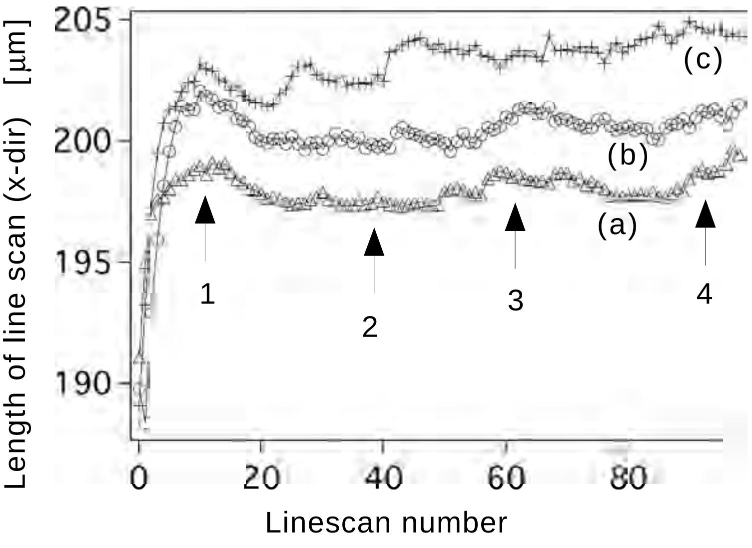

Figure 2.10: The linescan length as a function of linescan number for three subsequent 200×200 μm^2 FE maps (a)-(c). The length experiences a typical oscillating behavior indicated with numbers 1-4, where the average linescan length increases for every FE map.

In order to realize the spatially resolved FE image, the typically 100 consecutive linescans must be recorded over 100 parallel and adjacent thin film emitter linesegments and put together to form a two or three dimensional FE map. This put stringent requirements on the parallellity and inter-linescan distance on a μm level in order to obtain FE maps with μm resolution. It therefore has to be ascertained that adjacent linescans do not cross, touch or overlap each other and that the relative inter-linescan distance is maintained constant in the y direction. In fact a linescan is always recorded under small and continual deviations δy from the micro positioner direction of motion. Such unwanted sub-μm sidestep motions are super-imposed the principal direction of motion and may be caused by small dust particles, dirt or sub-μm scratches on the planar supporting guides (which defines the direction of motion) on which the micro positioner runs. In addition, we have to make sure that the linescan direction of motion coincides with the pre-defined x-axis. We will otherwise obtain a permanent run-out $\triangle$Y, where $\triangle$Y is the constant deviation in the y direction (measured at the end of each linescan) from the x-axis.

If $\triangle$Y is large we measure FE from a thin film area with the dimensions of a rhomb and not a square. However if we try to project a rhomb onto a quadratic area, we introduce a distortion into the FE map and we thus want to keep $\triangle$Y as small as possible. The total lateral run-out $\triangle\mathrm{Y}_{tot} = \triangle\mathrm{Y}+\delta\mathrm{y}$, is shown as a function of the linescan number for three independent 200×200 μm^2 FE maps (a)-(c) of each 100 consecutive linescans in Fig. 2.11. Whereas (a) and (b) correspond to two sequentially recorded FE scans from the very same CNT thin film emitter area, (c) is taken from another location of the same CNT film, after fine tuning of the direction of motion with the x-axis by turning the CCD pixel array. We therefore note that the integral run-out $\triangle\mathrm{Y} \approx 0.2$ μm of (c) is better than for (a) and (b) with $\triangle\mathrm{Y} \approx 0.7$ μm. However we consider $\triangle\mathrm{Y} < 1$ μm as acceptable for a 200×200 μm FE map. Finally we note from (a) and (b) that the differential run-out δy is always the same for several repeated linescans as long as the x micro positioner resides within the same 200 μm long region of the supporting guides. This is evident considering that δy is provoked by the same dirt and scratches along the same 200 μm long micro positioner runway for (a) and (b). The progression of δy for (c), which was obtained for a different 200 μm long spatial location of the x micro positioner, therefore look different compared to (a) and (b). $\triangle$Y and $\delta\mathrm{y}_{max}$ are only marked for (a) and (b) in

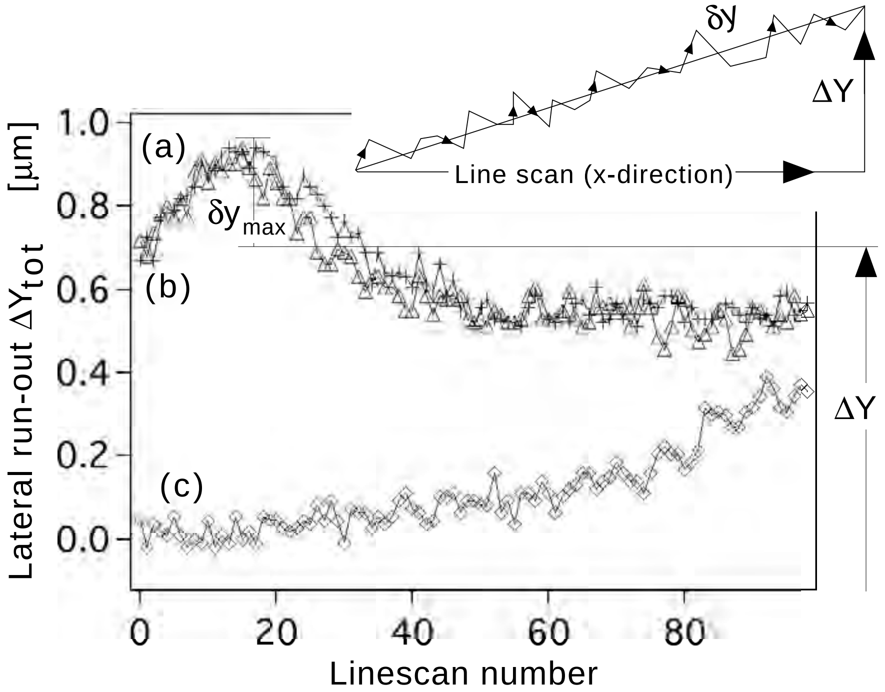

Figure 2.11: The lateral run-out △Y_{tot} for three different FE maps (a)-(c), where (a) and (b) corresponds to (a) and (c) of Fig. 2.10. △Y is the permanent lateral run-out due to non-parallellity between the x-axis and the x micro positioner direction of movement.

Fig. 2.11. The maximal differential run-out $\delta \mathrm{y}_{max}$ is less than 0.2 μm for (a)-(c), which is acceptable compared to the average step size of 2 μm. We have however also to compare $\delta \mathrm{y}_{max}$ with the inter-linescan distance △y to be sure that the micro positioner step size in y direction is sufficient.

Fig. 2.12 shows the single inter-linescan step size △y as a function of the linescan number (alternatively the step number in y direction), corresponding to the 100 consecutive linescans. The oscillating and irregular step size behavior may again be explained by dust or scratches on the micro positioner slide runway. We see that the average step size △y= 1.7 ± 0.1 μm is considerably larger than the differential run-out δy and that the linescans therefore to a good approximation run in parallel without touching or overlapping adjacent linescans. Note that the average step size △y= 1.7 ± 0.1 μm is less than the average x step size 2 ± 0.02 μm. As both step sizes △y and △x continuously are changed during the course of one or several FE scans, we conclude that it is difficult to adjust an

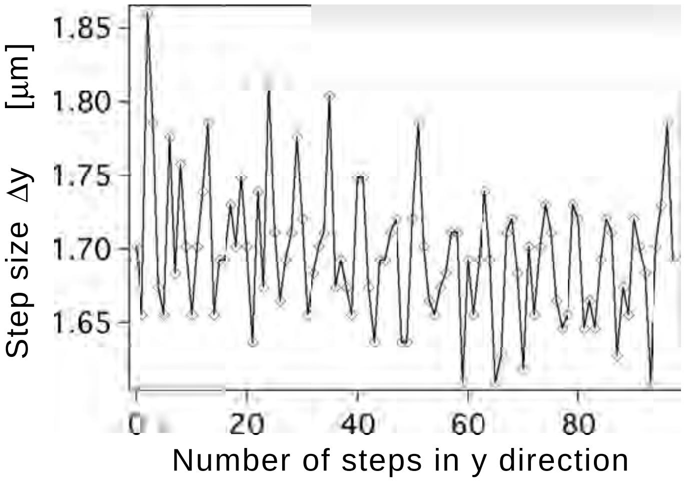

Figure 2.12: The step size △Y in y direction between every linescan as a function of the number of steps in y direction.

---

equal and constant step size for both the x- and y-axis between subsequent FE maps. Hence the FE maps are in general not recorded over an exactly quadratic thin film area, but this does not seem to distort the FE image, as we will see in the next section.

2.2.5.3 Field emission scanning procedure

In order to obtain a spatially resolved emission image we have to convert N_y one dimensional linescans into a two dimensional FE map. We therefore have to consider ways to correct position errors (e.g. due to the oscillations) during scanning. We use a home-made scanning software written in LabView to control the motion of the x/y micro positioner and to regulate the scan parameters as a function of temporal changes in the linescan length.

In order to compensate for the non-constant linescan lengths, each x translation step is composed of sub-steps, generally 8 to 12. Since the characteristics of the micro positioner motions are different in the forward (+x) and backward (-x) direction, the number of total sub-steps is different in the forward and backward direction.

The FE scanning process follows the flowchart of Fig. 2.33. After the start coordinate (t_x, t_y) and baseline x=t_x are set, the first linescan, during which the current or the voltage spot-wise is measured, is launched. The program saves the linescan end coordinate (X^e, Y^e) and returns to the baseline. The x-axis return coordinate X_g must not deviate too much from the baseline. If the difference between the linescan length and the return length surpasses a user pre-defined tolerance limit, generally set to 3-8 μm, the number of return steps is incremented to compensate for the difference in the following linescan. The anode-baseline distance may be additionally adjusted after return to the baseline, with refined sub-μm steps in an iterative sequence.

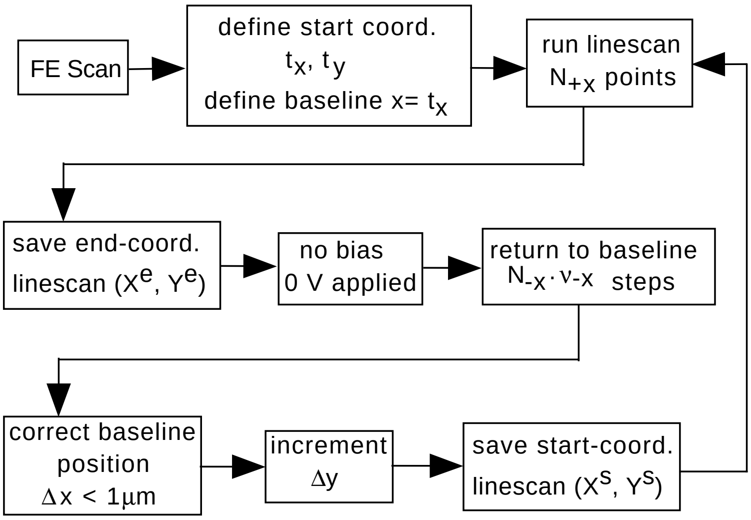

Figure 2.13: Flowchart scheme for the FE scanning procedure.

The $\triangle$y step movement consists in general of 3-6 sub-steps, which must be adjusted to make the total height of the FE scan in the y direction equal to the average linescan length. This is a matter of trial and error, since it is difficult to foresee the evolution of the x and y step sizes.

The raw data of 10^4 measurement points of the applied voltage from the 100 consecutive linescans (a) and (c) of Fig. 2.10 are obtained according to the flowchart above and depicted as two voltage V(x,y) FE maps over the same CNT thin film emitter area in Fig. 2.14(a) and (c). Dark spots corresponds to low extraction voltage and pin-points individual emission sites. Since the linescan lengths depends on the linescan number in y direction (see Fig. 2.10) only the average horizontal x length of the FE scan can be calculated for (a) and (c). The average width of the FE map is 198 μm for (a) and 203 μm for (c), whereas the height in y direction is 169 μm (a) and 162 μm (c). We cannot do much about the fact that the height in general not is equal to the width of the FE scan (except for cutting a quadratic window out of the FE map after the scan), but we may post-treat the linescans in order to equalize the lengths. With a home-made software written in Igor, a FE map can be normalized to the shortest linescan length l_n (generally the first linescan) and all linescan measurement points extending beyond l_n are discarded. This results in a number of linescans with less than 100 measurement points where all linescans are of equal length l_n. However we want to display 100×100 data points on a FE map and therefore we interpolate the reduced number of data points of a linescan onto 100 points.

The result of the interpolation of the raw data from (a) and (c) is shown in Fig. 2.14(b) and (d). The length induced inter-linescan mismatch, which creates discontinuities between adjacent lines in (a) and (c), is removed thanks to the interpolation and the images in (b) and (d) are smooth and continuous. The low voltage ripples at the start of each linescan at the baseline x=0 are due to the source-measure device, which unfortunately not was given enough time to increment the voltage from zero to the operating voltage before the linescans were launched. The time required to finish the FE scan (typically one hour) depends on several parameters but mainly on the measurement sensitivity of the source-measure device.

2.2.5.4 SAFEM image analysis and measurement capabilities

A closer look on the V(x,y) maps in the preceding paragraph, reveals significant differences in extraction voltage between individual emitting sites of the thin film. Whereas some sites barely are resolved from the background, others are strong emitters (with extraction voltage below 40 Volt) which are detected at large lateral distances of 10 μm from the anode.

The strong emitters in the V(x,y) map are normally also seen in a current map I(x,y), whereas the weak sites not are resolved due to the typically very steep field emission current-voltage (I-V) characteristics of the type seen in Fig. 2.5. Of the

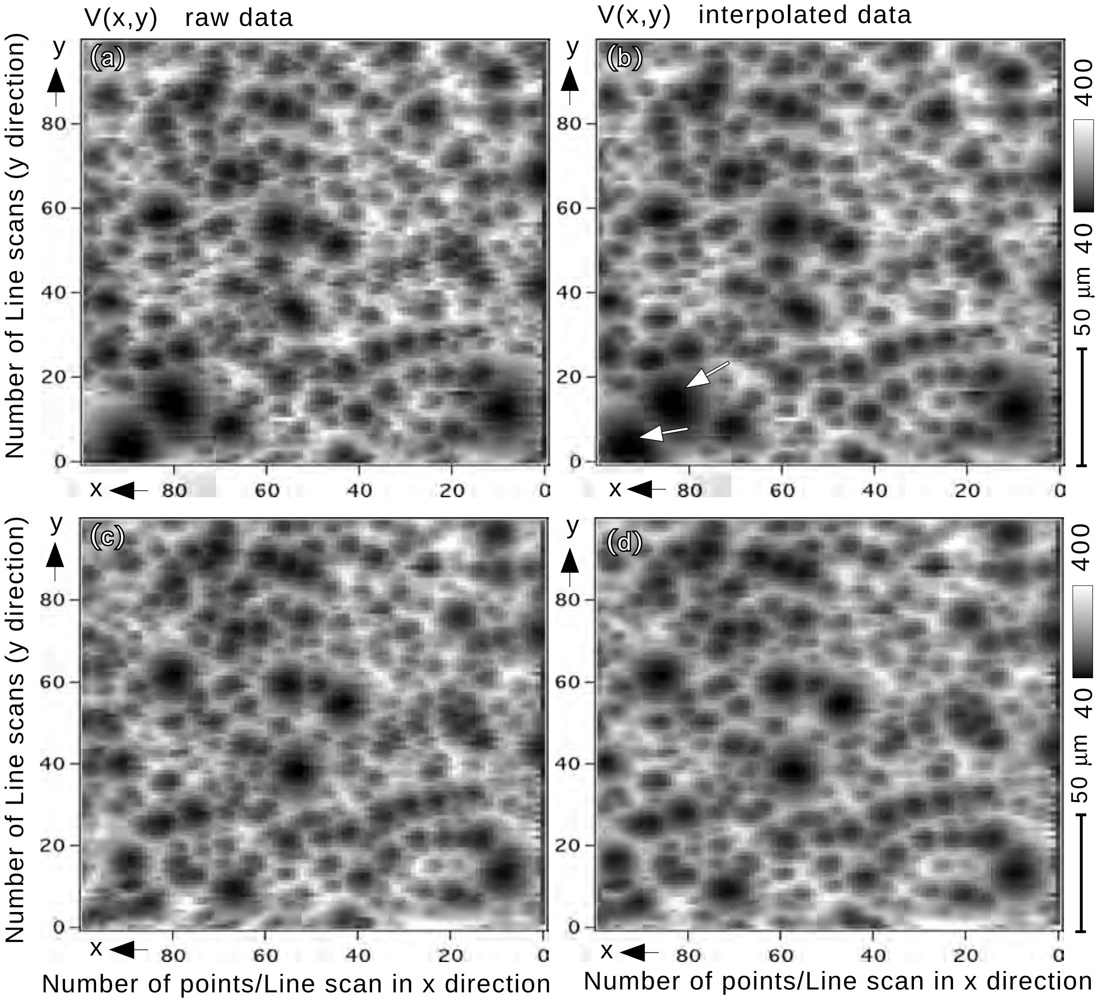

Figure 2.14: The raw data of the extraction voltage V(x,y) for 10 nA emission current (d ∼ 7 μm) of two sequentially recorded FE maps (a) and (c) corresponding to (a) and (c) of Fig. 2.10. (b) and (d) shows the same V(x,y) maps after linescan length error correction. Please note the two strong emitters in (c), marked by arrows, which have disappeared from the second V(x,y) scan in (d). The emission from these (arrows) blocked the emission from weaker sites underneath, seen in (d).

---

same reason we cannot expect to record the weak sites on a phosphor screen, which is operated in constant voltage mode. We conclude that the dynamic measurement range in constant current mode is larger than for the constant voltage mode, and that we therefore can detect and investigate sites in a V(x,y) map which are inaccessible in a I(x,y) map or with a phosphor screen [12].

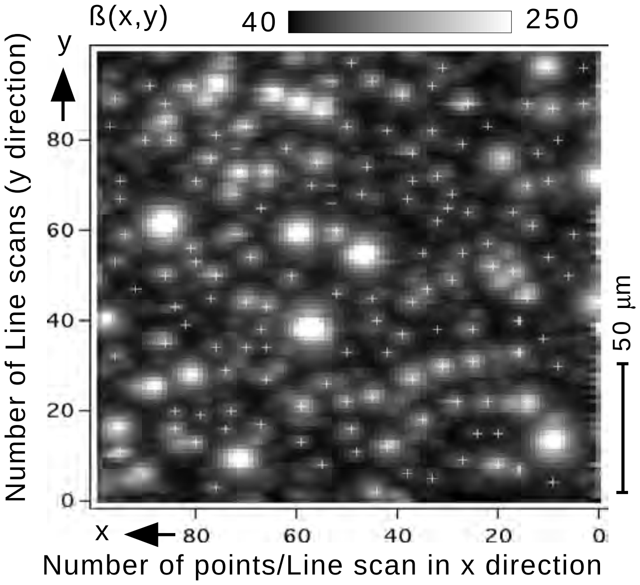

Figure 2.15: Calculation of the $\beta(x, y)$ map from V(x,y) in Fig. 2.14(d). The β peak values are marked by white crosses and correspond to individual emitters, where each emitter has a different I-V characteristic and thus different threshold field.

The large differences in voltage (required to produce 10 nA emission current per site) between the individual emitting sites makes it obvious why traditional I-V measurements over large emitting areas are unsatisfactory. Such large area I-V characterizations takes only a very small fraction of all sites, corresponding to the strongest sites with the highest field enhancement, into consideration. This small number is measured in parallel in contrary to the scanning anode. Considering these two facts, the quality of integral measured threshold fields or I-V characteristics on large area emitting films are questionable, since such quantities fail to acknowledge individual emission site characteristics. In contrast to integral techniques the SAFEM opens a spectrum of individual emission site characterization possibilities. Since a reference coordinate (t_x, t_y) is defined for each FE map, a number of FE maps can be independently recorded and individual sites can be spatially correlated. This allows multiple testing of single site emission characteristics as a function of intermediate increased current levels, current, voltage or time (single site emission stability). A specific site can be tracked and found in several different FE maps obtained under different conditions like in constant current mode or in constant voltage mode. Such comparisons are interesting as one like to compare e.g. emission currents in function of the corresponding field enhancement β of a specific site. Additionally single site I-V and I-t characteristics may be recorded as the SAFEM can be programmed to find and analyze all FE map peak values. This opens for statistical analysis, where the FE sites may be categorized according to saturation and degradation behavior, stability, time of life and spatial field enhancement β(x,y). As an example the spatial field enhancement β(x,y) is calculated from the V(x,y) map in Fig. 2.14(d) according:

$$\beta(x,y) = \frac{d \cdot E_{site}}{V(x,y)} \tag{2}$$

where the field at the emission site E_{site}= 3800 Vμm^{-1} for I= 10 nA according to the Fowler-Nordheim law as shown by energy resolved field emission spectroscopy [16] on CNT films, and d= 5 μm is the tip-sample distance. It should be pointed out that the applied field E= V/d [V/μm] between the anode and the sample surface is assumed homogeneous in the calculation (2) of the field enhancement. This is not entirely correct first because field enhancing structures or CNTs, whose β factors we would like to calculate, modify the equipotential lines and second because the anode radius of curvature induce an inhomogeneous applied field as compared to a parallel plate diode set-up. The applied field is over-estimated at the sample surface as compared to an inhomogeneous applied field by a factor 1.6 according to the simulation in Fig. 2.16(a).

Consequently the calculated field enhancement β(x,y) is correspondingly under-rated. The resulting β(x,y) map is shown in Fig. 2.15, where the β peak values have been marked by white crosses. By counting the number of emission sites with field enhancement in the range β to β+dβ we obtain a histogram, which normalized to 1 cm^2 corresponds to the β-distribution f(β). We derived f(β) for the very same CNT film in Fig. 2.7 in a higher field enhancement range using the phosphor screen. If we plot f(β) from both the screen measurement and the β(x,y)-mapping together, we can fit both measurements with an exponential characteristic f(β) $\propto$ exp(-k$_1\beta$) according to Fig. 2.17.

The emission properties, like the ESD, of thin emitting films are better characterized by f(β) than by a single parameter such as the threshold field. Our

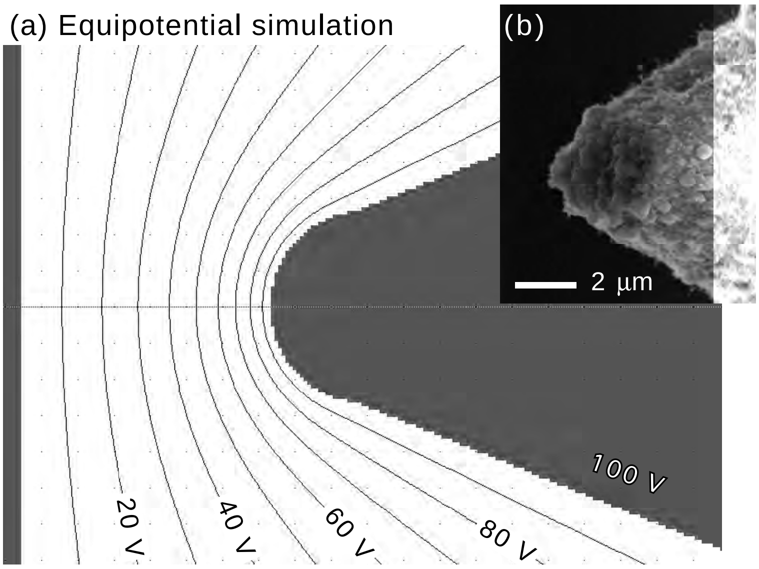

Figure 2.16: Simulation (a) shows the distribution of equipotential lines between the sample surface and the anode (radius of 1.5 μm). The distance sample surface-anode is 4 μm. Inset (b) shows the anode after several FE scans and contact measurements on CNT thin film emitters. The tip is blunted and covered by CNTs and catalytic metal particles which have been removed from the film due to the electrostatic forces.

investigations indicate that the emission properties can be tuned by modifying the slope and position of f(β), [12]. Even more important, whereas the emission from CNT films clearly is dominated by high field enhancement, the emission mechanism from DLC and other thin emitting films is still under dispute. However the functional dependence of f(β) recorded from CVD diamond films is similar to the exponential f(β) of CNT films. This would strongly suggest that the fundamental mechanism underlying the low threshold electron emission from a wide range of thin film emitters, and not only CNT films, is indeed high field enhancement.

2.2.6 FEM characterization of individual emitters

The microscopic techniques previously presented are liable on a μm scale. The μm resolution is well suited for statistical investigations of the low threshold emission from thin film emitter ensembles with regard to the ESD, collective

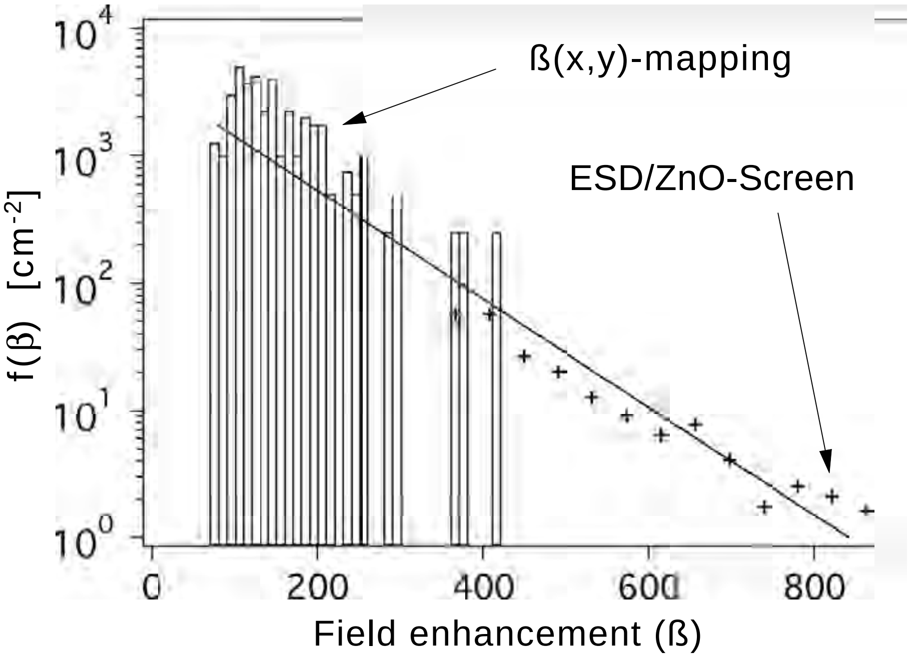

Figure 2.17: The β-distribution f(β) which is the number of emitting sites per unit area and field enhancement dβ as a function of the field enhancement for a CNT thin film emitter. f(β) as recorded with the screen of Fig. 2.7 (crosses) and with the scanning anode of Fig. 2.15 (bars), are plotted and fitted with an exponential f(β) characteristic.

---

emitter degradation behavior etc. However for some investigations of single site emission phenomena, a higher resolution is required. AFM/STM based FE microscopy does not reflect the same field enhancing conditions at the emission site with regard to the equipotential distribution since the field enhancing effect vanish as the anode is too close to the emission site. Therefore as we wish to investigate e.g. the spatial charge distribution of a single emission site on a sub-μm scale we need to ascertain that the anode-emission site distance is large compared to the typical size of the field enhancing structure. The situation where e.g. CNTs are mounted onto a tip or a filament and held at a distance of several cm under a phosphor screen in a field emission microscope (FEM), fulfill the requirement of a large anode-cathode distance with a magnification factor up to 10^6 times. The magnification is here given approximately as the ratio of the emitter-screen distance and the emitter tip radius of curvature [13]. The spatial emission current distribution of a single CNT tip apex obtained on the phosphor screen, reflects not only the local density of states but probably also effects of adsorbed molecules or species. Such adsorbed species may influence the spatial emission current pattern in at least two ways.

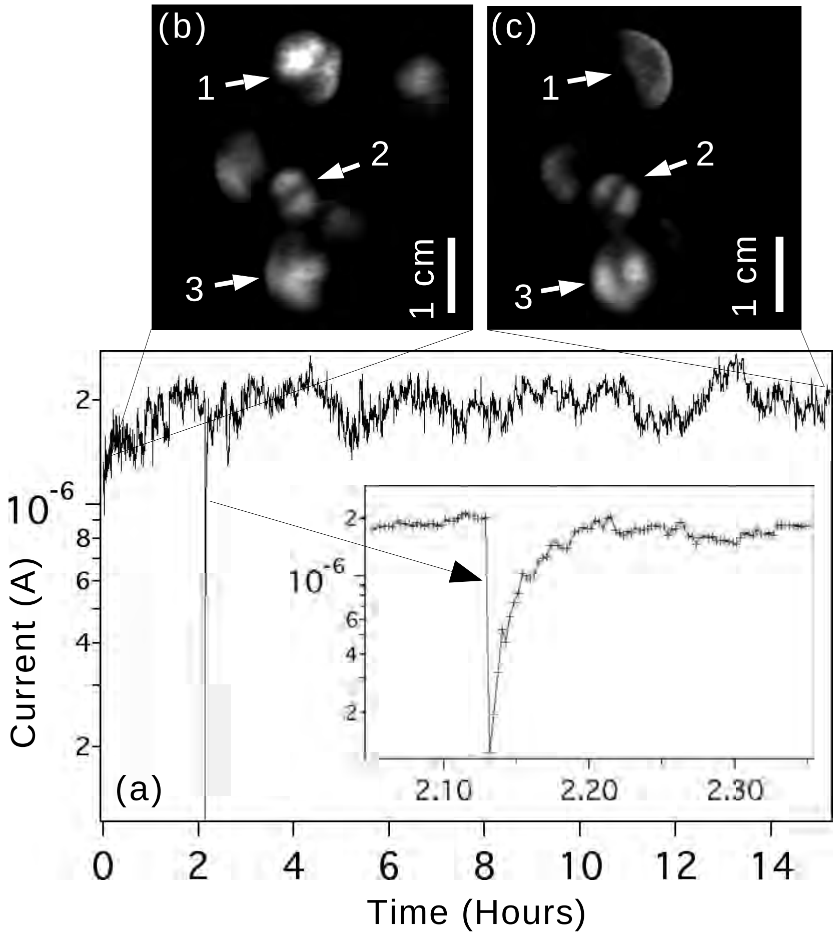

Figure 2.18: The emission current stability (a) of an ensemble of probably six emitting tubes in the FEM shown in the inset (a) and (c). Note the spontaneous rapid current drop at the time 2.13 hours and the afterwards continues current recovery. It can be speculated that the current drop is connected to the spontaneous loss or desorption of adsorbed species. It seems however that re-adsorption takes place on a time scale of six minutes due to impinging species. The different FEM patterns (1-3) seems to be created by different adsorption sites on the CNTs tip apex. The base pressure was about 10^{-9} mbar.

First of all the workfunction ϕ may be locally changed due to adsorbed species with an electron affinity different from the underlying carbon structure. Secondly the adhesion of species may on a nm level change the geometry of the field enhancing structure and thereby locally modify the field enhancing effect. It should however be pointed out that the workfunction and the field enhancement β are used to describe electronic and geometric properties of a material of macroscopic dimensions. One must therefore keep in mind that the description of the emission process on a molecular or atomic level may be better characterized by solutions to the Schrödinger equation under high field conditions for different atomic configurations at the emission site. The interpretation of the emission site spatial charge fluctuations seen in a FEM from CNTs in terms of changes of ϕ and/or β, is therefore not straightforward. It has been proposed by Dean et. al. [17] that the lobed and time varying FEM patterns of CNTs may be explained in terms of enhanced resonant tunneling states, created by molecules or species adsorbed to the CNTs tip apex. We observe these lobed patterns as well, Fig. 2.38(b) and (c). In such a case one could think of the species as atoms or molecules which become polarized in the presence of the high electric field around the CNTs. The dipols are therefore attracted to the CNTs and "feels" the presence of the CNTs from a much larger distance compared to when no field is present. Under these conditions it would be reasonable to assume that the rate of change in the FEM patterns would correlate with the rate of impinging dipols. However the nature and origin of the adsorbed species is not clear in this case. Our investigations indicate that the species originate from the phosphor screen rather than from the gas phase. If the CNT sample is heated and the adsorbed species thereby are desorbed, re-adsorption will take place at 300 K on a time scale of minutes depending on the state of the phosphor screen [15, 16].

Re-adsorption manifests itself through establishment of relatively stable FEM emission patterns and increased current levels. If the screen is well outgassed, thermally cleaned or electron scrubbed/sputtered for a long time, the time for re-adsorption after short heating is longer. If the screen is replaced by a flat alumina anode, re-adsorption does not seem to take place very fast or even at all, indicating that the active species responsible for enhancement of the tunneling current are contained in the phosphor and hence does not come from the gas phase (Fig. 2.19). Indeed, we investigated the effects of partial gas pressures of hydrogen, oxygen and water up to 10^{-5} mbar but could not record any enhanced tunneling states due to these gases. In contrary oxygen degrades the emission from single walled CNTs probably due to reactive ion etching. More work is

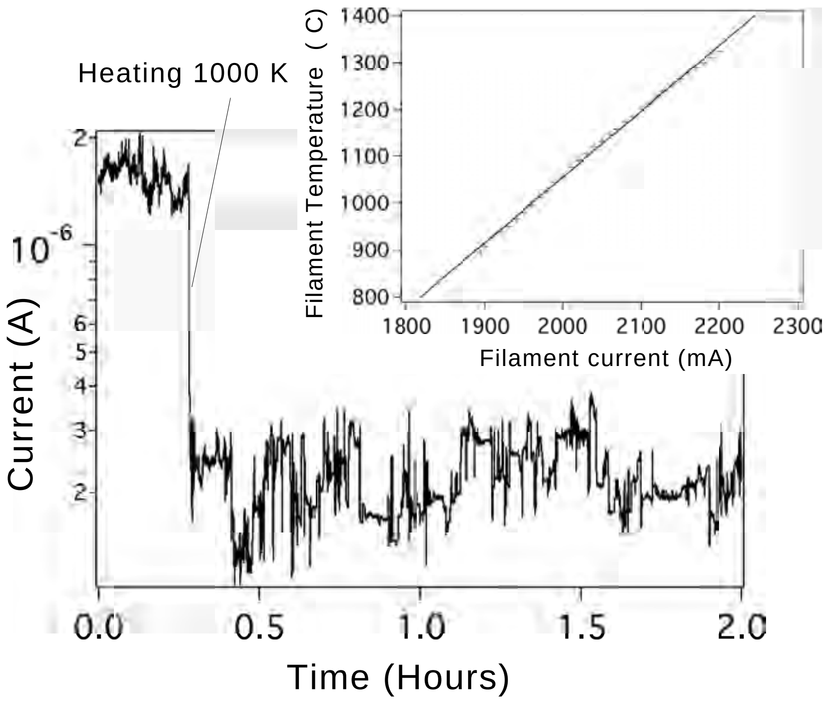

Figure 2.19: Whereas the emission current from CNTs in the FEM tends to increase to initial high values after heating of the tubes under a phosphor screen, the current remains on a low value after heating under a flat Al anode. The state of the anode seems to make a difference to the current recovery after heating of the tubes. The inset shows the filament (and CNT) temperature as a function of the filament current.

needed to clarify the nature of the FEM patterns from CNTs.

2.2.7 Conclusions and outlook

Macroscopic or integrated field emission characterization techniques alone, are inadequate for the description of the FE process from low threshold thin film emitters, since they fail to acknowledge individual emission site characteristics. However combined with scanning anode field emission microscopy on a μm scale, relevant information about the spatially divergent FE properties can be retrieved. Such information could help to classify the emitting sites of a thin film emitter ensemble into several groups of different current- time or current-voltage behavior. The combined experimental results of the phosphor screen and the SAFEM strongly suggests that the low threshold emission from several thin film emitters, mainly carbon-based, is best described in terms of the spatial field enhancement β(x,y). In contrast to electric threshold fields β(x,y) does not depend on the anode-cathode geometry. Field emission microscopy on single CNTs indicate that the presence of adsorbates may influence the electronic properties at the emission sites and therefore also the emission current. The geometry in which the FEM current-time behavior is measured, does however not reflect the influence of a large number of parallel emitting sites of a thin film emitter ensemble. We therefore like to continue the scanning anode field emission microscopy by single site current-time and current-voltage investigations in order to gain deeper insight of the low threshold emission process. The construction of a new μm sized focalization system of anode-guard ring should permit to increase the resolution of our system to the sub-μm regime, even with an anode-cathode separation of several μm. Such a large anode-cathode distance seems to be necessary in order to ensure the typical electrostatic conditions at the emission site on a low threshold thin film emitter.

2.2.8 Acknowledgment

The authors gratefully acknowledge financial support from Motorola and the Swiss National Science Foundation for the construction of the SAFEM. The realization of this project would not have been possible without the excellent hard- and software support of mainly Otto Zosso, Christoph Neururer, Elmar Mooser, Oswald Raetzo, and Francis Buorqui. The paper is dedicated to the very skillful mechanic Otto Zosso who spend a lot of time in setting up the equipment and after 40 years in duty of the university soon retires.

References for 2.2

[1] P.R. Schwoebl, I. Brodie, J. Vac. Sci. Technol. **B13**, 4, 1391 (1995).

[2] D. Temple, Mater. Sci. Eng. **R24**, 185 (1999).

[3] B. R. Chalamala, Yi Wei, B. E. Gnade, IEEE Spectrum **April**, 43 (1998).

[4] R. Fowler, L. Nordheim, Proc. R. Soc. London **A119**, 173 (1928).

[5] C.Wang, A.Garcia, D.C. Ingram, M. Lake, M.E. Kordesch, Electron. Lett. **27**, 1459 (1991).

[6] G.A.J. Amaratunga and S.R.P. Silva, Appl. Phys. Lett. **68**, 2529 (1996).

[7] J.-M. Bonard, J.P. Salvetat, T. Stöckli, W.A de Heer, L. Forró, A. Châtelain, Appl. Phys. Lett. **73**, 918 (1996).

[8] O.Gröning, O.M. Küttel, P.Gröning and L.Schlapbach, Appl. Surf. Sci. **111** 135 (1997).

[9] F.S.Baker, A.R.Osborn, J.Williams, J. Phys.D: Appl. Phys. **7**, 2105 (1974).

[10] M.W. Geis, J.C. Twichell, T.M. Lyszczarz, J. Vac. Sci. Technol. **B14**, 3, 2060 (1996).

[11] R.L. Fink, Z. Tolt, Z. Yaniv, Surface and Coatings **108-109**, 570 (1998).

[12] L. Nilsson, O.Groening, P. Groening, L. Schlapbach, subm. Jour. Appl. Phys. (2001).

[13] R. Gomer, Surf. Sci., **299/300**, 129 (1994).

[14] O.Gröning, O.M. Küttel, P.Gröning and L.Schlapbach, J. Vac. Sci. Techol. **B17**, 1970 (1999).

[15] L. Nilsson, O. Gröning, P. Gröning, O. Kuettel, L. Schlapbach, Proc. XIV Inter. Winterschool on Electr. Prop. of Novel Materials, Kirchberg, Tirol, Austria, 499 (2000).

[16] L.Nilsson, O. Gröning, P. Gröning, L. Schlapbach, Thin Solid Films **383**, 78 (2001).

[17] K.A. Dean, B.R. Chalamala, Appl. Phys. Lett. **75**, 3017 (1999).

2.3 Scanning field emission from patterned carbon nanotube films

L. Nilsson, O. Groening, C. Emmenegger, O. Kuettel, E. Schaller and L. Schlapbach
Institute of Physics, University of Fribourg, Pérolles, CH-1700 Fribourg, Switzerland

H. Kind, J.-M. Bonard and K. Kern
Department of Physics, EPFL, CH-1015 Lausanne, Switzerland

Published in Appl. Phys. Lett. **76**, 2071 (1999)

Abstract

The investigation of the field emission (FE) properties of carbon nanotube (CNT) films by a scanning anode FE apparatus, reveals a strong dependence on the density and morphology of the CNT deposit. Large differences between the microscopic and macroscopic current- and emission site densities are observed, and explained in terms of a variation of the field enhancement factor β. As a consequence, the emitted current density can be optimized by tuning the density of CNTs. Films with medium densities (on the order of 10^7 emitters/cm^2, according to electrostatic calculations) show the highest emitted current densities.

During the last decade different forms of carbon thin films, like diamond, diamondlike carbon (DLC), tetrahedral amorphous carbon (ta-C) etc. were found to show extraordinary FE properties from apparently flat surfaces [1–3]. It was believed that the reason for the enhanced FE was related to the electronic properties of the films [4]. This was very promising from a technological point of view since the incorporation of such materials in a gated structure, like a flat panel display (FED), could be done easily over large areas at low cost using standard chemical vapor deposition techniques [5,6]. However there is an increasing number of indications that the enhanced FE is due to intense local electric fields caused by protrusions in the μm- and nm range [7,8].

The production of such protruding field enhancing structures (FES) in gated patterns is a problem of technological relevance [25, 26]. To be competitive with more conventional cathodes a cheap and simple technique must thus be developed to reproducibly and selectively deposit carbon FES which, in addition, meet the prerequisites of uniformity ($>10^6$ emitters/cm^2) [6] and current density ($\sim 80\ \mu$A/cm^2) [11].

Recently, a simple nonphotolithographic technique, based on microcontact printing (μCP) of a catalytic precursor, was introduced to fabricate patterned carbon nanotube FES [12, 13]. In this letter we report on the field emission properties of patterned FES produced by this technique.

Ethanolic solutions containing 10-60 mM $Fe(NO_3)_3 \cdot 9H_2O$ were used as catalytic inks to be printed on the native oxide of silicon wafers. Samples were then mounted in a tube reactor and CNTs were grown at 720 °C in a mixture of acetylene and N_2 [12, 13]. The resulting pattern, Fig. 2.20, is covered by a film of multiwall CNTs, about 15 nm diameter and $\sim$5 μm height. The width of each line is 10 μm and the distance between the individual lines is 50 μm. An increase of the concentration of $Fe(NO_3)_3{\cdot}9H_2O$ results in an increased density of CNTs on the film, as shown on Fig 2.21(a)-(c).

The samples were investigated by means of a vacuum FE apparatus, which permits integrated FE using a phosphor screen as well as locally resolved FE using a X/Y-scanning tip. With integrated FE, emitter- and current-density on a macroscopic scale ($\sim$cm^2) is retrievable. To avoid artifacts due to the sensitivity of the screen, a constant voltage of $\sim$3000 V was applied to the screen-anode parallel to our grounded sample, and the field was changed by varying the screen-cathode distance. The X/Y scanning was performed over an area of typically 200 × 200 μm^2, divided into 100 × 100 pixels. The Pt-Ir anode with a tip radius of $2-5$ μm was biased to ∼100 V. The separation between anode and the surface of the emitting film was fixed at $\sim 3-5$ μm. Extracted FE currents were recorded with a Keithley 237 source-measure unit and plotted as a function of the tip position. The level of the noise was lower than 1 nA during scanning. Contact currents could be distinguished from the FE current by a sudden current increase and saturation of the source-measure device. The base pressure of the FE chamber was better than 10^{-7} mbar.

Integrated FE measurements on patterned samples with various densities of CNTs did not reveal significant differences in their emission properties. All started to emit at low fields ($2-3$ V/μm) but the emission was not homogeneous. As seen in the inset of Fig. 2.20, the emission was dominated by a comparatively small number (<100) of very strong emitting sites spread out over the entire sample surface.

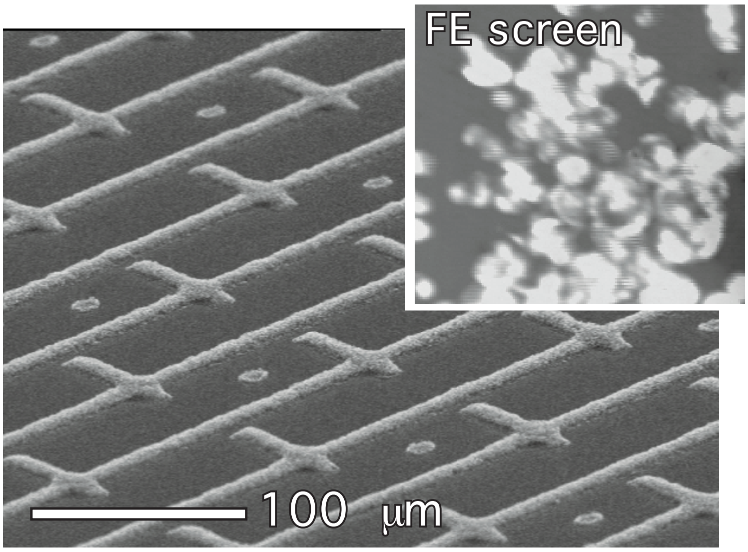

Figure 2.20: Low magnification SEM image of a CNT sample printed with an ethanolic solution of 40 mM $Fe(NO_3)_3{\cdot}9H_2O$. The inset shows a macroscopic emission image of 2.5 × 2.5 mm^2 on the phosphor screen at 5 V/μm.

This indicates that emitters with a lower length-to-diameter ratio (i.e. a lower field amplification factor β) are not detected. Indeed, the number of detectable emission sites depends on the size of the measured surface. A cm^2 area will include very few strong ($\beta \sim 1000$) emitting sites, whereas a local measurement in a $100 \times 100\ \mu\mathrm{m}^2$ window may reveal many emission sites with lower β-values (~100-200) when no strong emitters are present in this window. Furthermore, the resolution of the screen puts a limit to what is detectable on the sample, and emitters with a spatial separation of less than 100 μm are difficult to distinguish. These two facts show that traditional I/V measurements with large area anodes are insufficient for proper FE characterization.

To overcome these difficulties we performed FE-scans with a Pt-Ir tip and found indeed that there are in fact large differences between different samples. In Fig. 2.21 we compare three FE-scans on patterned samples with different densities of CNTs with the corresponding morphology seen in SEM. Fig. 2.21(d) shows the emission from a high-density CNT sample and is characterized by a rather inhomogeneous emission pattern. The lines and a few crosslines are recognizable, but a clear emission pattern is not obtained. A similar result [Fig. 2.21(f)] applies to the low density CNT sample, but the emission intensity is lowered by a factor of 10 and the pattern is even less pronounced. For the pattern with a medium CNT density, a much better emission image [Fig. 2.21(e)] is obtained: lines, crosslines and dashes can be easily distinguished. Emission from this sample and on this scale is very homogeneous.

The obtained emission behaviour is a combination of two effects. The poor emisson of high density films, as in Fig. 2.21(d), are explainable by an electrostatic screening effect provoked by the proximity of neighboring tubes. The solution of the Poisson equation governs the behavior of the potential penetration into the CNT deposit. The presence of many tubes per unit area (u.a.) means that there is more charge per u.a. and the charge reduces the potential drop perpendicular into the film. Since it is the local electric field ($\sim 3000 - 4000$ V/μm) at the emission site that governs the emission, the distance between the tubes remains a crucial parameter to optimize the FE. The limit of zero distance between the tubes would correspond to a flat metal surface without field penetration. The film depicted in Fig. 2.21(a) is close to this limit since the CNTs are densely packed. In fact, we observe some FE only because there are a few tubes that are branching out of the pattern. Low density films [Fig. 2.21(c)] also give poor emission but for another reason. As seen in the SEM image, the

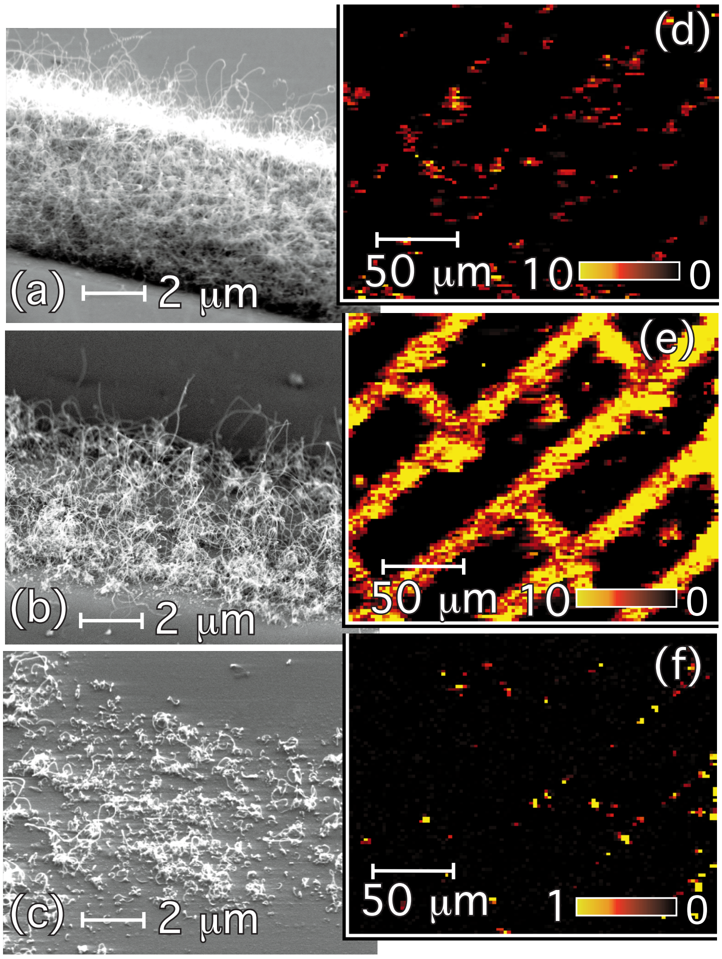

Figure 2.21: SEM images of patterned CNT films showing regions of (a) high, (b) medium and (c) low density, with the corresponding FE-maps of current density (d)-(f). The films were produced with ethanolic inks of 10 mM (a), 40 mM (b), and 60 mM $Fe(NO_3)_3{\cdot}9H_2O$. The FE-maps were taken under identical conditions using 100 V in constant voltage mode. The color scale corresponds to 0-10 μA/pixel for images (d), (e); and to 0-1 μA/pixel in image (f).

CNTs are short, bent, and not protruding out of the substrate. Only very few of them have a sufficient β-factor for an adequate emission. Thus the morphology of individual tubes is indeed of crucial importance for the FE properties. We conclude that a film with a medium density of high aspect ratio tubes shows optimal FE performance. These conditions are best fulfilled for the sample of Fig. 2.21(b).

In order to verify our experimental findings we performed electrostatic calculations of the field penetration between parallel standing tubes, as shown in Fig. 2.22(a). We assumed tubes of 1 μm length with a tip apex of 2 nm and decreased the distance between the tubes. The equipotential lines and thus the field enhancement factor β are seen to be strongly affected as the intertube distance is decreased. The field enhancement factor β is displayed as a function of the distan ce in Fig. 2.22(b), along with the density of emitting sites. Inserting β and emitter density into the Fowler-Nordheim equation yields the current density as a function of the distance and applied macroscopic field, shown in Fig. 2.22(c). In accordance with the experiment we find an optimum intertube distance of 2 μm where the emission is strongest. It is worth noting that this effect is dominated by the field penetration, which is determined by the relative height of the CNTs compared to the intertube distance. A variation in the tube tip apex changes the magnitude of the field amplification but does not influence significantly the optimum distance.

By comparing the current density versus distance in Fig. 2.22 with the FE-maps of Fig. 2.21, we conclude that three different emission regimes can be defined. Emission from low density CNT films is poor because there are few emitting sites of unsufficient β-factors, whereas emission from densely packed CNT films is poor because of reductions in the field enhancement factor due to screening effects. In the intermediate regime, the distance between CNTs is sufficient to reach substantial local fields, and the available emitter density is still sufficient for adequate emission currents.

In summary, completely different values of current and emitter density are obtained using a screen technique as compared to a scanning tip technique. The reason for the discrepancy is found in the composition of few high β-emitters ($\beta \sim$1000) and a majority of low β-emitters ($\beta \sim$100). When our samples are measured with a large anode, the emitters with the highest β dominate the emission. Since they represent a very small fraction of all possible emitters, the emission is not homogeneous and the obtained current densities are low. When microscopically investigated, the low β-emitters are also recorded and much higher local current densities, $\sim$100 A/cm^2, are observed from individual pixels as seen in Fig. 2.21(e). Local current densities are thus a factor 10^5 higher than during macroscopic FE and it appears that an improved monodispersivity

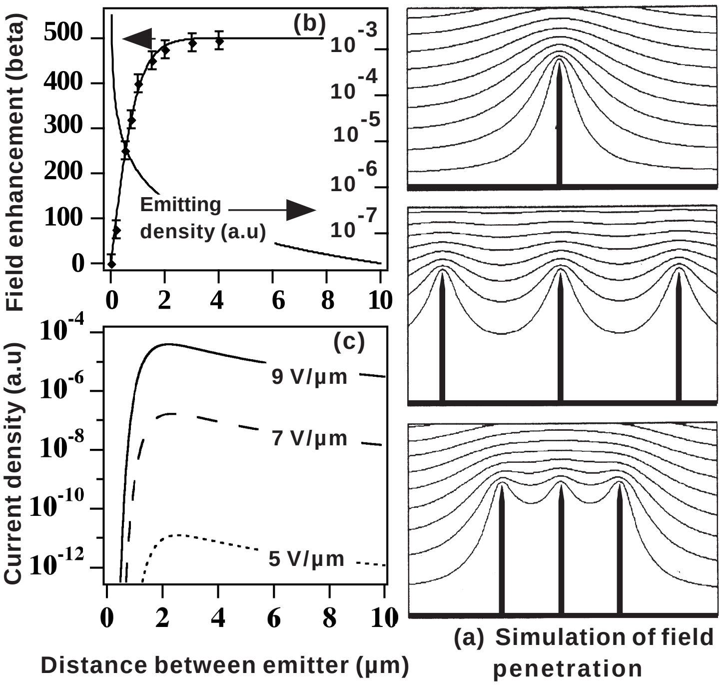

(a) Simulation of field penetration

Figure 2.22: (a) Simulation of the equipotential lines of the electrostatic field for tubes of 1 μm height and 2 nm radius, for distances between tubes of 4, 1, and 0.5 μm; along with the corresponding changes of the field enhancement factor β and emitter density (b), and current density (c) as a function of the distance.

---

of the β-factors is necessary to obtain homogeneous high currents over a large anode. We have shown experimentally and theoretically that the density of the nanotubes plays a crucial role for the FE properties. CNT films of low density yield low currents essentially because the emitter density and the β-factor are low. For high density films, screening effects reduce the field enhancement and thus the emitted current. For films of medium density, there is an ideal compromise between the emitter density and the intertube distance, which is sufficiently large to avoid screening effects. A better control of density and morphology (and hence of the β factors) of the films is thus clearly required for future applications. Our calculations predict that an intertube distance of about 2 times the height of the CNTs optimises the emitted current per unit area. For straight tubes of 1 μm height, this would correspond to an ideal density of $2.5 \cdot 10^7$ emitters/cm^2, or equivalently to ~625 emitters per 50×50 μm^2 pixel.

This work was supported by Motorola and NFP 36 of the Swiss National Science Foundation.

References for 2.3

[1] C.Wang, A.Garcia, D.C. Ingram, M. Lake, M.E. Kordesch, Electron. Lett. **27**, 1459 (1991).

[2] G.A.J. Amaratunga and S.R.P. Silva, Appl. Phys. Lett. **68**, 2529 (1996).

[3] O.Gröning, O.M. Küttel, P.Gröning and L.Schlapbach, Appl. Surf. Sci. **111** 135 (1997).

[4] M.W. Geis, J.C.Twichell and T.M. Lyszcyarz, J. Vac. Sci. Technol. **B14**, 2060 (1996).

[5] J.E. Jaskie, MRS Bulletin **21**, 59 (1996).

[6] R.L. Fink, Z. Tolt, Z. Yaniv, Surface and Coatings **108-109**, 570 (1998).

[7] O.Gröning, O.M. Küttel, P.Gröning and L.Schlapbach, J. Vac. Sci. Techol. **B17**, 1064 (1999).

[8] J.-M. Bonard, J.P. Salvetat, T. Stöckli, W.A de Heer, L. Forró, A. Châtelain, Appl. Phys. Lett. **73**, 918 (1996).

[9] S. Fan, M.G. Chapeline, N.R. Franklin, T.W. Tombler, A.M. Cassell, H. Dai, Science **283**, 512 (1999).

[10] Z.F. Ren, Z.P. Huang, D.Z. Wang, J.G. Wen, J.W. Xu, J.H. Wang, L.E. Calvet, J. Chen J.F. Klemic, M.A. Reed, Appl. Phys. Lett. **75**, 1086 (1999).

[11] J.E. Jaskie, private communication.

[12] H. Kind, J.-M. Bonard, C. Emmenegger, L.O. Nilsson, K. Hernadi, E. Maillard-Schaller, L. Schlapbach, L. Forró, K. Kern, Adv. Materials **11**, 1285 (1999).

[13] H. Kind, J.-M. Bonard, L. Forró, K. Kern, K. Hernadi, L.O. Nilsson, L. Schlapbach, unpublished (2000).

2.4 Characterization of thin film electron emitters by scanning anode field emission microscopy

L. Nilsson, O. Groening, P. Groening, O. Kuettel and L. Schlapbach
Institute of Physics, University of Fribourg, Pérolles, CH-1700 Fribourg, Switzerland

Accepted for publication in Journal of Applied Physics (2001)

Abstract

Scanning anode field emission microscopy (SAFEM) is used to map the electron emission current I(x,y) under constant anode voltage and the electron extraction voltage V(x,y) under constant emission current as a function of tip position on carbon based thin film emitters. The spatially resolved field enhancement factor β(x,y) is derived from V(x,y) maps. It is shown that large variations in the emission site density (ESD) and current density, can be explained in terms of the spatial variation of the field enhancement β(x,y). Comparison of β(x,y) and I(x,y) show that electron emission currents are correlated to the presence of high aspect ratio field enhancing structures.

We introduce the concept of the field enhancement distribution f(β), which is derived from β(x,y) maps to characterize the field emission properties of thin films. In this context f(β)·dβ gives the number of emitters on a unit surface with field enhancement factors in the interval [β, β+dβ]. It is shown experimentally for the investigated carbon thin film emitters, that f(β) has an exponential dependence with regard to the field enhancement factor β. The field enhancement distribution function f(β) can be said to give a complete characterization of the thin film field emission properties. As a consequence, the emitted current density and ESD can be optimized by tuning f(β) of the emitting thin film.

Keywords: Field enhancement distribution, microscopy, carbon, nanotubes

2.4.1 Introduction

During the last decade chemical vapor deposition (CVD) diamond, diamond like carbon (DLC) and nanotube (CNT) [1] thin films have met a great deal of interest due to extraordinary low-field electron emission (FE) [2–6]. Carbon-based thin film cold cathodes could prove to be advantageous over classical field emitter arrays (FEA's) [7, 8] due to potentially simpler and cheaper cathode design. Field electron emission occurs due to quantum mechanical tunneling of electrons from a solid into vacuum and becomes apparent only at high electric fields on the order of 3000 V/μm [9]. Due to the high electric field, the surface potential barrier, which confines the electrons within the solid, is lowered and becomes triangular in shape. As the width of the surface potential barrier at the Fermi energy approaches 2 nm, electrons will have a non-negligible probability to tunnel from the highest occupied states of the solid into vacuum. In order to create the fields necessary for FE, the field enhancing effect of tip-like structures is exploited. In the first approximation such field enhancing structures (FES), amplify the applied field E_a by a factor (beta) β, which is of the order of the aspect ratio h/r of the FES. h is here the height of the tip and r the radius of curvature of the tip apex. E_a represents the global or overall electric field, applied between the anode and the cathode in a typical FE experiment. The amplified field E_{site} at the tip apex of the FES is given by $E_{site}=\beta \cdot E_a$. As the emission current from a single FES is limited to a few nA up to μA, the success of gated field emission electron sources lies in the integration of a large number of FES confined to small μm-sized areas. For several years etched silicon or evaporated metal micro tips, produced by conventional lithographic patterning techniques, have been used as FEA's [10–12]. The fabrication of such micro tips however, requires expensive processes. The tips suffer from emission degradation caused by sputter erosion or chemical contamination and therefore require a high vacuum environment for operation [6,9]. For this reason there is a strong incentive to simplify both the production and design of the cathode in FEAs and carbon based thin film emitters. A thin planar film, emitting at exceptionally low applied fields below 20 Vμm^{-1}, not spot-wise but homogeneous over the entire film surface would invoke a number of technological advantages in FEAs. Current generation of micro tip based FED require ~70 Volts gate-to-cathode bias for operation [13]. A reduction of this driving voltage, achievable with low electric threshold thin film emitters, would lead to lower driver costs and reduced power consumption. Compared to silicon or metal micro tips a flat, homogeneously emitting thin film would be less sensitive to sputter erosion. Since the typical gate-cathode separation as compared to conventional cathodes can be increased, the capacitance and therefore the switching time could be reduced. Homogeneous electron emission from the entire thin film surface would further reduce the power dissipation and joule per unit area (u.a) heating of the surface, as compared to micro tips which can become disrupted and blunted [11]. DLC and CVD diamond thin films, exhibiting e.g. the negative electron affinity [14, 15] property, were thought to deliver such thin film emitters. However it is shown in a number of works that the emission mechanism of carbon-based thin films seems to be Fowler-Nordheim (FN) tunnelling like, due to field enhancement β from μm- and nm-structures [16–18]. In addition it has been shown that sp^2 rich thin films are favorable for efficient FE [19–22], and that the FES therefore can be graphitic structures on the thin film surface [23] or sp^2 conducting channels inside an isolating sp^3 matrix [18]. Thus from a physical point of view, the carbon-based thin film emission is analogous to the classic tip array emission, where FES like e.g. carbon nanotubes, sharp whiskers or protrusions are responsible for amplifying the applied field to cause sufficiently large microscopic fields to promote FE. However unlike the well ordered micro tip arrays, the FES of thin electron emitting films exhibit a stochastic nature, with regard to the field enhancement factor. The ideal FEA is thought to have a narrow Gaussian distribution of aspect ratios where the distance between every tip can be controlled with rather accurate precision even in the sub-μm range. In contrast to the micro tip arrays, the thin film FES are randomly distributed with a large variation of field enhancing factors β. The random spatial distribution and large spread in β values of the FES on thin emitting films are problems of technological importance, as they strongly influence the homogeneity of the field emission current. Therefore, in order for a gated FEA to have uniform emission intensity (e.g. in a field emission flat panel display (FED)), every sub-pixel must be made up of a large number of FES. Additionally the variation of the aspect ratios within and between different sub-pixels must not be too high, due to the steep current-voltage characteristics of the FN tunnelling. Consequently the FES has to be deposited in a controlled manner [24–30] confined to well defined patterns in the μm range, preferably inexpensive and over large area substrates. Clearly, since the field enhancing properties such as the ESD are crucially determined by the random distribution of β values, we need to characterize the spatial field enhancing properties β(x,y) of the thin film emitter, in order to optimize the ESD. To optimize the ESD, the FES spatial distribution has to be microscopically monitored. To do that we have developed a scanning anode field emission technique.

2.4.2 Basic considerations

To start our general discussion on the field emission behavior of thin film emitters we first have to find a realistic description of the emission current I of a single emitter as a function of the local electric field E$_{site}$ at the emission site. Field emission spectroscopy on carbon thin film emitters such as CVD diamond, DLC and nanotube thin films has shown that the emission from these carbon based emitters is due to FN-tunnelling at local electric fields E$_{site}$ on the order of 3000 Vμm^{-1} or more and with typical emitter work functions ϕ around 5 eV [31]. Based on this finding we assume that the current-field characteristic of a single emission site obeys the Fowler-Nordheim law [9]:

$$I = A \cdot \frac{1.56 \cdot 10^{-6}}{\phi t^2(y)} E_{site}^2 \exp\left(\frac{-6.83 \cdot 10^7 \phi^{1.5}}{E_{site}} \cdot v(y)\right) \tag{1}$$

with

$$y = \sqrt{\frac{e^3 E_{site}}{4\pi\varepsilon_0\phi^2}}$$

I is the emission current in ampere [A]. A in [cm^2] denotes the pre-exponential factor, ϕ [eV] the emitter work function and E$_{site}$ [Vcm^{-1}] the local field at the emission site. The expressions t(y) and v(y) are the Nordheim elliptic functions, which can be approximated by $t^2(y) \simeq 1.1$ and $v(y) \simeq 0.95 - y^2$ [11].

Though A has the dimension of an area and theoretically only takes account of the emitting area, in experiment the pre-exponential factor A will also depend on the bandstructure of the emitter [32].

In order to describe the emission current I of a single emitter over a wide range of electric fields, we use the simplified FN-formula as proposed by Spindt et al. [11], where the elliptic functions v(y) and t(y) are approximated, as indicated above:

$$I = A \cdot \frac{1.5 \cdot 10^{-6}}{\phi} E_{site}^2 \exp(\frac{10.4}{\sqrt{\phi}}) \exp\,(\frac{-6.44 \cdot 10^7 \phi^{1.5}}{E_{site}}) \tag{2}$$

In order to account for experimentally observed emission currents of carbon thin film emitters, A takes values of 10^{-11}- 10^{-9} cm^2. A value of 5.0 eV seems reasonable for the workfunction of carbon emitters, as indicated by photoelectron and field emission spectroscopy [16]. Putting A=10^{-9} and ϕ=5.0 eV in expression (2) gives us a relation for the emission current, which depends only on the local field E_{site}.

In a typical field emission experiment, the emission current is measured as a function of the bias voltage V between the anode and the cathode, and not directly with respect to the local field E_{site} at the emission site. For a given anode-cathode geometry a kind of global or average field can be determined. We refer to this field as applied field E_a hereafter. The applied field E_a is generally approximated for a planar diode electrode configuration by

$$E_a \simeq \frac{V}{d} \tag{3}$$

Where the V is the voltage between the anode and the cathode, and d is the anode-cathode distance. The local field E_{site} at the emission site depends linearly on the applied field with the field enhancement β as the proportionality factor.

$$E_{site} = \beta \cdot E_a \tag{4}$$

It has to be stressed that effects like space-charge or current saturation can lead to deviation from this linearity, but only for very high emission current densities. As indicated earlier β depends on the geometry of the FES and may take values of several hundred in case of a good emitter. By substituting (4) into (2) we note that for a constant applied field E_a, the emission current I depends dominantly on the field enhancement factor β, since the FN expression (1) and (2) only depends linearly on the pre-exponential factor A and the workfunction ϕ is approximately constant. A small variation of ϕ may occur due to adsorbates as observed in field emission microscopy (FEM) [33–35]. β goes however into both the quadratic as well as the exponential factor of expression (2). The relative change of the emission current dI/I as a function of the relative change of the field enhancement $d\beta/\beta$ can be calculated from (2), where ϕ is taken to 5.0 eV:

$$\frac{dI}{I} = (2 + \frac{6.15 \cdot 10^8}{E_a \cdot \beta})\frac{d\beta}{\beta} \tag{5}$$

We see that the emission current I is strongly depending on β. If we take one single FES with field enhancement 150, which is subjected to E_a= 22 Vμm^{-1} as an example:

$$\frac{d\beta}{\beta} = 1\% \qquad \Rightarrow \qquad \frac{dI}{I} = 21\%$$

Consequently a small variation or increase of β has a strong impact on the current and a "good" emitter is thus characterized by a high value of β. However, a high field enhancement factor β is not alone the only criteria of a good thin film emitter, as the emission properties (such as the ESD) are determined by an ensemble or a large number of emitters. Therefore we like to extend the discussion to the emission behavior of an ensemble of many parallel emitting structures randomly distributed on a surface. We assume that the emission current from all emission sites to a good approximation follows the FN tunnelling expression (2). Further we assume that all the emitters have the same work function (justified by the fact that the emitters are made of the same material) and that the emission area A is the same for all emitters (justified by the assumption that the emitters are of the same dimensions and that the emission current only depends linearly on A).

Under these assumptions and for a constant applied electric field E_a, the only remaining parameter determining the emission current is the field enhancement factor β at the location of emission on the thin film. The spatial distribution of the emission current I(x,y) and the ESD can be directly related to the spatial distribution of the field enhancement β(x,y). β(x,y) again is related to the topographic structure h(x,y) of the thin film emitter, and we may readily expect a scatter or spread in the field enhancement β depending on the position.

In this picture the field emission properties of a thin film emitter can be represented by the function f(β), where the number of emitter dN on a surface area A with field enhancement factors in the interval β to β+dβ is given by dN(β)=A·f(β)·dβ. As we will see later on, the function f(β) can be derived from the field enhancement map β(x,y). We define the f(β)-distribution, or for short the β-distribution, as

$$f(\beta) = \frac{1}{A}\frac{dN}{d\beta} \qquad [Emitter/cm^2] \tag{6}$$

According to the definition, f(β) is proportional to the probability of having a FES in the range β to β+dβ per unit area. Consequently one may view f(β) as a probability distribution. The measurement of the electric field (usually called threshold field), where a given threshold field emission current sets on, can be understood as measuring a threshold field enhancement β_{max}. With E$_{site}$=E$_{threshold}$ · β_{max}, where E$_{threshold}$ is the measured threshold field in the experiment and E$_{site}$ is the electric field at the emission site which generates the threshold current. Since f(β) and thus also A·f(β) can be appreciated as a probability function, the probability P(β_{max}) to observe the strongest emitter, i.e. dN(β_{max})= 1, in the window [β_{max}-dβ, β_{max}] is proportional to A·f(β_{max})dβ. Therefore we can expect to observe β_{max} with higher probability on a large surface area A. The threshold field will therefore decrease with increasing surface measured. The characterization of the emission properties of a thin film emitter just by stating the threshold field is thus limited, since anode-cathode geometry (and consequently E$_{threshold}$) differs from one experiment to another. We need other means and parameters of characterization.

Since the emitting site density (ESD) critically depends on β(x,y) and as we will see consequently on f(β), thin film emitters have to be characterized in terms of these two quantities and in the following section we will illustrate the impact of different β-distributions on the ESD. We use three computer simulated distributions with randomly distributed emission sites on a unit surface A=1 to illustrate the emission properties on a phosphor screen. We assume that the current from every site follows the FN expression (2) and that the total or integral emission current for the whole ensemble is kept around a constant value I$_{tot}$ close to 0.3 mA.

In the first example we assume that all FES have β values in a narrow range around a mean value β_0. One may think of such an ensemble of FES, as randomly distributed metal tips, with idealized field enhancement kept around an average value β_0. This corresponds to a gaussian β-distribution:

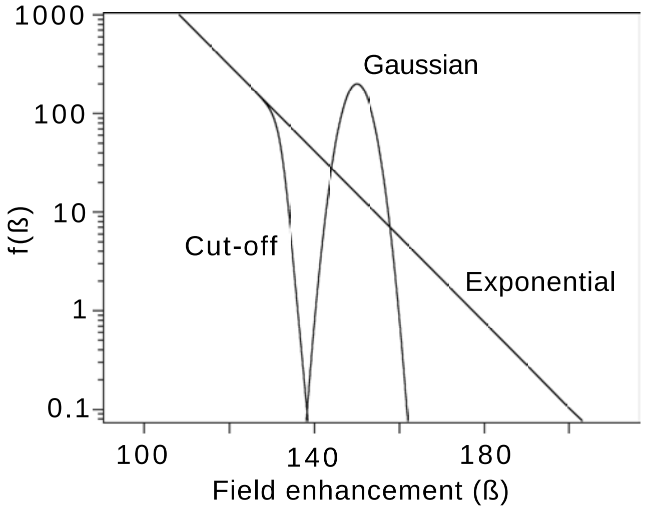

Figure 2.23: Simulation of three β-distributions. The Gaussian f(β) with idealized narrow spread of field enhancement values. The exponential f(β) with decreasing density of sites. The cut-off f(β) is obtained from the exponential distribution if the highest field enhancement FES are removed.

$$f(\beta) = 200\exp\left(-\frac{(\beta-\beta_0)^2}{18.02}\right) \qquad (FWHM = 10) \qquad (7)$$

The narrow shape of the gaussian β-distribution is shown in Fig. 2.23 and is thought of as being typical for randomly distributed metal cones with an average field enhancement β_0=150.

It should be pointed out that real metal FES have a much broader distribution and thus higher variation of $E_{threshold}$ between different tips. Therefore f(β) in equation (7) corresponds to an idealized β-distribution. Typical values of the simulation are:

Gaussian: E_a=21.25 Vμm^{-1} I_{tot}=0.304 mA

The resulting FE image is depicted in Fig. 2.24(a), where the level of the gray scale is linear between 0 to 0.9 mA/ unit area (u.a) and saturated white above. The situation depicted on the simulated screen in Fig. 2.24(a) resembles the ESD as obtained on an ordinary phosphor screen from a "good" thin film emitter.

In the case of a thin film emitter such as a nanotube thin film the situation may be different. Due to the random length and orientation of the tubes, there is a priori no reason to believe that the field enhancement is kept in a narrow β range or that the distribution function f(β) is gaussian. Consequently the gaussian distribution, typical of idealized metal tip emitters, is not likely to be a good description of such a kind of thin film emitter, since there is in general no pre-requisite that all aspect ratios of thin emitting films should be equal or even in the same range.

As β(x,y) depends on the surface topography h(x,y), an analogy to the surface roughness can be drawn. Atomic force measurements (AFM) have shown that surface roughness exhibits a power law dependence on the horizontal length scale on self-affine [36] thin films. In this picture the geometric shape of asperities can be described at all length scales in a fractal regime, normally limited by a transition length L_0, which demarcates two regimes of power law behavior [37, 38]. In such a case f(β) takes the shape of a function steadily decreasing with increasing β and we therefore assume an exponential β-distribution (with assumed constants) in analogy to the power law dependence of asperities on surfaces such as:

$$f(\beta) = 5 \cdot 10^7 \exp\left(-0.1\beta\right) \tag{8}$$

The exponential f(β) is shown in Fig. 2.23. Equivalently to the gaussian distribution, the emission behavior is simulated on a phosphor screen, Fig. 2.24(b). Typical values of the simulation are:

Exponential: E_a=20.10 Vμm^{-1} I_{tot}=0.294 mA

Note that although the applied field and the total emission current is about the same for the gaussian and the exponential β-distribution, the emission current is delivered only by a relatively small number of emission sites in the latter case.

Using the concept of the β-distribution, the ESD as a function of the applied field E_a can be written as:

$$ESD(E_a) = \int_{\beta_{min}=\frac{E_{thr}}{E_a}}^{\infty} f(\beta)\, d\beta \qquad [cm^{-2}] \tag{9}$$

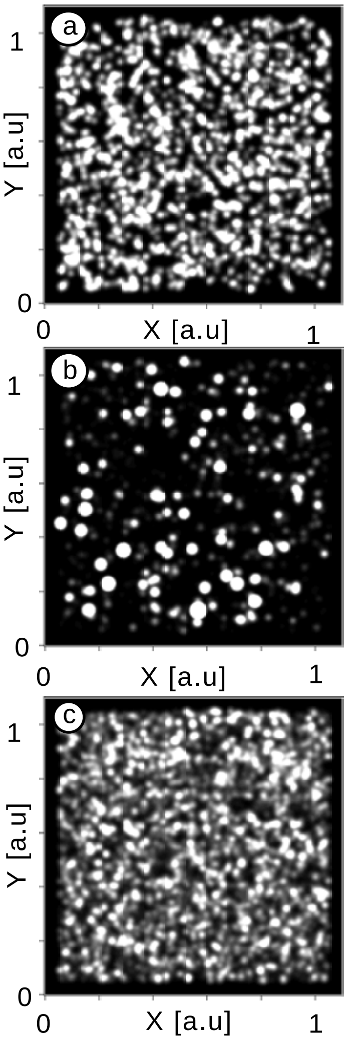

Figure 2.24: Simulations of the FE currents on a phosphor screen from randomly distributed FES with field enhancement according to (a) the gaussian f(β) equation (7) (E_a= 21.25 Vμm^{-1}), (b) the exponential f(β) equation (8) (E_a= 20.10 Vμm^{-1}) and (c) the cut-off f(β) equation (10) (E_a= 24.75 Vμm^{-1}). The total current amounts to ~0.3 mA in (a)-(c) and white corresponds to 0.9 mA/u.a. or more.

E_{thr} is the local field at an emission site required to produce a minimum recordable emission current I_{thr}. On a phosphor screen I_{thr} corresponds to the minimum emission site current, required for the eye to observe the emission spot. β_{min} corresponds to the lowest field enhancement value which can be detected at E_a, with regard to I_{thr}. Since the applied field E_a is constant this mode of operation is called the constant voltage mode (CVM). In the simulations a site becomes visible for $I_{thr} \simeq 1$ nA corresponding to $E_{thr} \simeq 3000$ Vμm^{-1}. The maximum E_a is restricted by the total current limit condition ~0.3 mA and since E_a only varies slightly between the two simulations, β_{min} is approximately the same for the gaussian (β_{min} ~141) and the exponential (β_{min} ~149) distribution. We obtain an ESD of 1500 sites/u.a (u.a = unit area) for the gaussian f(β) and 165 sites/u.a for the exponential f(β) according to expression (9).

The physical interpretation of the difference between the ESD of the gaussian and exponential f(β) is explained as follows. The exponential f(β) contains a small number of high field enhancement sites. These sites are not present in the gaussian f(β). The current-voltage characteristic of equation (2) is very steep and therefore the current from the high β sites is several orders of magnitude higher than from FES with lower field enhancement in the gaussian f(β). Since the total current is limited to 0.3 mA and the major part of the total current is delivered by the high β FES (which have a low density), the ESD of the exponential distribution is low. Hence the current load is very high for the high field enhancement FES and negligible for the low β FES. The gaussian f(β) in contrast, contains sites confined in a narrow β range. The small variation of the gaussian field enhancement leads to comparable turn-on fields and magnitude of emission currents from site to site. Since the density of sites in the gaussian range is high and all sites deliver currents of approximately same order of magnitude, the ESD is higher than for the exponential f(β). The current level per site is therefore lower in the case of the gaussian f(β).

We will show later that the emission characteristics of typical thin film emitters in fact are due to an exponential β-distribution. This leads to the paradoxical conclusion that the ESD for a real electron emitting film is limited by a small number of high field enhancement emitters. By a small number we refer to a density of FES $\leq 10^4$ cm^{-2}, namely those sites spotted on a phosphor screen. In order to make the homogeneity of FEAs sufficient for application in e.g. flat panel displays, we want primarily to increase the ESD up to at least 10^6-10^7 emitting sites per cm^2 [13]. A higher density of tubes (assumed at least 1 μm long) is not recommended since electrostatic screening effects become dominant for densities above 10^8 cm^{-2} [27]. One approach to achieve higher ESD would be to eliminate or burn the high β sites, e.g. through high currents. Once eliminated, they do not obstruct the emission from sites with lower β and higher density. The distribution one may obtain through the high β emitter elimination, is actually a modified exponential β-distribution, which we refer to as "cut-off". An example of such a cut-off distribution is shown in Fig. 2.23 and is given as:

$$f(\beta) = 5 \cdot 10^7 \exp(-0.1\beta) \frac{1}{1 + \exp(\beta - 132)} \tag{10}$$

Emitters in the range $\beta \in$ [140,200] have been eliminated, or "burned" by high current levels. Since the strongest sites are removed, the applied field must be increased as compared to the exponential distribution for the total current to remain approximately 0.3 mA:

Cut-off: E_a=24.75 Vμm^{-1} I_{tot}=0.292 mA

Since E$_a$ is increased, $\beta_{min} = E_{thr}/E_a \simeq 121$, is shifted towards lower field enhancement and thus a higher density regime of FES. The result is a simulated current map I(x,y) with higher ESD (~1850 sites/a.u.) and homogeneity (Fig. 2.24(c)) than the original exponential distribution.

If we return to the initial question whether a "good" emitter only is characterized by the field enhancement, we see that the response depends to a great extent in which way the emission source is intended to be used. If only one single emitter is needed, e.g. in a scanning electron microscope where a high brilliance electron source is desirable, it is clear that a high field enhancement will reduce the driving voltage. If many parallel electron sources are required, like in a FEA, the homogeneity of the emission will be equally important. The trade-off between the driving voltage and the homogeneity is determined by the application.

As shown in the simulations, the knowledge of the β-distribution f(β) gives an almost complete characterization of the FE behavior of thin film emitters. Therefore the experimental characterization of such films should include the determination of f(β). f(β) can be obtained from the field enhancement map β(x,y), where every point x,y on a thin film can be assigned a field enhancement value. In theory β(x,y) can be calculated from the topography of a surface h(x,y), e.g. by solving the Poission equation at the surface. However in a general case of a thin emitting film, we do not know the solution to the Poission equation and have to resort to other methods of deriving β(x,y). Through relation (2), β(x,y) is directly related to I(x,y). The measurement of I(x,y) could theoretically be used to calculate β(x,y).

Scanning anode FE measurements, with a constant voltage applied to the anode, can be used to obtain a spatially resolved FE current image I(x,y) with $\sim \mu$m resolution. The sequentially obtained current is recorded with a source measure unit, which has dynamic measurement range from a few pico-ampere up to milli-ampere. Consequently, by recording the FE current, point-by-point, one is in principle able to re-calculate the β value of every point from equation (2). However since the anode is located very close to the surface, the variation in the surface roughness and the local field enhancement causes the applied field to fluctuate several times from one site to another. Such a change of the electric field causes the emission current to fluctuate several orders of magnitude into a regime of resistor limited emission and emitter degradation. Since a β re-calculation based on expression (2) does not include resistor limited emission, we cannot use I(x,y) to calculate β(x,y).

In order to derive β(x,y) and avoid current saturation effects, not to say emitter destruction, the scanned electron emission has to be performed in another mode of operation, which we call the constant current mode (CCM). In CCM the voltage V applied to the anode is changed as a function of anode position over the thin film surface, in order to maintain the same emission current for every point. If the current is reasonably low, like 50 nA, we will obtain a spatially resolved FE image of the extraction voltage V(x,y), without current saturation effects or emitter destruction. This is both experimentally and conceptually beautiful since V(x,y) is actually an inverted image of the field enhancing landscape β(x,y). This can be realized if we use the approximation (4) of the applied field E_a=V/d, where d is the anode-cathode distance and get $E_{site}=\beta \cdot V/d$ for the field at the emission site. As energy resolved FE measurements from thin emitting films have shown, an emission current of 50 nA approximately corresponds to an electric field E_{site}= 4000 Vμm^{-1} at the tip apex of the emitting structure [16]. Therefore, since the current I to a good approximation dominantly depends on β according to expression (2), the field enhancing landscape β(x,y) is calculated:

$$\beta(x,y) = \frac{d \cdot E_{site}}{V(x,y)} \tag{11}$$

where both d and E_{site} are constants. If the β(x,y) map contains N(β) number of peak values (where β is the corresponding field enhancement factor) and A is the scanned surface area, f(β) can be calculated according to definition (6). Note that several assumptions are involved in the calculation of expression (11). First, the applied field has been approximated for a planar diode configuration. In reality the field lines are concentrated at the anode as compared to a planar configuration, since the anode radius of curvature R $\leq$ d. This leads to a slight overestimation of the applied field up to a factor 1.5, and the field enhancement is accordingly underrated. Second, the anode-cathode distance d is not constant, but varies with the surface roughness. The surface roughness peak-to-peak is estimated to 4 μm on a length scale of 20 μm. If the average d= 7 μm , we can expect d to vary between 5 and 9 μm, i.e in the interval [$\frac{5}{7}$d, $\frac{9}{7}$d]. Therefore if the real distance is d*=d*(x,y) corresponding to a real β^* at position (x,y), the calculated $\beta \in [\frac{7}{9}\beta^*, \frac{7}{5}\beta^*]$. It is however reasonable to believe that roughly 50 % of the FES are recorded at a distance d $\in [\frac{5}{7}d$, d] and the other half in [d, $\frac{9}{7}$d]. Consequently if a sufficiently large number of FES, e.g 6 or more, are recorded in $[\frac{7}{9}\beta^*, \frac{7}{5}\beta^*]$, it can be argued that the average field enhancement β of these sites is well approximated by expression (12). This is an important remark, since on a statistical basis, fluctuations in β do not affect the shape of the distribution function f(β). Finally we note that in our fundamental assumption of expression (2), the workfunction ϕ is assumed to be 5 eV similar to graphite. This is true in the case of a nanotube film as long as the typical diameter of the CNTs does not become comparable with the typical tunneling length 2 nm, which is the case for single walled nanotubes (SWNT). Field emission microscopy reveals also that the emission current from a single site is divided into time varying lobed patterns [33–35]. Such spatial current variations can be explained in terms of adsorbates which changes either the field enhancement or the workfunction ϕ localized at the position of the adsorbate. As a consequence the electric field E_{site} required for a constant emission current I per site, may vary slightly from one site to another. It can be evaluated for a constant current I= 50 nA that if the workfunction is changed by 10 % due to adsorbates, i.e. from 5.0 to 4.5 eV, the calculated field enhancement varies by 14-15 %. Hence the true field enhancement $\beta^* \in [0.85\times\beta,\ 1.15\times\beta]$ if we assume a workfunction variation of 10 %. Again, if a sufficiently large number of sites are recorded in the interval $[0.85\times\beta,\ 1.15\times\beta]$, we may expect the average field $E_{site} \simeq 4000$ Vμm^{-1} and the calculated average field enhancement $\beta=\beta^*$. A variation of 10 % of ϕ does thus not affect the shape of the distribution f(β).

Scanning anode FE in CCM is attractive because it is non-destructive with a high spatial resolution compared to the phosphor screen. Nevertheless the phosphor screen can be used to obtain complementary information about the β-distribution in a higher range of field enhancement. Since f(β) is connected to the ESD through expression (9) we have the possibility to calculate f(β) by taking the derivative of the ESD on a phosphor screen. According to expression (4) we can write $E_{thr} = \beta \cdot E_a$ where $E_{site}=E_{thr} \simeq 3700$ Vμm^{-1} is the threshold field needed to produce an emission current of 10 nA, where 10 nA is the current which is required for an emission site to be recorded, i.e. to be visible, and to contribute to the ESD on the phosphor screen. Therefore we take the derivative of the ESD=ESD($E_a(\beta)$) and of expression (9) to obtain

$$f(\beta) = \frac{dESD}{dE_a}\left(\frac{E_{thr}}{\beta^2}\right)\Bigg|_{E_a=\frac{E_{thr}}{\beta}} \tag{12}$$

Depending on the efficiency of the phosphor and the operating voltage, the current needed to produce a visible spot on the screen may vary slightly between different phosphor screens. $E_{thr} \simeq 3700$ Vμm^{-1} is only marginally affected due to the very steep current-voltage characteristics of expression (2) and different phosphor types do not change the characteristics of expression (12).

The high ESD range ($> 10^4$ cm^{-2}) is difficult to explore with the phosphor screen due to annoying micro discharges caused by the high β emission sites. Since the probability of a small number of very strong, i.e. very high field enhancement FES, is higher on a large than a small sample area, the applied field E_a can normally not be increased above 10 Vμm^{-1}. As a consequence the phosphor screen is limited to the low electric field range, where only a minority of the sites in the high field enhancement regime can be investigated. Additionally an ESD higher than $\sim 10^4$ cm^{-2} is difficult to resolve on the screen due to overlapping emission spots. In order to investigate the FE behavior of the inactive majority of FES, the emission must be performed in CCM. Furthermore, to overcome the problems of limited resolution, scanning anode FE is a better option than FE with a screen in CVM. Nevertheless FE with the phosphor screen is a valuable tool, first because it provides additional information about f(β) which allows us to double check the results from the scanning anode FE measurements in CCM, and second because it is easy from an experimental point of view.

In the remaining part of this paper we will concentrate on measurements of β(x,y) and calculations of f(β). We will show that spatial variations in the current I(x,y) are directly linked to the spatial field enhancement β(x,y). Finally we will give experimental evidence, that the ESD is linked to the shape of the f(β)-distribution, and that the electric threshold E_{thr} in traditional diode-type FE experiments, indeed is by itself a poor parameter as a quality mark of the emitting properties of thin film emitters.

2.4.3 Test samples and experimental set-up

Two carbon thin films (sample A and sample B) were deposited by hot filament assisted chemical vapor deposition (HFCVD) onto a metal- coated ceramic substrate. A hydrogen/methane gaseous mixture was introduced into a reactor chamber and activated by hot filaments. Process parameters such as filament and substrate temperature, gas flow rate and gas composition were carefully monitored during the growth process to obtain films with good electron emission properties. Scanning electron micrographs of the samples are shown in Fig. 2.25.

The overall surface topography on a length scale of tens of μm is given by the ceramic substrate and is therefore not very different between the samples, with a typical roughness ~5 μm peak to peak. The field enhancement is however most probably created by different types of field enhancing structures on the samples. On sample A we observe a small number of particles covered by coralline like carbon structures, which exhibit sharp whiskers in the sub-μm range, Fig. 2.25(c). The coralline structures are not observed on sample B, where carbon nanotubes are present instead. The carbon nanotubes (CNT) can be several μm long with an average diameter of 20 nm. The coralline particles are sparely common on sample A, as compared to the CNT density on sample B.

The samples were investigated by means of a vacuum FE apparatus operating

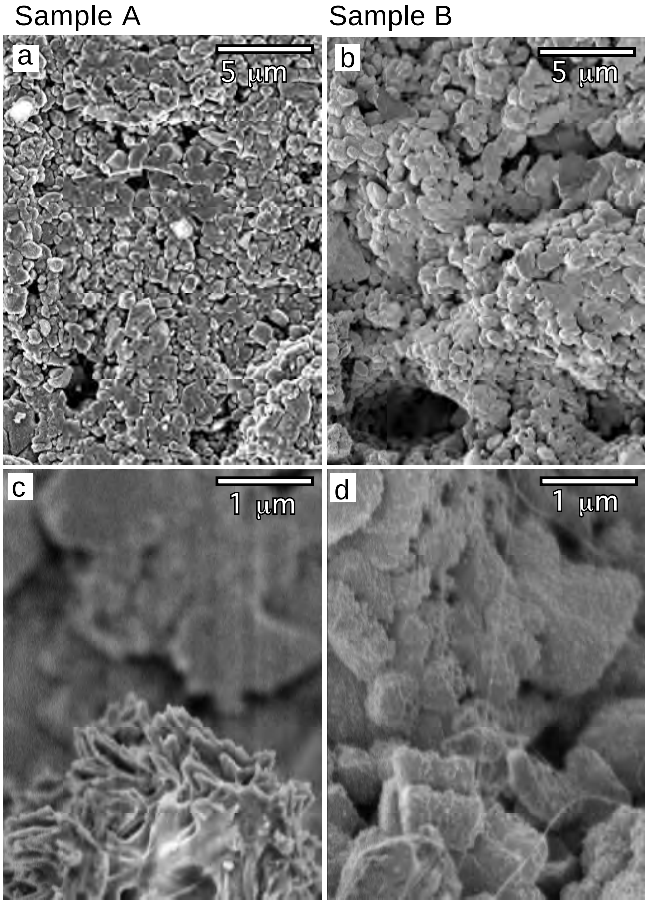

Figure 2.25: SEM of (a) sample A and (b) sample B shows a rough topography due to the ceramic substrate. The white bar in (a) and (b) is 5 μm, in (c) and (d) 1 μm. Sample A (c) and sample B (d) exhibit structural differences on a sub-μm scale including different carbon allotropes. Sample A has isolated carbon nanocoralline like particles with sharp whiskers, which does not seem to be present on sample B. Sample B is instead covered by carbon nanotubes (CNTs) with an average inter-tube distance of 30-50 μm.

---

at a typical base pressure of 10^{-7} mbar. Macroscopic or integral emission behavior was investigated using a phosphor screen diode type set-up (see Fig. 2.26). Integral FE can be understood as parallel electron emission from a large number of FES on the thin film surface, while applying a constant voltage of 3000 Volts to a phosphor screen. The ESD and the current was recorded as a function of the applied field from a ~cm^2-sized thin film emitter, kept at ground potential. The applied field is defined as the voltage V divided by the sample-screen separation

d. By keeping the voltage constant and changing the sample-screen separation d, artifacts due to the voltage dependent efficiency of the phosphor screen and due to spacer leakage currents were avoided.

FE on a microscopic level was performed with a scanning anode field emission apparatus, Fig. 2.26(a). The sample was mounted on a computer controlled piezo driven x/y-translation stage and a tip Pt-Ir anode (tip radius of $\sim$5 μm) was approached to the sample in steps of 100 nm, and thereafter held at a constant height d. The tip height d is chosen larger than the surface roughness of the sample under investigation, typically $\sim$ 10 μm. The tip-sample distance can be changed without hysteresis. The FE current I(x,y) or the extraction voltage V(x,y) is recorded as a function of tip position with a Keithley 237 source-measure unit. We call the these two measurement modes of field emission Constant Voltage Mode (CVM) and Constant Current Mode (CCM). In CVM the applied voltage is kept constant (typically 100-300 Volts) and the measured FE current is recorded as I(x,y). In CCM the extraction voltage V(x,y) applied to the tip is adjusted between 0 - 1100 Volts depending on the tip position in order to maintain the FE current on a constant level, e.g. 50 nA. Sample areas of $200\times200\mu\text{m}^2$ up to 800×800 μm^2 were scanned with $\sim$5 μm resolution depending on the tip-sample separation. Tip re-positioning can be achieved with sub-μm resolution on a surface up to 5×5 mm^2. The level of the current noise was lower than 1 nA during scanning and contact currents could be distinguished from the FE current by a sudden current increase and saturation of the source-measure device. The measured samples in this paper does not show such contact currents.

2.4.4 Scanning anode field emission on thin film emitters

As discussed in the the earlier section it is the probability distribution of emitting sites on a thin film, called the β-distribution, which determines the emitting site density, electric threshold field and current per unit area. Therefore we first like to investigate the emission properties of sample B in order to derive f(β) and to compare the emission in CVM and CCM using scanning anode FE.

An area of 800×800 μm^2 on sample B was scanned at a constant anode-sample distance d $\sim$16 μm, with an applied voltage of 320 Volts (E_a $\sim$ 20 $V\mu m^{-1}$). Figure 2.27(a) and (b) shows the resulting I(x,y) map obtained under these conditions, where the intensity is displayed in (a) logarithmic and (b) linear

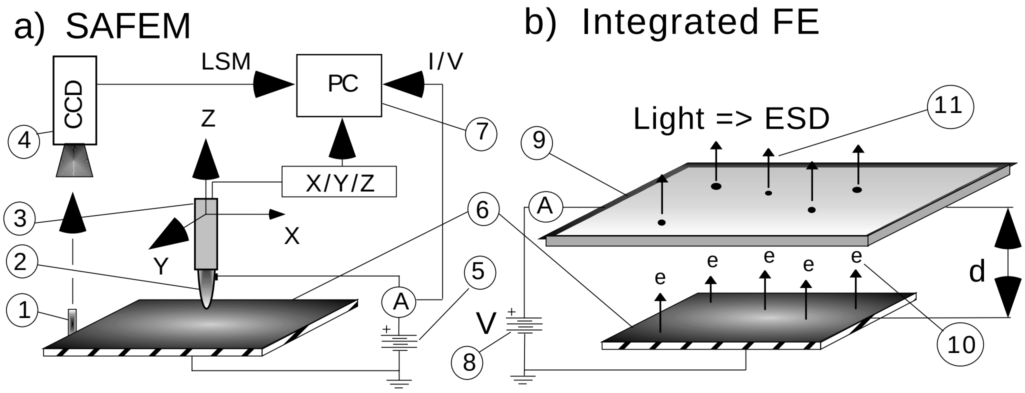

Figure 2.26: FE apparatus: a) Scanning Anode Field Emission Microscope b) Integratal field emission with a phosphor screen. 1) Reference light source for sample positioning. 2) x/y/z-movable scanning FE Pt-Ir tip (radius ~5μm). 3) x/y/z piezo step motors. 4) Charge coupled device (CCD) camera for motion monitoring. 5) Source-measure device (1100 Volts/10 mA). 6) Carbon thin film emitter. 7) Computer-controlled sample motion, current (A) and voltage (V) monitoring. 8) High Voltage Supply 3000 Volts. 9) Phosphor screen with variable separation d. 10) spot-wise electron emission. 11) Electron stimulated fluorescence of the phosphor screen ⇒ emission site density (ESD).

scale. It is interesting to note that the differences in detail between (a) and (b) are due to the choice of intensity scale. The current shows a large scatter between some $\sim$ nA/pixel, in the level of the noise, up to tens of μA. That is, the current ranges over about four orders of magnitude. four orders of magnitude current can easily be resolved on a logarithmic intensity scale, but not on a linear scale as on a phosphor screen. We calculate an emitting site density of $\sim 60{\cdot}10^3$ cm^{-2} for $E_a \sim 20$ Vμm^{-1}.

The advantage of the SAFEM is thus that we are not only able to determine the ESD with higher resolution and at higher fields, but moreover the dynamic range of the detected emission current is larger as compared to a phosphor screen. Keep in mind that an applied field of ~ 20 Vμm^{-1} during scanning in CVM, is likely to destroy several high β sites due to elevated current levels. Consequently the I(x,y) map is not trusted for calculation of β(x,y). Instead we derive β(x,y) in the CCM without emitter destruction and correlate the individual peaks in the I(x,y) and β(x,y) maps. Such a comparison enables us to estimate at which current levels the current saturation in fact occurs. We will see that current

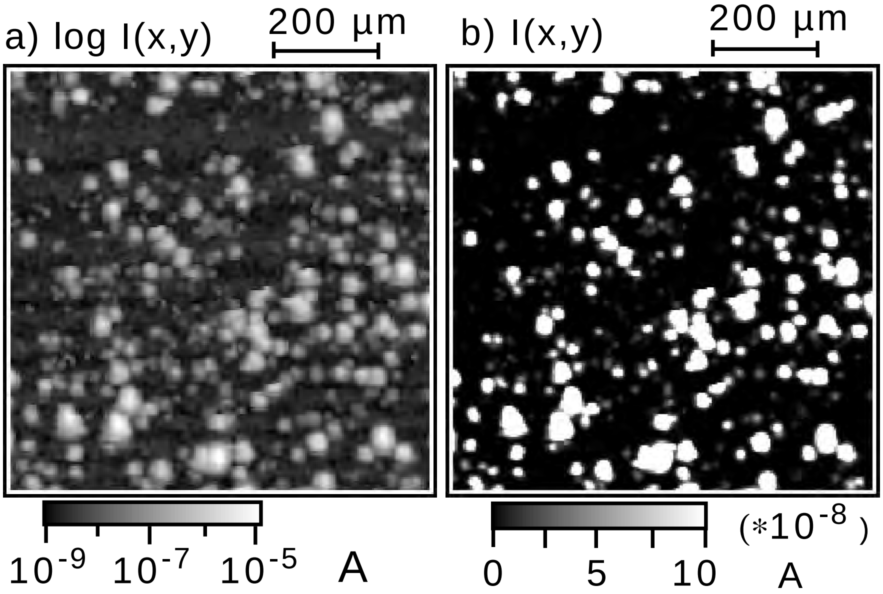

Figure 2.27: The spatially resolved emission current I(x,y) on sample B for (a) logarithmic and (b) linear intensity scale. (a) Weak emitters are observed due the dynamic logarithmic range, but since the ESD normally is calculated using a linear intensity scale, the log-image is not representable for a phosphor screen. (b) The intensity scale is cut above 0.1 μA, and emitters in the range 0.1 - 10 μA appears white saturated. The ESD$\sim$ 60 $\times$ 10^3 is calculated for $E_a \simeq 20$ V/μm.

---

saturation effects start already around 300 nA per site and become noticeable for applied fields ≥ 5 Vμm^{-1}.

Therefore we compare the β(x,y) map of the same emission area in Fig. 2.28(b) with the I(x,y) map of Fig. 2.27. The β(x,y) map was derived from the voltage map V(x,y) for a constant emission current of 50 nA, before the the current map I(x,y) was measured. The gray scale is linear in Fig. 2.28 and we note that V(x,y) is more circumstantial than I(x,y) on a linear scale. This is understandable if we consider that the current change dI inflicted by a change dβ in CVM is drastic, due to the steep I/V Fowler-Nordheim characteristics (see eq. (5)). However the voltage change dV in order to maintain a constant E_{site} of about 4000 V/μm for a change dβ is comparatively low. Thus $|\frac{dI}{d\beta}|_{V=const} >> |\frac{dV}{d\beta}|_{I=const}$ and the intensity of the I(x,y) map ranges over four orders in magnitude, whereas the β(x,y) map over less than one order. As a consequence on a linear scale the

β(x,y) image is indeed more circumstantial than the CVM map and very weak emitters, not detected in CVM, are recorded.

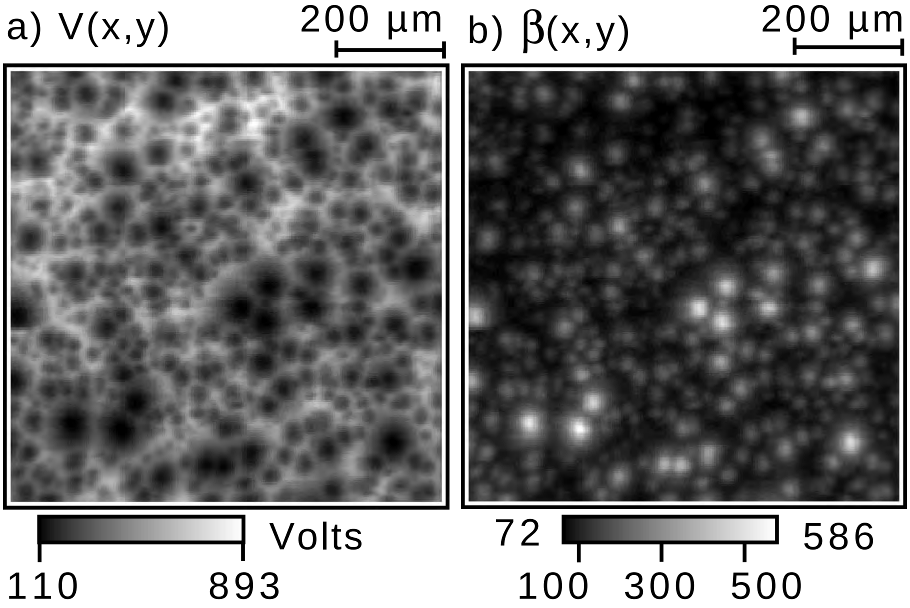

Figure 2.28: (a) The spatially resolved Voltage map V(x,y) and (b) the corresponding field enhancement β(x,y) map from the same scanned area as the I(x,y) map of Fig.2.27 on sample B. Correlation of peak positions in Fig. 2.27(a) and 2.28(b) shows that high local emission currents are connected to high local field enhancement β. The V(x,y) image was obtained for a constant FE current of 50 nA and a tip-sample separation d= 16 μm.

Nevertheless we clearly see that the images in Fig. 2.27(a) and 2.28(b) coincides quite well and that individual peaks in the current image can be assigned to the corresponding field enhancement counterpart. Remember that the two images are independently obtained. To complete the physical interpretation of I(x,y) and the β(x,y) map, we recall that β(x,y) is related to the topography h(x,y) in the high field enhancement range of the thin film, and we thus have:

$$h(x,y) \qquad \Rightarrow \qquad \beta(x,y) \qquad \Rightarrow \qquad I(x,y)$$

To evaluate the emission saturation we insert the measured field enhancement, obtained from the peaks in the β(x,y) map, into expression (2) for E_a= 20 Vμm^{-1}. The resulting FN current (diamonds) is displayed as a function of the field enhancement in Fig. 2.29. We see that the highest field enhancement $\beta \sim$

586, would give rise to FE currents in excess of 10 mA for E_a= 20 Vμm^{-1} according to (2). One may argue that 10 mA would create physically unrealistic high current densities at the emission site, and in fact the measured peak FE currents in the I(x,y) map, correlated with the corresponding β peak values (crosses in Fig. 2.29), are much lower. We see how the measured (crosses) current deviates from the calculated Fowler-Nordheim current (diamonds) above $\beta \sim 200$, and that the deviation starts in the range 100 to 300 nA. As a consequence the high emission current up to 13 μA, is a weaker function of the field enhancement than the corresponding Fowler-Nordheim curve above $\beta \sim$200.

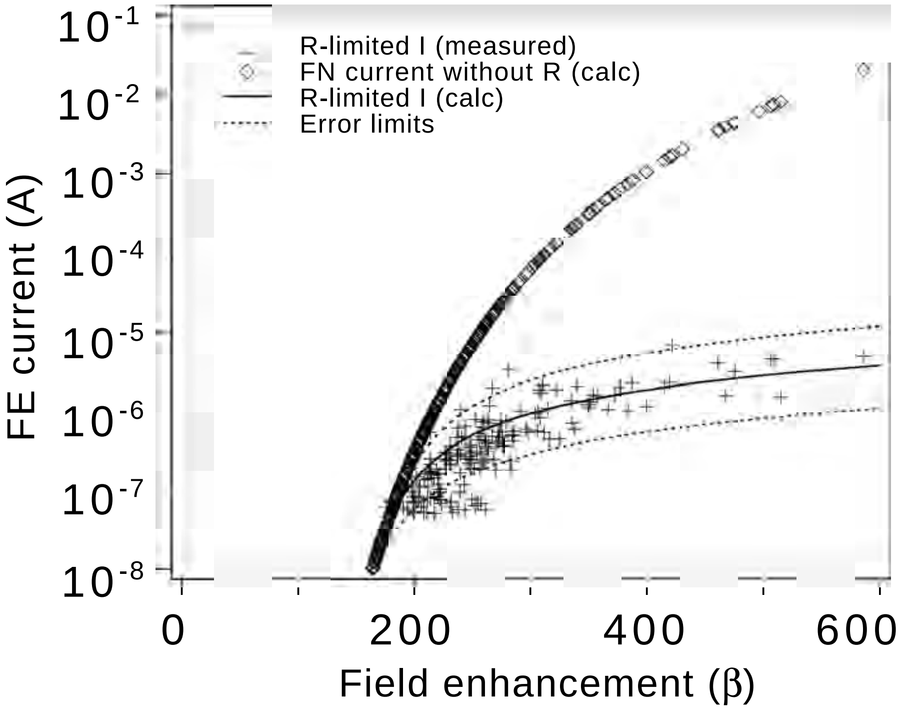

Figure 2.29: The measured (from the I(x,y) and β(x,y) maps) and calculated FE current for a constant applied field $\sim$ 20 Vμm^{-1} as a function of the field enhancement β. Comparison shows a deviation from the expected FN tunneling behavior due to current saturation effects starting around 300 nA. The saturation can be explained using the concept of a ballast resistor in serie with the FES (solid line).

The saturation can be explained in a resistor (R) limited emission model, where part of the applied voltage is lost over a resistor R in series with the emitter. The calculated R-limited emission current I can with good agreement be fitted to the recorded R-limited current I. The variation of the recorded FE current from the calculated R-limited current (up to 120 % as indicated by the error limits), is probabably mainly due to variations in the contact resistances between the emitting FES and the substrate. We also keep in mind that the R-limited emission model does not account for field penetration into the emitting FES.

The CCM resolves the problem of current saturation and emitter destruction with both experimental and conceptual ease, as the emission current can be fixed at values where current saturation does not occur. It now remains to exploit the β(x,y) map to find out exactly what the f(β)-distribution actually looks like. Our starting point must be definition (6), which tells us that we have to find the number of emitting FES dN in a small interval dβ. This information is contained in the β(x,y) map and may be obtained as a histogram. We process the β(x,y) map with home-made software which allows us to find and to localize the maximums (or peak values) of the field enhancement corresponding to single emitters. The peak values may be counted as N number of maximums and assigned the corresponding field enhancement value β. Additionally a histogram $\triangle$N as a function of β is obtained, where $\triangle$N is the number of peaks in the interval $\triangle\beta$, which equally is the bin width of the histogram. The amplitude of the histogram is however depending on the choice of bin width $\triangle\beta$, and to get the normalized distribution dN/dβ, $\triangle$N is divided by $\triangle\beta$. The normalized distribution dN/dβ equals the scanned area A times f(β) and the measured dN/dβ, is displayed for three scanned areas A_1, A_2 and A_3 as bars in Fig. 2.30 (Histogram H1, H2 and H3). A_1 equals $64\cdot10^{-4}$ cm^2 and is the area of the scan which is shown in Fig. 2.28. The scanned FE maps of A_2= $16\cdot10^{-4}$ cm^2 (~400 × 400 μm^2) and A_3= $4\cdot10^{-4}$ cm^2 (~200 × 200 μm^2) are not shown here, but are essentially very much alike Fig. 2.28. The number of FES is decreasing according to (6) if the surface A is decreasing, and this is observed in Fig. 2.30.

We are investigating the functional dependence of f(β) and the first observation we do, concerns the shape of dN/d$\beta \propto$ f(β), which at a first glance appears to have the shape of an asymmetric peak located at β value of 200. The apparent asymmetric behavior, most clearly evident from the histogram H1 (~800 × 800 μm^2), is however due to a measurement artifact. The true f(β) is a steadily, monotone decreasing exponential function, which (multiplied with the proper

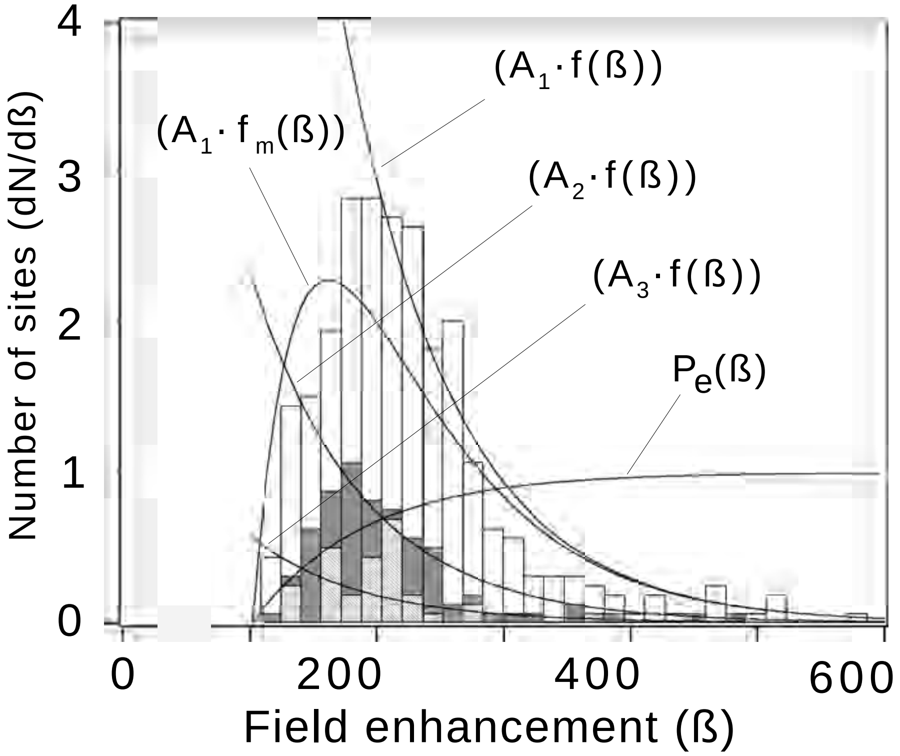

Figure 2.30: The number of peak values in three β(x,y) maps of surface area A$_1$= 64·10^{-4} cm^2, A$_2$= 16·10 $^{-4}$ cm^2 and A$_3$= 4·10^{-4} cm^2 has been counted as a function of the field enhancement and give three histograms H$_1$ (white bars), H$_2$ (dark grey bars) and H$_3$ (light grey bars). The negative slope of H$_i$ can be fitted with A$_i$·f(β), where i=1-3. FES with field enhancement below $\beta_{cut-off} \simeq 100$ are not recorded due to emission from adjacent sites with higher field enhancement. The low field enhancement cut-off of H$_1$ is simulated using the function P$_e$(β), where f$_m$(β)=f(β)· P$_e$(β) is the "as measured" β-distribution.

---

area A$_i$) can be fitted to the negative slope of each of the three measured histograms. In order to obtain reliable data we concentrate on the histogram H1 obtained from the FE map on ∼800 × 800 μm^2, since the number of peaks N and thus the statistical reliability is higher as compared to the other scans. We fit A$_1 \cdot f(\beta)$ to the negative slope of the histogram H1 and obtain:

$$f(\beta) = 4.6 \cdot 10^3 exp(-0.0115\beta) \tag{13}$$

The exponential dependence of f(β) is one of the main results in this paper, and it will be confirmed using the CVM technique in the next section.

The histograms H2 and H3 are also fitted with $A_2 \cdot f(\beta)$ and $A_3 \cdot f(\beta)$. The exponential dependence is confirmed, although as the area A is decreased, the quality of the statistics is reduced. The probability of finding dN FES in the interval dβ is increased if the scanned area A is enlarged and therefore we cannot expect the fit of H3 (where several bins are empty) to be as good as to H1. In this picture we realize that if we choose the scanned window sufficiently small, the field enhancement in the window is a strong function of where this window is measured and that f(β) indeed can be interpreted as a probability function.

There seem to be no emitter with β values below a cut-off field enhancement around $\beta \sim 100$. There is however no reason to believe that only high aspect ratio protrusions are present on the emitter surface. On the contrary, we may expect more low than high aspect ratio structures. The reason for the cut-off is that the weak emitters are concealed by the strong ones. As can be seen in Fig. 2.28(a) emission from the strong (high β) emitters occupy a larger emission spot surface than low β sites, i.e. strong sites are "seen" at a larger distance from the anode and thereby cover weak sites. In Fig. 2.31 the scale of field enhancement of the β map is chosen to maximum 200 and 150. The surface being covered by emission from FES with $\beta \geq 200$ is more than 50 % of the totally scanned area. We also see that the surface being covered by emission from FES with $\beta \geq 150$ is more than 90 % of the total scanned area. If the maximum of the field enhancement scale is set to 100, the scanned area is completely covered by emission, meaning no more available space for further emission spots from FES with $\beta < 100$. Consequently the field enhancement cut-off is approximately 100 and sites with $\beta < \beta_{cut-off}$= 100 are not recorded in the β-distribution. Aside from the field enhancement the spot size depends on the tip sample separation and the radius of curvature of the anode. Theoretically, if the tip could approach the sample more (without crashing) and if the radius of the tip is reduced, the cut-off limit may be reduced to lower β values.

We can quantitatively estimate the limit of resolution at which neighbor emission spots overlap by multiplying $A_1 \cdot f(\beta)$ with a probability factor $P_e(\beta)$. $P_e(\beta)$ converges towards 1 for high field enhancement since the probability of recording a high β value is high, and towards 0 for low $\beta \sim$100 since low field enhancement sites are "hidden" by other FES with higher field enhancement. We write the probability function as:

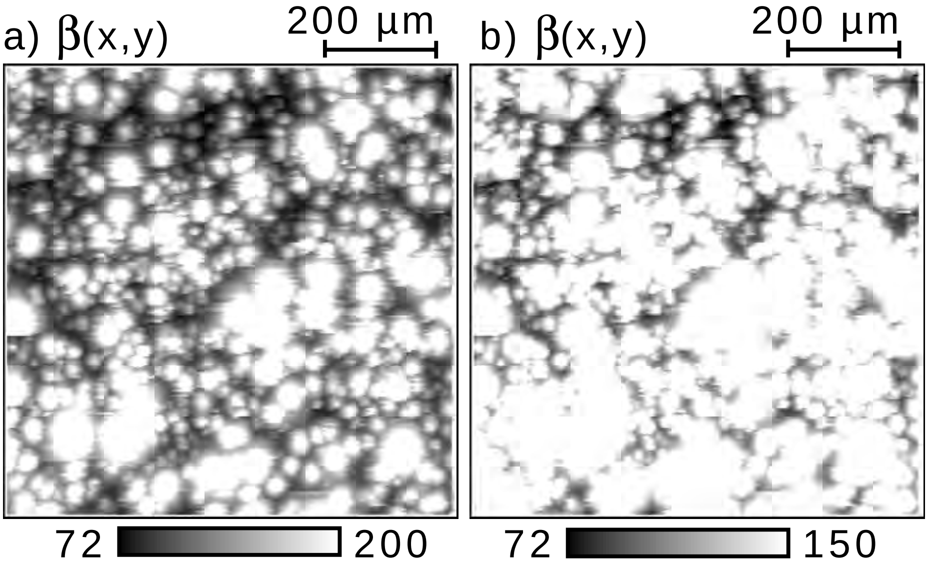

Figure 2.31: (a) and (b) shows the same β(x,y) map of sample B as in Fig. 2.28(b) but in different scales. White corresponds to emission spots from sites with field enhancement higher than (a) 200 and (b) 150. The β(x,y) map is almost completely covered by emission spots (white) if the scale of the maximum field enhancement is set to $\beta_{cut-off} \simeq 100$.

$$P_e(\beta) = 1 - \int_{\beta}^{\infty} f(\beta) A_0 \, d\beta \tag{14}$$

A_0 is the average area (spot size) at height d above the sample which is covered by emission from a single site. $P_e(\beta)$ is shown in Fig. 2.30 and inserting $P_e(\beta_{cut-off} = 100) = 0$, we obtain $A_0 = 7.9 \cdot 10^{-6}$ cm^2. The radius of A_0 is equally a measure of the resolution or cut-off radius $\sim$ 16 μm in the β map. This value is consistent with the average tip-sample separation, tip radius and surface roughness. We can now make a fit to the experimentally obtained histogram H1 according to:

$$(\frac{dN}{d\beta})_{measured} = A_1 \cdot f_m(\beta) = A_1 \cdot f(\beta) \cdot P_e(\beta) \tag{15}$$

Where $f_m(\beta)$ is the graph fitted to the experimental asymmetric gaussian-like β-distribution. The agreement between histogram H1 and $A_1 \cdot f_m(\beta)$ is reasonably good.

2.4.5 The CVM and the β-distribution

The β map and f(β) are obtained in the constant current mode without inflicting damage to the sample because the emission current is fixed at a constant level where no saturation occurs. In order to verify the results obtained for the β-distribution (13), we investigate the ESD with the phosphor screen in constant voltage mode. As a bonus f(β) can be investigated in a higher field enhancement range.

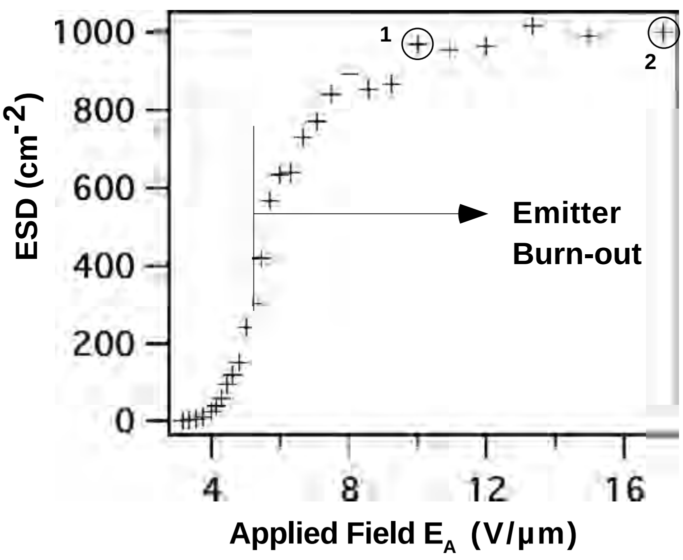

Figure 2.32: The emitting site density (ESD) as a function of the applied field E_a. The ESD does not increase exponentially above 5 V/μm since the sites are partly destroyed due to high current levels above 300 nA. Point 1 and 2 corresponds to the super-imposed images in Fig. 2.33

The ESD as a function of the applied field E_a for sample B is shown in Fig. 2.32. The ESD increases exponentially for low E_a, but remains almost constant for E_a >10 Vμm^{-1}. The flattening of the curve is not consistent with equation (13) without a proper explanation. We observed how some emission spots on the screen disappeared as the field E_a was increased. At the same time new spots turned on, but with less intensity. The newcomers are FES with lower β values than the initial emitting sites on the screen. The ESD remains therefore on a constant level for high fields E_a above 10 Vμm^{-1}.

If we subtract the FE image of the screen at 10 Vμm^{-1} from the image at

17 Vμm^{-1} (point 1 and 2 in Fig. 2.32), we obtain the super-imposed image of Fig. 2.33. White spots are new emitting sites that were not present at the lower field of point 1 but have arisen at point 2 due to the increased field. Dark spots are emission from FES that were present at point 1, but disappeared due to elevated current levels and emitter disruption as the field was increased. Since the highest aspect ratio FES deliver the highest currents in CVM, these are first destroyed or "burned". We appreciate that emitter burning starts for currents of 300 nA per site and upwards and that this effect is seen as a not exponential increase of the ESD for applied fields above 5 Vμm^{-1} in Fig. 2.32.

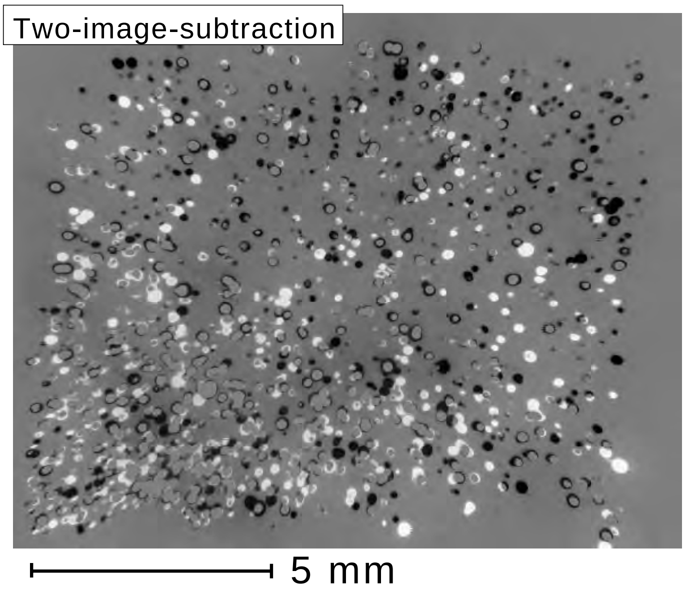

Figure 2.33: The image of the phosphor screen at point 1 (10 V/μm) has been subtracted from point 2 (17 V/μm) in Fig. 2.32, and white spots corresponds to emission sites, not present at point 1 but at point 2. Dark spots corresponds to sites which have disappeared due to emitter burn-out at higher fields. Therefore the ESD remains approximately constant for $E_a > 10$ V/μm.

Obviously we should not consider measurement points above 5 Vμm^{-1} when we calculate f(β) according to (11), since the measurement itself has modified the shape of f(β). f(β) is plotted as diamond dots in Fig. 2.34. The values start to deviate from the exponential slope at β= 740 due to emitter burning. The calculation of f(β) in the range $\beta \in [740, 1100]$ is done in the low applied field range, and does thus not suffer from measurement artifacts.

The β-distribution (histogram H1 normalized for one cm^2) measured in CCM with the SAFEM is shown as bars in Fig. 2.34. The fitted graph f(β) of equation (13) coincides with both histogram H1 (bars) and $f(\beta)_{screen}$ (diamonds). The agreement between the two independent experimental techniques is convincing, not only because the functional dependence of f(β) has been verified over nearly five orders of magnitude, but also because the exponential distribution seems to make good sense as emitter probability function. This observation is consistent with the surface roughness dependence in typical AFM measurements where a similar behavior with regard to the distribution of asperities can be shown. The resemblance in functional behavior of f(β) and the distribution of surface asperities is a strong circumstantial evidence that the reports on low threshold emission from carbon, convincingly can be explained in terms of field enhancement from an ensemble of protrusions and surface structures.

2.4.6 Comparison sample A and B

The deposition and growth methods of thin film emitters influence the FE behavior since more or less rough surfaces are produced as a function of the deposition parameters. Some emitter ensembles have a higher density of FES in the high field enhancement range than others and therefore different f(β). Such thin films may start to emit electrons at similar applied threshold fields (E_{thr} some few $\sim$Vμm $^{-1}$) but have different ESD due to different f(β). Differences in the FE behavior become more apparent the smaller the sample surface is. A small surface contains in general no exceptionally strong emission sites, because these are rarely encountered on most samples. However strong sites do occasionally appear, and lead to exceptionally low E_{thr}. Therefore diode-type FE measurements are incomplete.

In order to show that these considerations are consistent with experimental observations, we will compare two samples (sample A and B) with different β-distributions. We have chosen the measured area small ($\sim 200 \times 200\ \mu m^2$) to illustrate how the presence of one or a small number of high field enhancement FES may crucially influence the current density. The β(x,y) maps in Fig. 2.35 were obtained under identical CCM conditions with a sample-tip separation $\sim$ 7 μm and 50 nA emission current.

The number of FES with $\beta > 20$ was 74 for sample A and 102 for sample B.

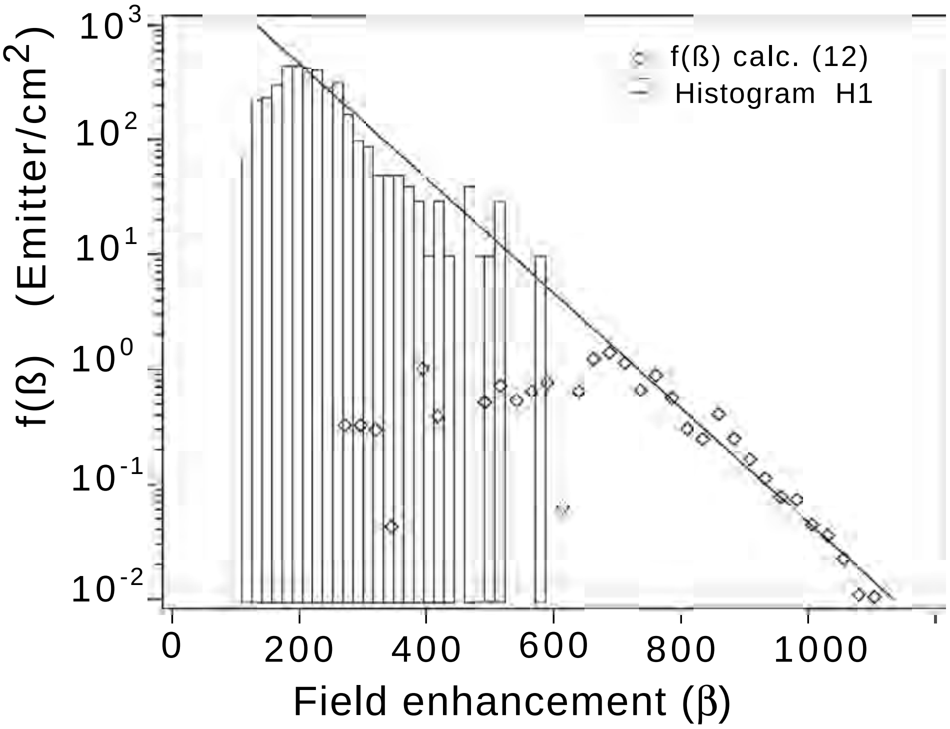

Figure 2.34: Simulation of three β-distributions. The Gaussian f(β) with idealized narrow spread of field enhancement values. The exponential f(β) with decreasing density of sites. The cut-off f(β) is obtained from the exponential distribution if the highest field enhancement FES are removed.

From the β(x,y) maps we see that the average field enhancement per FES on sample A is lower than for sample B. We also see that the scatter in the field enhancement is higher on sample A, where we were lucky (or unlucky) enough, to record a strong FES with β ~1564. It does thus seem that the topography h(x,y) is rougher on sample A than on sample B, with the presence of a small number of high β >500 FES on sample A. In fact, the measured electric threshold field is actually lower on sample A than on sample B indicating very high local field enhancement. If we take a look at the β-distributions from A and B in Fig. 2.36, we clearly see that the FE maps of these two particular regions look quite different in terms of the field enhancement. The 102 sites found on sample B are located in a rather narrow range of field enhancement (45< β <286). The FES on sample A are scattered over a larger range (25< β <1564) where two

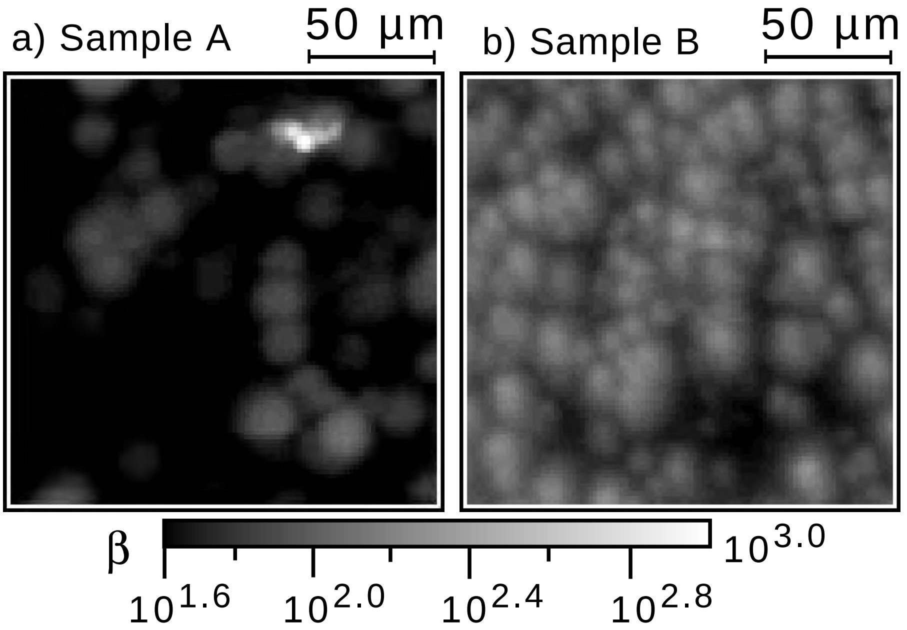

Figure 2.35: The field enhancing landscape β(x,y) is shown for two equally sized areas of sample A and B. The scatter in the field enhancement is less prounounced and the number of sites is higher on sample B. The scanned window on sample A contains a single strong β ~1564 which gives a very low electric threshold field and creates inhomogeneous current density along the surface.

FES are located around β ~550 and one very strong site at β ~1564. These few high field enhancement sites may indeed create very high local currents (emitter disruption not counted for) at low applied fields. However the large scatter of field enhancement on sample A is devastating for the ESD. This is verified as we map the FE over the two regions in Fig. 2.35 a second time in CVM. We maintain the tip-sample separation and record the current for the constant bias 320 Volt. The resulting current maps I(x,y) are depicted on a logarithmic scale in Fig. 2.37. On sample A 13 sites are recorded compared to 152 sites on sample B. The ESD is thus indeed higher on sample B ($\mathrm{ESD}_A \sim 41{\cdot}10^3$ cm^{-2} and $\mathrm{ESD}_B \sim 290{\cdot}10^3$ cm^{-2}).

However due to the high applied field $\sim$ 40 Vμm^{-1} we locally destroy the samples on these areas and the values of the ESD are thus given for comparison and not as reproducible values. Furthermore the majority of the sites on sample

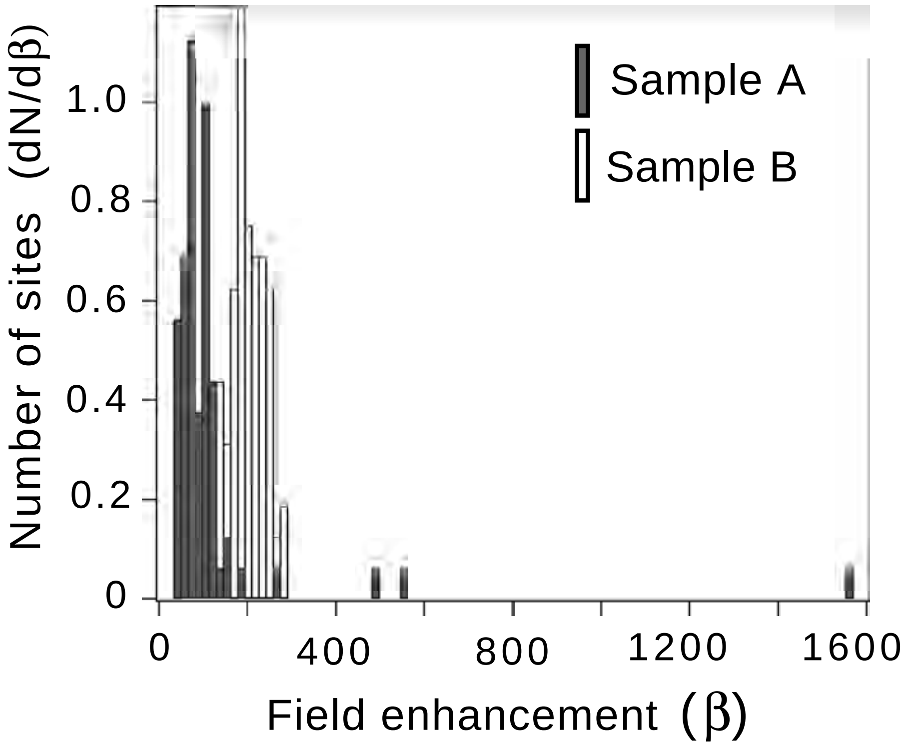

Figure 2.36: β-distributions from the β(x,y) maps of sample A and B in Fig. 2.35. The field enhancement of the sites on sample A is scattered over a larger range than sample B. Sample B has a higher average field enhancement concentrated in a narrow β range. Due to the small spread of β on sample B, the sites have comparable turn-on fields.

A deliver less than ~1 μA with the exception of one FES with current ~14 μA and one strong ~51 μA site in the right rear part of Fig. 2.37(a). This site corresponds spatially to β ~1564.

On sample B the spread in height of the individual FE current peaks is less pronounced and the average inter-FES distance is lower. The maximum measured individual current on B is 13 μA and the average current is about 4 μA/site, which is more than for A. The current density (calculated as the sum of the current peak values divided by the respective film area) is estimated to 200 mA/cm^2 for sample A and 10 A/cm^2 for sample B. These high current density values are not possible to attain for a cathode (of macroscopic dimensions) in useful operation due to the exponential characteristics of f(β) and emitter

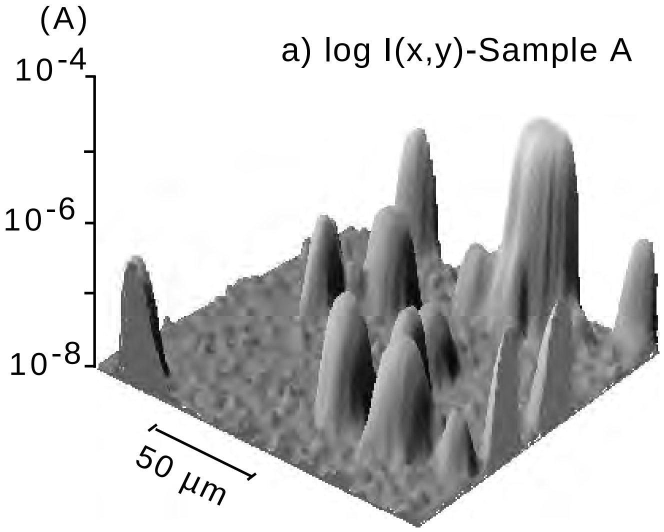

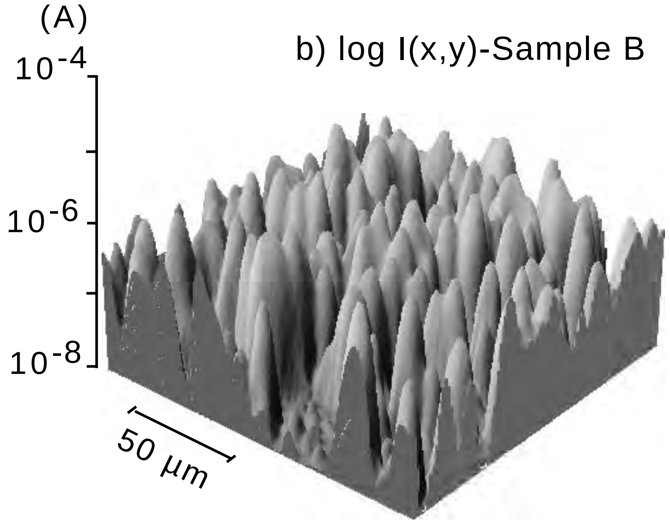

Figure 2.37: The current maps I(x,y) of (a) sample A and (b) sample B correspond to the regions in Fig. 2.35, with $E_a \sim 40$ Vμm^{-1}. Comparison of the I(x,y) and β(x,y) maps shows firstly that current peaks are located at positions with high local field enhancement. Secondly, that a small scatter in β is favorable for a high ESD. The strong emitter on sample A creates a low threshold field but the ESD is low.

---

disruption. Clearly the small variation in the field enhancement β of sample B is favorable for both a high ESD and current density. The small variation in β is the result of a steep slope in f(β). Although the ESD on sample A is low, the current density is not as low as might be expected due to the single strong $\sim$51 μA emitter. If this is excluded (which from a statistical point of view is acceptable due to the small probability) the current density is reduced by a factor of five to ~40 mA/cm^2. If the current density is varying as much as five times or possibly more dependant on the spatial position, a cold cathode device cannot be expected to have a homogeneous current distribution along the emitter surface. A μm-sized area with a single strong site (i.e. high β), has a lower E_{thr} field and a higher current density than other comparable areas. As a final example of how a large scatter in the field enhancement is unfavorable for the ESD, we compare the ESD on the phosphor screen for samples A and B, Fig. 2.38. The applied field is constant at 4.5 Vμm^{-1}. Since the sites on sample B have comparable field enhancement factors, they turn on simultaneously and the ESD of sample B is higher than on sample A.

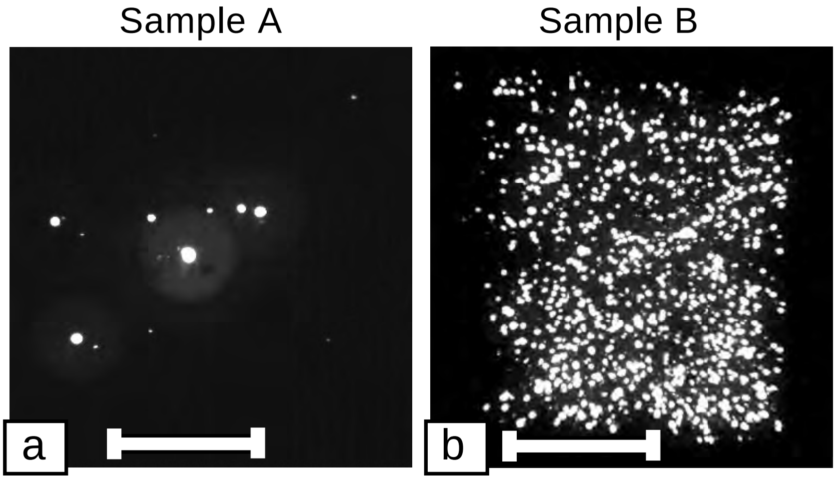

Figure 2.38: The macroscopically measured ESD of the entire surface of sample A and B for $E_a \sim$ 4.5 Vμm^{-1} on a phosphor screen confirms the large difference in the microscopically recorded ESD. The white bar corresponds to 5 mm.

2.4.7 Conclusions and outlook

We believe that the reported low threshold electron emission from a wide range of thin film emitters may be accurately described by Fowler-Nordheim tunnelling. The Fowler-Nordheim tunnelling requires high electric fields generated by an ensemble of field enhancing structures (FES) like protrusions, whiskers or nanotubes on the thin film surface. The amplification factor of the applied field is called the β-factor and the emission from thin films can be characterized in terms of the spatial field enhancement map β(x,y). The variation in β for different FES leads to a β-distribution f(β), which can be seen as a probability function of field enhancing structures. The β-distribution can be said to give an almost complete characterization the FE properties, in contrast to the threshold field of thin film emitters.

f(β) has been shown to be exponential for the samples presented in this paper. From other experiments, we believe that the exponential distribution is typical for most electron emitting thin films. The exponential distribution has a high density of field enhancing structures in the low field enhancement range and a low density with high field enhancement.

In order to obtain a field emission array with uniform emission intensity and high ESD, stringent requirements must be placed on the permitted spatial variation of emitting sites and the variation of β. Homogeneous emission from an ensemble of FES, defined as dI/I$<$ 50 %, requires that the relative variation of the field enhancement must be small $d\beta/\beta < 4$ %. Therefore it is desirable to optimize the density of sites close to the highest field enhancement of the ensemble to the limit of electrostatic screening effects. This criteria can be satisfied in two ways. First if the exponential slope of the pristine or as-produced f(β) is made sufficiently steep during deposition of FES. Or second, if the FES in the high field enhancement regime are removed through high currents and emitter disruption. By removing the high β FES a cut-off may be introduced in the exponential slope and the shape of f(β) is modified. Since a small spatial variation of β is difficult to achieve over a large area substrate, the cathode has to be combined with a serial resistive layer. In which case higher applied fields are required in order to get field emission.

The future task in order to engineer a carbon based thin film emitter device is comprised by finding a method, by which a defined number of FES with well defined aspect ratio's can be deposited on small μm-sized areas over large substrates in a controlled way.

The authors are grateful to L.H. Thuesen, R. Fink and Z. Yaniv of FEPET Inc., Austin, USA for supplying the two CVD carbon thin film emitter samples. This project was funded by the Swiss National Science Foundation and Top-Nano 21.

References for 2.4

[1] Yu.V. Gulyaev, L.A. Chernozatonskii, Z.Ja. Kosakovskaja, N.I. Sinitsyn, G.V. Torgashov, Yu. F. Zakharchenko, J. Vac. Sci. technol. B, **13(2)**, 435 (1995).

[2] C.Wang, A.Garcia, D.C. Ingram, M. Lake, M.E. Kordesch, Electron. Lett. **27**, 1459 (1991).

[3] G.A.J. Amaratunga and S.R.P. Silva, Appl. Phys. Lett. **68**, 2529 (1996).

[4] O.Gröning, O.M. Küttel, P.Gröning and L.Schlapbach, Appl. Surf. Sci. **111** 135 (1997).

[5] F.S.Baker, A.R.Osborn, J.Williams, J. Phys.D: Appl. Phys. **7**, 2105 (1974).

[6] E.I. Givargizov, V.V. Zhirnov, A.N. Stepanova, E.V. Rakova, A.N. Kiselev, P.S. Plekhanov, Appl. Surf. Sci. **87/88**, 24 (1994).

[7] J.E. Jaskie, MRS Bulletin **21**, 59 (1996).

[8] R.L. Fink, Z. Tolt, Z. Yaniv, Surface and Coatings **108-109**, 570 (1998).

[9] R. Fowler, L. Nordheim, Proc. R. Soc. London **A119**, 173 (1928).

[10] D. Temple, Mater. Sci. Eng. **R24**, 185 (1999).

[11] I. Brodie, C. Spindt, Advances in electronics and electron physics **83**, 1 (1992).

[12] B. R. Chalamala, Yi Wei, B. E. Gnade, IEEE Spectrum **April**, 43 (1998).

[13] A. Tallin, B. Coll, E. Menu, J. Markham, J. Jaskie, Proc. 1st Inter. Special. Meeting on Amorp. Carbon **97**, 329 (1997).

[14] J. van der Weide, Z. Zhang, P.K. Baumann, M.G. Wensell, J. Bernholc, R.J. Nemanich, Phys. Rev. B, **50**, 5803 (1994).

[15] J. Liu, V.V. Zhirnov, W.B. Choi, G.J. Wojak, A.F. Myers, J.J. Cuomo, J.J. Hren, Appl. Phys. Lett. **69**, 4038 (1996).

[16] O.Gröning, O.M. Küttel, P.Gröning and L.Schlapbach, J. Vac. Sci. Techol. **B17**, 1970 (1999).

[17] J.-M. Bonard, J.P. Salvetat, T. Stöckli, W.A de Heer, L. Forró, A. Châtelain, Appl. Phys. Lett. **73**, 918 (1996).

[18] F.Lacher, C.Wild, D.Behr, P.Koidl, Diamond and Rel. Mat.**6**, 1111 (1997).

[19] B.S.Satyanarayana, J. Robertson, W.I. Milne, Journ. Appl. Phys. **87**, 3126 (2000).

[20] J.B. Cui, M. Stammler, J. Ristein, L. Ley, Journ. Appl. Phys. **88**, 3667 (2000).

[21] A. IIie, A.C. Ferrari, T. Yagi, J. Robertson, Appl. Phys. Lett. **76**, 2627 (2000).

[22] J.P. Zhao, Z.Y. Chen, X. Wang, T.S. Shi, T. Yano, Appl. Phys. Lett. **76**, 191 (2000).

[23] A.N. Obraztsov, A. Volkov, I. Pavlovsky, Diam. Rel. Mater. **9**, No 3-6, 1190 (2000).

[24] H. Kind, J.-M. Bonard, C. Emmenegger, L.O. Nilsson, K. Hernadi, E. Maillard-Schaller, L. Schlapbach, L. Forró, K. Kern, Adv. Materials **11**, 1285 (1999).

[25] Z.F. Ren, Z.P. Huang, D.Z. Wang, J.G. Wen, J.W. Xu, J.H. Wang, L.E. Calvet, J. Chen J.F. Klemic, M.A. Reed, Appl. Phys. Lett. **75**, 1086 (1999).

[26] S. Fan, M.G. Chapeline, N.R. Franklin, T.W. Tombler, A.M. Cassell, H. Dai, Science **283**, 512 (1999).

[27] L. Nilsson, O.Gröning, C.Emmenegger, O.Kuettel, E.Schaller, L.Schlapbach, H. Kind, J-M. Bonard, K. Kern, Appl. Phys. Lett. **76**, 2071 (2000).

[28] H. Murakami, M. Hirakawa, C. Tanaka, H. Yamakawa, Appl. Phys. Lett. **76**, 1776 (2000).

[29] J.Li, C. Papadopoulos, J. M. Xu, M. Moskovits, Appl. Phys. Lett. **75**, 367 (1999).

[30] C. Bower, W. Zhu, S. Jin, O. Zhou, Appl. Phys. Lett. **77**, 830 (2000)

[31] O. Gröning, "Field emission properties of carbon thin films and carbon nanotubes", Inaugural-Dissertation no **1258**, University of Fribourg (1999).

[32] W. Zhu, G.P. Kochanski, S. Jin, L. Seibles, Journ. Appl. Phys. **78**, 2707 (1995).

[33] K. Dean, B.R. Chalamala, Appl. Phys. Lett. **75**, 3017 (1999).

[34] L. Nilsson, O. Gröning, P. Gröning, O. Kuettel, L. Schlapbach, Proc. XIV Inter. Winterschool on Electr. Prop. of Novel Materials, Kirchberg, Tirol, Austria, 499 (2000).

[35] L.Nilsson, O. Gröning, P. Gröning, L. Schlapbach, (In press) Thin Solid Films (2000)

[36] B. Mandelbrot, Phys.Scr., **32**, 257 (1985).

[37] M. Collaud Coen, G. Dietler, S. Kasas, P. Gröning, Appl. Surf. Sc. **103**, 27 (1996).

[38] B. Bhushan, Handbook of Micro/Nano Tribology 2nd Ed., CRC Press LLC, 195 (1999).

2.5 Scanning anode field emission microscopy on carbon nanotube thin films

L. Nilsson, O. Groening, P. Groening, L. Schlapbach
Institute of Physics, University of Fribourg, Pérolles, CH-1700 Fribourg, Switzerland

Published in The Electrochemical Society Proceedings, **2000-28**, 52 (2001).

Abstract

Scanning anode field emission measurements are used to obtain spatially resolved electron emission images of carbon nanotube thin film emitters, which can be used to derive the spatial field enhancement map β(x,y). The emitting sites, which are randomly distributed on the surface, obey a statistical probability distribution, which has been calculated.

2.5.1 Introduction

Chemical vapor deposition (CVD) diamond, diamondlike carbon (DLC) and nanotube (CNT) thin films have met a great deal of interest during the last decade due to extraordinary low-field electron emission (FE) [1–4]. Carbon-based thin film cold cathodes could replace classical tip emitter arrays [5, 6] in field emission arrays (FEAs) due to potentially simpler and cheaper cathode design [7]. Electron emission from tip emitters is based on the Fowler-Nordheim tunneling and needs high electric fields of the order of 3000 V/μm, to extract electrons from the solid into vacuum. Due to the high electric field, the surface potential barrier, which confines the electrons within the solid, is lowered and becomes triangular in shape. As the width of the surface potential barrier approaches 2 nm, electrons will have a non-negligible probability to tunnel from the highest occupied states of the solid into vacuum. Usually the high fields are created using tip-like structures, which cause field enhancement at the tip apex. In a first approximation these field enhancing structures (FES), amplify the applied field E_a by a factor β which is of the order of the aspect ratio h/r, where h is the height of the tip and r the radius of curvature of the tip apex. Ea can be defined as a global or overall electric field, applied between an anode and cathode in a typical FE experiment. The amplified field E_{site} at the tip apex of the FES is calculated as $E_{site}=\beta\cdot E_a$. Due to geometrical restrictions imposed by the gated structure of FEAs, the FES are confined to μm-sized dimensions, where h $\sim$ μm and r $\sim$nm create β factors up to $\sim$ 100-200. Etched silicon or evaporated metal micro tips, created by conventional lithographic patterning techniques, have been used in FEAs for a long time [6, 8]. The production of such metal micro tips however, requires expensive processes. They suffer from emission degradation caused by sputter erosion and chemical contamination and therefore require a high vacuum environment for operation [6, 9]. There is thus a strong incentive to simplify both the production and design of the cathode in FEAs and carbon based thin film emitters turned out to be very interesting in this respect. Thin planar film emitters, emitting at low electric fields below 2 Vμm^{-1} homogenous over the whole emitter surface would lead to a number of technological advantages in e.g. FEAs. Current generation of micro tip based FEAs require $\sim$70 Volts gate-to-cathode bias for operation [10]. A reduction of this driving voltage, achievable with low threshold thin film emitters, leads to lower driver costs and reduced power consumption. Compared to field enhancing metal tips in the μm range, which are subjected to ion sputter during FE, a flat homogeneously emitting thin film would offer technological advantage [11]. Homogeneous electron emission from the entire thin film surface, would reduce the power dissipation and joule heating per unit area of the surface, as compared to micro tips which can become disrupted and blunted. DLC and CVD diamond thin films were thought to deliver such thin film emitters. However it is shown in a number of works that the emission mechanism of carbon-based thin films seems to be Fowler-Nordheim (FN) tunneling, due to field enhancement β from μm- and nm-structures [12–14]. Thus from a physical point of view, the carbon-based thin film emission is analogous to the classic metal tip array emission, where FES like e.g. carbon nanotubes, sharp whiskers or protrusions are responsible for amplifying the applied field to cause sufficiently large microscopic fields to promote FE. However unlike the well ordered metal tip FEAs, the FES of thin electron emitting films exhibit a stochastic nature, with regard to the distribution of field enhancement. Whereas the metal microtips are idealized with a narrow Gaussian distribution of aspect ratios, and the distance between every tip can be controlled with rather high precision in even the sub-μm range, the thin film emitters are randomly distributed with so far uncontrollable field enhancing factors. The random spatial distribution and large spread in β values of thin emitting films is a problem of technological importance. In order for the FEAs to emit electrons homogeneously over larger area substrates, the variation of the field enhancement within and between individual pixels must not be too large for the same applied field. Consequently the FES has to be deposited in a controlled manner [15–18] in the gated structure of the FEA. In this case it is of great importance that the number of the emitting sites/pixel as well as the inter-FES distance and the distribution of β values can be controlled and kept in a narrow range. Clearly, since the random distribution of β values is directly linked to current and emitting site density (ESD), we need to characterize the spatial field enhancing properties β(x,y) of the thin film emitter, in order to optimize the ESD. To optimize the ESD, the FES spatial distribution has to be microscopically monitored and to do that we have developed a scanning anode field emission technique.

2.5.2 Basic considerations

At the basis of our consideration of an ensemble of emitters on a planar surface, stands the description of the current-field characteristics of a single emitter. Field emission spectroscopy [19] on various carbon thin film emitters such as CVD diamond, DLC and nanotube thin films has shown that the emission of these films is classical FN-tunneling at fields of the order of 3000 Vμm^{-1} or more and with typical emitter work functions around 5 eV.

In order to describe the emission current of a single emitter over a wide range of fields, we use the simplified FN-formula as proposed by Spindt et al. [6], where the elliptic functions v(y) and t(y) are approximated:

$$I = A \cdot \frac{1.5 \cdot 10^{-6}}{\phi} E_{site}^2 \exp(\frac{10.4}{\sqrt{\phi}}) \exp(\frac{-6.44 \cdot 10^7 \phi^{1.5}}{E_{site}}) \tag{1}$$

I is the emission current in Ampere, A is the emitting area in cm^2, E$_a$ is the applied electric field in Vcm^{-1} and β is the field enhancement factor of the emitter. It has to be pointed out that although A has the dimension of area, it also accounts for the DOS and the band structure of the emitter. In order to get realistic values of the emission current, consistent with energy resolved measurements [12, 19], A=10^{-9}-10^{-10} cm^2 and the workfunction ϕ= 4.5-5.0 eV. For the following considerations we will assume that all the emitters have the same work function (justified by the fact that the emitter are made of the same material) and that A is the same for all emitters (justified by the assumption that the emitter are of the same dimensions and that emission current only depends linearly on A).

This means that for a constant applied electric field E$_a$, the only remaining parameter determining the emission current from expression (1), is the field enhancement factor β. Under these assumptions the field enhancement map β(x,y) gives a complete description of the spatial emission current I(x,y). β(x,y) again is related to the topographic structure h(x,y) of the thin film emitter.

Since the field enhancement β is the dominant factor in expression (1), and critically controls the emission current I(x,y), we can in principle describe the ESD and current density if the spatial field enhancement β(x,y) is known.

In this picture the field emission properties of a thin film emitter can be represented by the function f(β), where the number of emitter dN on a given surface area A with a field enhancement factor in the interval β to β+dβ is given by dN(β)=A·f(β)·dβ. As we will see, the function f(β) can be derived from the field enhancement map β(x,y). We define the f(β)-distribution, or for short the β-distribution:

$$f(\beta) = \frac{1}{A}\frac{dN}{d\beta} \qquad [Emitter/cm^2] \tag{2}$$

To illustrate the influence of the f(β)-distribution on the emitting site density (ESD) we take the emission characteristics of a metal tip FEA, where the aspect ratios are approximately the same, as an example. The field enhancement is thus ideally kept around an average value β_0 and has a gaussian β-distribution:

$$f(\beta) = 200\exp{(-\frac{(\beta-\beta_0)^2}{18.02})} \qquad (FWHM = 10) \tag{3}$$

The narrow shape of the gaussian β-distribution is shown in Fig. 2.39 and is thought of as being typical for randomly distributed metal tips with an average field enhancement β_0= 150.

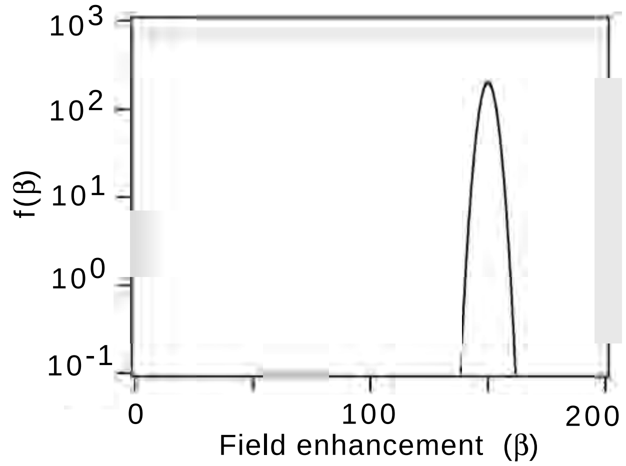

Figure 2.39: A gaussian emitter distribution f(β), representing randomly distributed metal tip FES with an average field enhancement of 150 (FWHM=10).

With the aid of expression (1) we may simulate the emission on a phosphor screen, if the emitting sites of expression (3) are randomly distributed over an arbitrary surface area A=1. Typical values of the simulation are given:

E_a=21.25 Vμm^{-1} I_{tot}=0.304 mA "A"=10^{-9} cm^2 (eq.1) ϕ= 5.0 eV

The resulting FE image is depicted in Fig. 2.40, where the level of the gray scale is linear between 0 to 9 mA/cm^2. White corresponds to 9 mA/cm^2 and above. The situation depicted on the simulated screen in Fig. 2.40 resembles the ESD as obtained on an ordinary phosphor screen from a "good" thin film emitter.

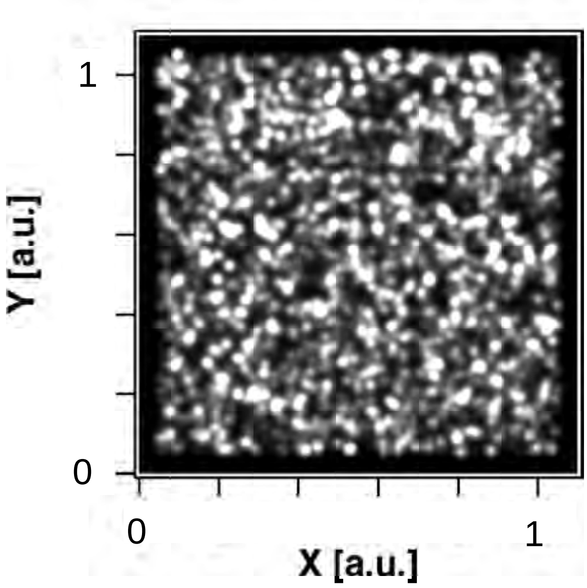

Figure 2.40: Simulation of the current image I(x,y) of randomly distributed metal tip FES subjected to E_a= 21.25 Vμm^{-1}. The emitting sites are given field enhancement according to a gaussian β-distribution f(β) and the emitted current/site is calculated according to the FN expression (1). White corresponds to currents of $\sim$ 9 mA/cm^2.

In contrast to an array of well ordered metal tips with similar aspect ratios, a thin film emitter such as a nanotube thin film, has a high density of emitters with low β and a low density of FES with high β. Due to the random length and orientation of the tubes (see Fig. 2.42), there is no a priori reason to believe that the aspect ratios of the CNTs are kept in a narrow gaussian range and therefore cannot the distribution function f(β) be assumed to be gaussian anymore. In such a case f(β) takes the shape of a function steadily decreasing with increasing

β. The measurement of the electric field (usually called threshold field), where a given threshold field emission current sets on, can be understood as measuring a threshold field enhancement βmax. With $E_{site} = E_{threshold} \cdot \beta_{max}$, where $E_{threshold}$ is the measured applied threshold field in the experiment and E_{site} is the electric field at the emission site which generates the threshold current. From (2) we see that β_{max} will depend on the area on which the threshold field is measured, as the probability to find an emitter with a given field enhancement factor will increase with increasing surface. In other words, the measured threshold field will decrease with increasing surface measured. The characterization of the emission properties of a thin film emitter just by stating the threshold field is therefore questionable.

Certainly the function f(β) is a far better characterization of a thin film emitter than the threshold field (which is determined by the highest aspect ratio β_{max} of the thin film emitter ensemble). The ESD can be calculated from f(β) according to:

$$ESD(E_a) = \int_{\beta_{min}=\frac{E_{thr}}{E_a}}^{\infty} f(\beta)\, d\beta \qquad [cm^{-2}] \tag{4}$$

The number of emitting sites (ESD) per unit area (cm^{-2}) is given as the integral of f(β) from β_{min} to β_{max}, as a constant field E_a is homogeneously applied to the thin film surface. E_{thr} is the lowest threshold field at the tip apex of the emission site, required for the site to be recorded. Since the ESD is recorded for a constant applied field, we call this mode of operation the Constant Voltage Mode (CVM), which is the basis of most applications, including FE with a phosphor screen. A current of 10 nA is sufficient for a site to be detected on a phosphor screen. E_{thr} is approximately 3700 V/μm at the site for an emission current of 10 nA.

Since our prime interest is to increase the ESD to fit the requirement of at least 10^6 emitting sites per cm^2 [10], the integral expression (4) has to be increased, but not over 10^8 emitters/cm^2 in order to avoid screening effects [17]. In order to optimize (4) we have to be able not only to simulate but moreover to determine f(β) according to (2) for a carbon nanotube (CNT) thin film emitter. We thus ask what does f(β) of a CNT thin film emitter look like? And how can f(β) be modified in order to maximize the ESD according to expression (4)? To answer these questions, there exist several approaches, which can be adopted to measure or calculate the β-distribution. We present the experimental measurement principles to obtain f(β) in the next section.

2.5.3 Measurement principles

According to the definition of the ESD (4), f(β) and the ESD are directly linked. Consequently, since the ESD=ESD($\mathrm{E}_a(\beta)$) where $\mathrm{E}_{thr}= \beta \cdot \mathrm{E}_a$ is the local field at an emitting site in order to spot that site on a phosphor screen, the β-distribution is calculated from the ESD [20] according to:

$$f(\beta) = \frac{dESD}{dE_a}\left(\frac{E_{thr}}{\beta^2}\right)\Bigg|_{E_a=\frac{Ethr}{\beta}} \tag{5}$$

where the derivative is taken for expression (4) and ESD($\mathrm{E}_a(\beta)$). We may readily assume that for a FES to contribute to the ESD (i.e. be visible on the screen), the FE current should be = 10 nA or more. Based on the current-voltage characteristics of expression (1), which in turn is based on energy resolved FE measurements, we may approximate the local emission site field $\mathrm{E}_{thr} \sim 3700$ Vμm^{-1} corresponding to $\mathrm{I}_{site}= 10$ nA. It can be shown [20] that f(β) can be computed according to expression (5). However the screen suffers from the drawback of not being able to resolve ESD higher than $\sim 10^4$ cm^{-2} due to the divergence of the electron beam. Since we need to monitor and investigate emission site densities in excess of $\sim 10^6$ cm^{-2}, the poor resolution of the phosphor screen is a problem. Additionally the use of a large area anode causes the local field and the corresponding currents to be extremely divergent from low β to high β sites. Whereas some sites do not even appear on the screen, others may be destroyed due to excessive current levels caused by large local fields. However there are other ways of to obtain the ESD with higher resolution.

Scanning anode FE may be used to obtain a spatially resolved FE current image I(x,y) with $\sim$ μm resolution in CVM. If a movable $\sim$ μm-sized anode is scanned at 5-10 μm sample-anode distance, the spatial resolution is significantly improved, compared to the screen. The current, which is sequentially obtained using the scanning anode, is recorded with a source measure unit, which has dynamics measurement range from a few pico-ampere up to milli-ampere. Consequently, by recording the FE current, point-by-point, one is in principle able to re-calculate the β value of every point from equation (1). The only problem with this approach is within the CVM mode of operation, where a constant voltage is applied to the scanning anode. A small change of β or anode-site separation (and thus the local field $E_site{=}\beta{\cdot}E_a$ at the site) may cause the current to fluctuate over several orders of magnitude according to (1), and therefore will the strongest emitting sites suffer from both resistive current saturation and destruction due to joule heating. The consequence will be that the calculation of β according to (1) will be incorrect, since the Fowler-Nordheim expression does not account for current saturation effects.

Since we want to avoid current saturation effects, not to say emitter destruction due to joule heating, the scanned electron emission has to be performed in another mode of operation, called the constant current mode (CCM). In the CCM the emission current is constant for every point, and the voltage V applied to the anode is changed in order to maintain the same current as a function of the anode position above the thin film surface. If the current is reasonable low, such as 50 nA, we will obtain a spatially resolved FE image of the extraction voltage V(x,y), without current saturation effects or emitter destruction. This is both experimentally and conceptually beautiful since V(x,y) is actually an inverted image of the field enhancing landscape β. This can be realized if we approximate the applied field E_a= V/d, where d is the anode-cathode separation, to get E_{site}= β·V/d for the field at the emission site. Since 50 nA approximately corresponds to a constant E_{site}= 4000 Vμm^{-1} according to (1), which is based on energy resolved FE, and V(x,y) is known, we may readily obtain the field enhancing landscape β(x,y) according to:

$$\beta(x, y) = \frac{d \cdot E_{site}}{V(x, y)} \tag{6}$$

where both d and E_{site} are constants. Since we neglect the radius of curvature and assume a homogeneous applied field (the field lines are actually concentrated close to the anode as compared to the cathode and the real applied field at the cathode is therefore lower than the calculated E_a= V/d), the value of β in expression (6) is slightly under-estimated.

If the β(x,y) image contains N(β) number of peak values (where β is the corresponding field enhancement factor) and A is the scanned surface area, we can obtain f(β) according to (2).

2.5.4 Experimental set-up

The samples were investigated by means of a vacuum FE apparatus operating at a typical base pressure of 10^{-7} mbar. Microscopic FE measurements were performed with a scanning anode field emission apparatus (Fig. 2.41).

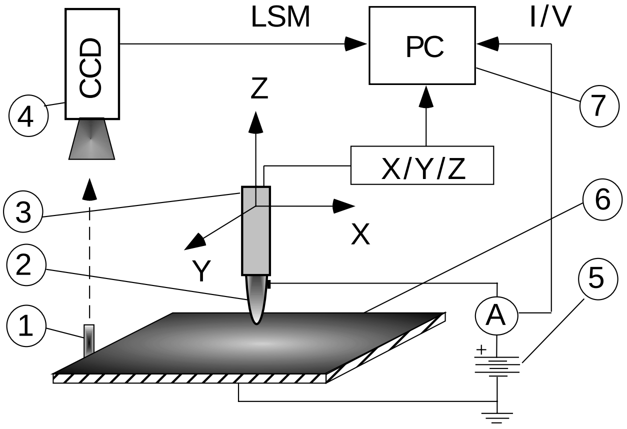

Figure 2.41: The Scanning Anode Field Emission Microscope. 1) Light source (reference) 2) Anode 3) Z Pico-motor 4) Camera for control of the translation of the sample 5) Keithley Source Measure unit 6) Thin film emitter 7) Computer control

The sample was mounted on a computer-controlled piezo driven x/y-translation stage and a tip Pt-Ir anode (tip radius of 2-5 μm) was approached to the sample in steps of 100 nm. Changing the tip-sample separation can be done without hysteresis. The FE current I or the voltage V, can be recorded as a function of tip position as the sample is scanned in x- and y- directions. The tip was held at a constant height, typically 7-15 μm, which is larger than the surface roughness, and the electron current was recorded with a Keithley 237 source-measure unit. The field emission was recorded in two ways: A) Constant Voltage Mode (CVM) and B) Constant Current Mode (CCM). In CVM the applied voltage was kept constant (typically 100-300 Volts) and the measured FE current was recorded as I(x,y). In CCM the FE current was kept constant, e.g. 50 nA, and the extraction voltage V(x,y) applied to the tip was adjusted between 0-1100 Volts depending on the tip position. Sample areas of $200 \cdot 200$ μm^2 up to $800 \cdot 800$ μm^2 were scanned with $\sim$ 5-10 μm resolution depending on the tip-sample separation. Tip re-positioning can be achieved with sub-μm resolution on a sample surface up to 5·5 mm^2. The obtained FE-map in either CVM or CCM however, is a convolution of tip-sample distance, surface topography and tip radius. The level of the noise was lower than 1 nA during scanning and contact currents could be distinguished from the FE current by a sudden current increase and saturation of the source-measure device.

2.5.5 Scanning anode FE on CNT thin film emitters

In order to illustrate the considerations made previously, we will show how the functional dependence of f(β) can be obtained for a carbon nanotube (CNT) thin film emitter. These films were produced by pyrolysis using a acetylene/nitrogen gas mixture at temperatures around 900 °C.

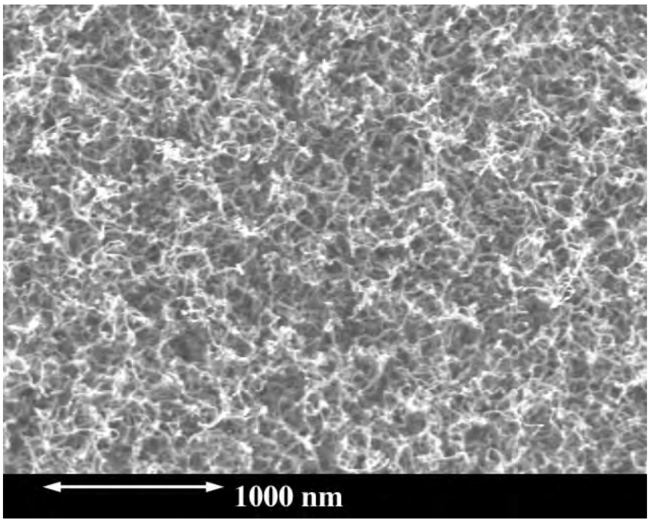

Figure 2.42: Densely packed forest of carbon nanotubes (CNTs) produced by catalytic decomposition of methane using sputtered Ni as catalyst. Diameter of the CNTs ~20 nm.

Figure 2.42 shows the SEM image of such a nanotube thin film where Nickel was sputtered on the silicon substrate and used as a catalyst. Scanning FE was performed in CCM at a tip-sample distance d ~5 μm with constant emission current I= 50 nA, and the resulting map (raw data) of the extraction voltage V(x,y) as a function of tip position, is shown in Fig. 2.43(a). The voltage is changing between 30 to 426 Volts depending on tip position, but the gray scale is chosen between 30 to 350 Volts. Dark regions or spots correspond to low electric threshold or efficient emission due to field enhancement by carbon nanotubes.

In order to obtain the field enhancement map β(x,y), we invert the V(x,y) map according to expression (6), where we take E_{site} to be 4000 V/μm at the tip apex of the CNTs corresponding to 50 nA emission current. The resulting β(x,y), which is an image depicting the local field enhancing properties of the CNTs, is shown in Fig. 2.43(b). Since we have neglected that the field is not homogeneous, the field enhancement values are probably slightly underestimated. Furthermore, E_{site} is affected by differences in electronic cap states, adsorbed molecules and utterly by differences in the work function of different tubes. Thus, we cannot exclude that Esite is slightly varying around 4000 V/μm in order to obtain an emission current of 50 nA per site. Such a variation is of course not accounted for in the calculation (6), but is thought to play a minor role as opposed to the field enhancement effect.

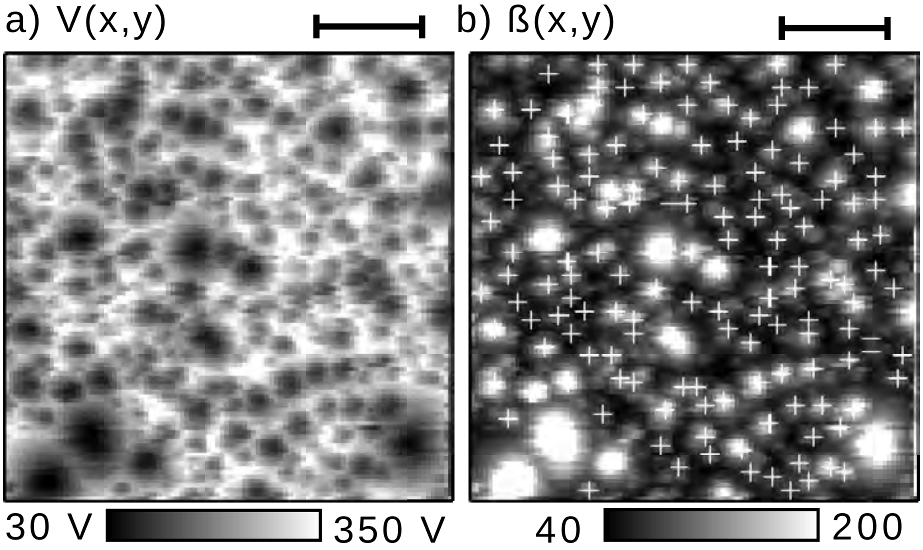

Figure 2.43: (a) The voltage required to obtain a constant current of 50 nA from a CNT thin film has been plotted as a function of anode position V(x,y). (b) The image in (a) is transformed into the field enhancement map β(x,y) according to expression (6). The positions of β peak values (N=157) in β(x,y) have been marked with white crosses. The black bar corresponds to 50 μm.

The gray scale is linear for β values ranging from 40 to 200, where white corresponds to emitting sites with $\beta \geq 200$. β values up to 650 are detected on the film area A= $4{\cdot}10^{-4}$ cm^2, and the total number of emitting sites N is 157. The white markers in Fig. 2.43(b) indicate the positions of β peak values. Figure 2.44 displays the histogram of the 157 peak values, with a bin width of dβ= 12.5. A higher or lower value of E$_{site}$ will not affect the shape of f(β), but merely shift the histogram.

We see that dN, is a rapidly decreasing function from maximum around $\beta \sim$ 130 down to only 4 emitting sites above β= 350. The probability of recording FES with β values >350 is small on A= $4{\cdot}10^{-4}$ cm^2, since dN obeys a statistical probability distribution as indicated by the fitted line in Fig. 2.44. Nevertheless we recorded 4 FES above β= 350, with a large scatter in β. Repeated scanning at different positions on the sample surface show this unpredictable occasional presence of one or a few high β FES. However in order to obtain reliable statistical data, each bin in Fig. 2.44 should contain at least 10 points. With the fitted line in Fig. 2.44:

$$\mathrm{dN}=\mathrm{A}\cdot 15\cdot 10^5\exp(-0.024\cdot\beta)\cdot \mathrm{d}\beta$$

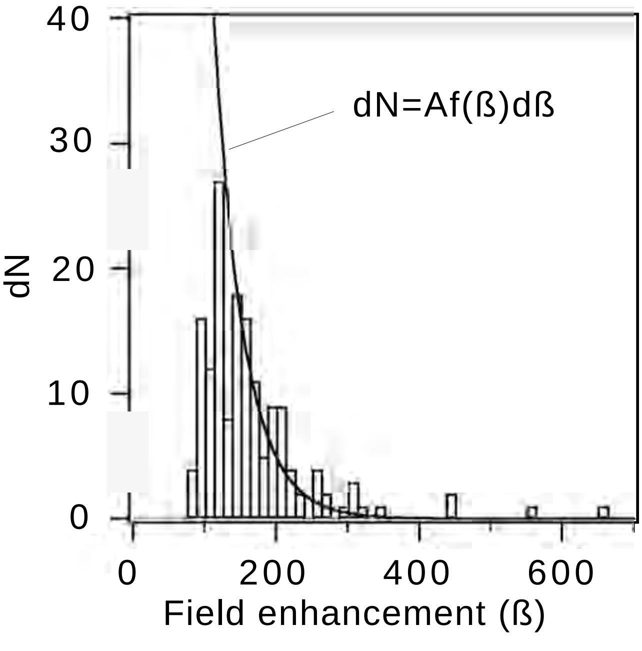

Figure 2.44: dN is proportional to the β-distribution f(β), where N is the number of peaks in the β(x,y) image. f(β) is exponential which is explained by the surface roughness created by the carbon nanotubes.

we obtain the β-distribution as:

$$f(\beta)= 1.2\cdot 10^5 \exp(-0.024\cdot\beta) \qquad [\text{Emitters/cm}^2]$$

according to expression (2), where $A= 4\cdot 10^{-4}$ cm^2. According to $f(\beta)$ we can expect $\sim 10^3$ emitters/cm^2 with a β between 200 and 201.

In order to get a histogram with better statistics, compared to Fig. 2.44, we do not only take the peak values into account, but all 10000 points of the field enhancement map β(x,y) as shown in Fig. 2.45. The slope of $f(\beta)$ can then be determined with better accuracy than in Fig. 2.45. For the fit to the data of Fig. 2.45, only data points larger than 10 are taken into consideration. Consequently points above $\beta= 300$ are not used, since they are considered statistically unreliable. However the distribution in Fig. 2.45 is not the true β-distribution, since all points of the β(x,y) image have been used (instead of only the peak-values). Thus we only use Fig. 2.45 to obtain the slope of $f(\beta)$. We observe a low β cut-off around $\beta= 130$ in Fig. 2.45. The cut-off is due to measurement resolution limitations. Low β (<100) FES are not "seen" by the scanning anode since stronger, i.e. higher β (>130) FES both screen and amplify the applied field more than β <100. During scanning this effect becomes obvious from the size of each emission spot in the β(x,y) map. High field enhancement emitters create larger emission spots and thus cover smaller emission spots from low β emitters. The low β cut-off can therefore be simulated using the emission spot area [20]. The exponential dependence of $f(\beta)$ is understandable from a statistical point of view. The probability of high β (>300) FES is low or at least considerable lower, than the probability of low β (<200) FES per unit area (cm^{-2}). This can be correlated with the surface roughness (in this case CNTs), which is found to be exponentially dependent on the length scale in atomic force microscope measurements. Consequently, the number of low aspect ratio protrusions is exponentially higher than the number of high aspect ratio protrusions for a given surface area A.

We have also measured exponentially dependent $f(\beta)$ on chemical vapor deposited diamond surfaces [20], using both scanning CCM and a phosphor screen in CVM (see equation (5)). It does thus seem that the exponentially dependent β-distribution is a common feature of electron emitting thin film surfaces.

We see that the exponential β-distribution predicts only few field enhancing structures (4 FES for β >350) in the high β range on the surface $A= 4\cdot 10^{-4}$ cm^2.

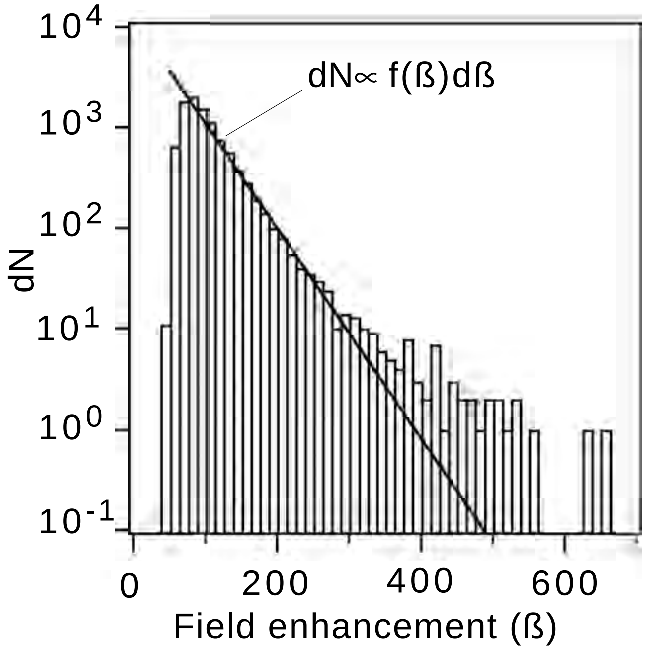

Figure 2.45: dN is proportional to the β-distribution f(β), where N is the total number of points in the β(x,y) image. f(β) is exponential with a slope proportional to -0.024.

We earlier assumed a narrow gaussian distribution for metal tip FEAs. Since the density of emitting sites is higher in the narrow gaussian range than in the high field enhancement range of the exponential f(β), the ESD calculated with a screen (4), should be higher for metal tip FEAs. This observation is confirmed by the high and homogeneous ESD, simulated in Fig. 2.45. Due to homogeneity in aspect ratios, the turn-on field is only weakly varying from one idealized metal tip to another. Consequently the ESD is high and homogeneous in the simulation. The typical exponential f(β) thin film emitter however, possesses few FES with high aspect ratio and low turn-on electric field as compared to the majority of the low β emitting sites on the film. This does not necessarily imply that the ESD of thin film emitters cannot be increased above the ESD of metal tip FEA. There exists ways to circumvent the low density of exponential f(β) characteristics of thin films. On possibility is to "burn" high aspect ratio emitters with elevated current levels, leading to an increased slope of f(β). In order to do so, the applied electric field is slowly increased and the current levels of the highest β sites will increase more than for low β sites and consequently the high β sites will be disrupted. This will induce a cut-off for high β values in the f(β) characteristics and as a consequence the integral value (4) of the ESD will increase. The second option concerns the use of ohmic ballast resistors in series with the emitters. Resistors change the characteristics of the FN equation (1), as the current levels of the high β sites will be more damped than the low β sites. The ESD will thus appear homogeneous, although higher electric fields are required to promote electron emission.

Consequently we see that the emitting properties can be very well described in terms of β(x,y) and f(β). The ESD is closely linked to f(β) according to (4) and we see that if the shape and/or the slope of f(β) is modified, the ESD can be tuned to the desired application. However in doing so, one should keep in mind that there is a trade-off between the desired ESD and the turn-on field. If f(β) is modified with "burning" or ballast resistors are used, the turn-on field will inevitably increase.

2.5.6 Acknowledgements

The authors gratefully acknowledge funding for this work by the Swiss National Science Foundation NFP36, Top-Nano21 and Motorola Labs, Tempe, Arizona.

References for 2.5

[1] C.Wang, A.Garcia, D.C. Ingram, M. Lake, M.E. Kordesch, Electron. Lett. **27**, 1459 (1991).

[2] G.A.J. Amaratunga and S.R.P. Silva, Appl. Phys. Lett. **68**, 2529 (1996).

[3] O.Gröning, O.M. Küttel, P.Gröning and L.Schlapbach, Appl. Surf. Sci. **111** 135 (1997).

[4] F.S.Baker, A.R.Osborn, J.Williams, J. Phys.D: Appl. Phys, **7**, 2105 (1974).

[5] B. R. Chalamala, Yi Wei, B. E. Gnade, IEEE Spectrum **April**, 43 (1998).

[6] I. Brodie, C. Spindt, Advances in electronics and electron physics **83**, 1 (1992).

[7] R.L. Fink, Z. Tolt, Z. Yaniv, Surface and Coatings **108-109**, 570 (1998).

[8] D. Temple, Mater. Sci. Eng. **R24**, 185 (1999).

[9] K. Dean, B.R. Chalamala, Appl. Phys. Lett. **75**, 3017 (1999).

[10] A. Talin, B. Coll, E. Menu, J. Markman, J. Jaskie, Amorphous carbon: State of the Art, Edited Silva, Robertson, Milne, Amaratunga, Proc. 1st Intern. Specialist Meeting on Amorpous Carbon, 329-337 (1997).

[11] J.E. Jaskie, MRS Bulletin **21**, 59 (1996).

[12] O.Gröning, O.M. Küttel, P.Gröning and L.Schlapbach, J. Vac. Sci. Techol. **B17**, 1064 (1999).

[13] J.-M. Bonard, J.P. Salvetat, T. Stöckli, W.A de Heer, L. Forró, A. Châtelain, Appl. Phys. Lett. **73**, 918 (1996).

[14] F.Lacher, C.Wild, D.Behr, P.Koidl, Diamond and Rel. Mat.**6**, 1111 (1997).

[15] S. Fan, M.G. Chapeline, N.R. Franklin, T.W. Tombler, A.M. Cassell, H. Dai, Science **283**, 512 (1999).

[16] Z.F. Ren, Z.P. Huang, D.Z. Wang, J.G. Wen, J.W. Xu, J.H. Wang, L.E. Calvet, J. Chen J.F. Klemic, M.A. Reed, Appl. Phys. Lett. **75**, 1086 (1999).

[17] L. Nilsson, O.Gröning, C.Emmenegger, O.Kuettel, E.Schaller, L.Schlapbach, H. Kind, J-M. Bonard, K. Kern, Appl. Phys. Lett. **76**, 2071 (2000).

[18] H. Kind, J.-M. Bonard, C. Emmenegger, L.O. Nilsson, K. Hernadi, E. Maillard-Schaller, L. Schlapbach, L. Forró, K. Kern, Adv. Materials **11**, 1285 (1999).

[19] O. Gröning, "Field emission properties of carbon thin films and carbon nanotubes", Inaugural-Dissertation no **1258**, University of Fribourg (1999).

[20] L. Nilsson, O. Groening, P. Groening, L. Schlapbach "To be published".

2.6 Collective emission degradation behavior of carbon nanotube thin-film electron emitters

L. Nilsson, O. Groening, O. Kuettel, P. Groening and L. Schlapbach
Department of Physics, University of Fribourg, Pérolles, CH-1700 Fribourg, Switzerland

Accepted for publication in Applied Physics Letters (2001)

Abstract

The current-induced emission degradation of a carbon nanotube (CNT) thin-film electron emitter is studied under constant emission current for different current levels, using a scanning anode field emission microscope. A permanent emission degradation is observed for emission currents higher than 300 nA per CNT and is associated with resistive heating at the CNT-substrate interface for the sample under investigation. A second field-induced emission degradation mechanism, associated with the removal of CNTs from the substrate, is also reported.

Due to the development of field emission electron sources based on carbon nanotubes (CNT), e.g. for flat panel display (FPD) applications, much effort has been devoted lately to find inexpensive and efficient ways for controlled deposition of CNTs on large area substrates [1–6]. With the advances in the field of controlled growth, more technological aspects of the field emission such as life time, emission degradation [7–10] and the short- and long-term emission stability [11, 12] become more and more relevant. In a CNT based field emitter technology, emitter life time and degradation will be key parameters to be controlled. However up to now only very few investigations in this direction have been undertaken. The reason for this might reside in the fact that emitter life time and emitter degradation are not general properties of CNT emitters, but will depend on the technological configuration and environment in which the emitter is operated. Experiments performed with single multi-walled CNT (MWNT) mounted on metallic tips have shown that emission currents of the order of 0.1 mA repeatedly can be obtained from a single CNT without short term degradation [10]. However this value may be not relevant in the case of a CNT film emitter since other effects may dominate the emitter degradation due to the differences in cathode geometry. In most devices the CNTs are not operated as single "stand-alone" units but as a group or ensemble with electrostatic screening effects [6] and statistical variations of defects, adhesion and contact resistances. Therefore the sources of emitter degradation can be multiple such as high contact resistances, ignition of arcs, tubes flying of the substrate etc. The extrapolation of the current limitation behavior from a single straight, possibly defect free and ballistically conducting CNT to an ensemble of CNTs is therefore not straight forward. To elucidate the degradation behavior and the single site current limit of an ensemble of thin film CNT emitters under conditions close to the operating environment in e.g. FPDs, we performed scanning anode field emission microscopy with constant emission current per site [13].

We investigated MWNT catalytically grown on silicon wafer by thermal CVD. The silicon substrate was sputter coated by nickel and introduced into the reactor where multi-walled CNTs where catalytically grown in a acetylene/nitrogen atmosphere at 700 °C for 30 minutes. The substrate was homogeneously covered by a thick CNT deposit (Fig. 2.46(a)).

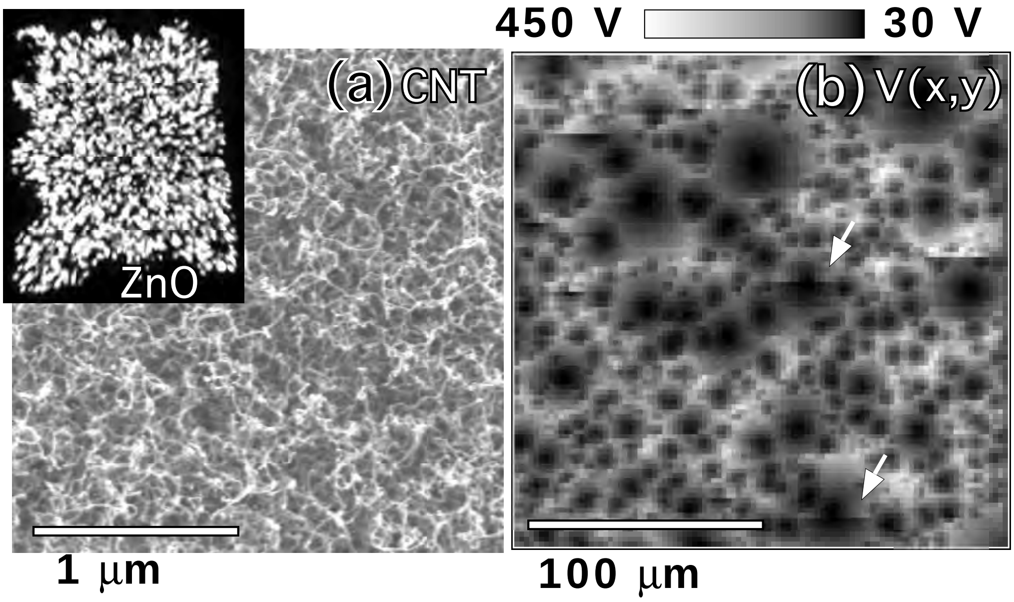

Figure 2.46: (a) Scanning electron micrograph of catalytically deposited CNTs. Inset shows the emission on a ZnO anode (emission area $\sim 4\times5$ mm^2) for $E_{applied}= 12$ Vμm^{-1}. (b) V(x,y) map (scan 1) for a constant emission current of 10 nA. White arrows indicate suddenly decreased emission typical for the first scan.

The electron emission properties of the CNT thin films were investigated using a phosphor screen (typically operated at 3000 V) and a home-made scanning anode FE microscope (SAFEM) operated at a base pressure of 10^{-8} mbar. In the SAFEM a Pt-Ir tip of radius $\sim$1 μm is used as anode for high resolution thin film emitter investigations and can be scanned over a surface area of up to 5×5 mm^2 with sub-μm accuracy. The field emission is measured with a Keithley 237 source measure unit with voltage range of 0-1100 V and a current detection limit of $\sim$ 1 pA.

Fig. 2.46(a) shows a scanning electron micrograph (SEM) of the CNT thin film under investigation. Due to the random orientation and length of the nanotubes, the field enhancement β values between the individual tubes show a large scatter. This because some tubes stick up above the average CNT film deposit and therefore exhibit a large β as compared to the electrostatically shielded tubes that are entangled deep in the CNT film deposit. Therefore it is natural to assume that there is a spatial variation of the field enhancement β(x,y). The

SAFEM can be used to map the emission voltage V(x,y) at a fixed emission current level as a function of the tip position. The field enhancement β(x,y) map may then be derived from the V(x,y) map [13] according to:

$$\beta(x,y) = \frac{d \cdot E_{site}}{V(x,y)} \tag{1}$$

where E_{site} denotes the local electric field present at each emission site, necessary to obtain the constant emission current (in our case 10 nA) at which the V(x,y) scan was performed. From field emission spectroscopy of multi-walled CNTs we know that for an emission current of 10 nA, E_{site} is about 3800 $V\mu m^{-1}$ [14]. d $\sim$ 5 μm is the tip-sample distance.

From the field enhancement β(x,y) map the number N of peak values corresponding to single emitting CNTs can be determined as a function of the field enhancement. In this picture the β-distribution f(β) is defined by dN=f(β)dβ, where dN is the number of CNTs with field enhancement $\in$ [β, β+dβ] per unit area. In this paper however, we use the convention that dN represents all measured points/pixels (and not peak values) with field enhancement $\in$ [β, β+dβ] per unit area in the β(x,y) map. Therefore strong emitters are slightly over weighted in f(β) but the statistical quality is considerably enhanced.

From SAFEM investigations on various kinds of carbon field emitters including CNT thin films [13], it has become clear that f(β) has the form of an exponentially decreasing function with increasing field enhancement β (i.e. f(β) $\propto$ exp(-$k_1\beta$)). This means that the number of emission sites rapidly decreases with increasing value of the field enhancement β.

For the sample under investigation there are about 10^4 emitters $\cdot cm^{-2}$ at an applied field of 12 V/μm which deliver emission currents exceeding 10 nA (inset of Fig.2.23(a)). Compared to the high nanotube density of about 10^{10} cm^{-2} present on the CNT film deposit, the number of active emitters is therefore very small, just about 1 ppm. Hence a current driven degradation mechanism will act only on very few "active" CNT emitters in a constant applied field. But one has to consider that the degradation of such an active tube also can affect numerous non active tubes in its vicinity wherefore a complex degradation pattern may result. Hence the individual emission site disruption current level is difficult to evaluate in a typical current-voltage (I-V) or current-time (I-t) emission measurement, where a large number of emitters are simultaneously

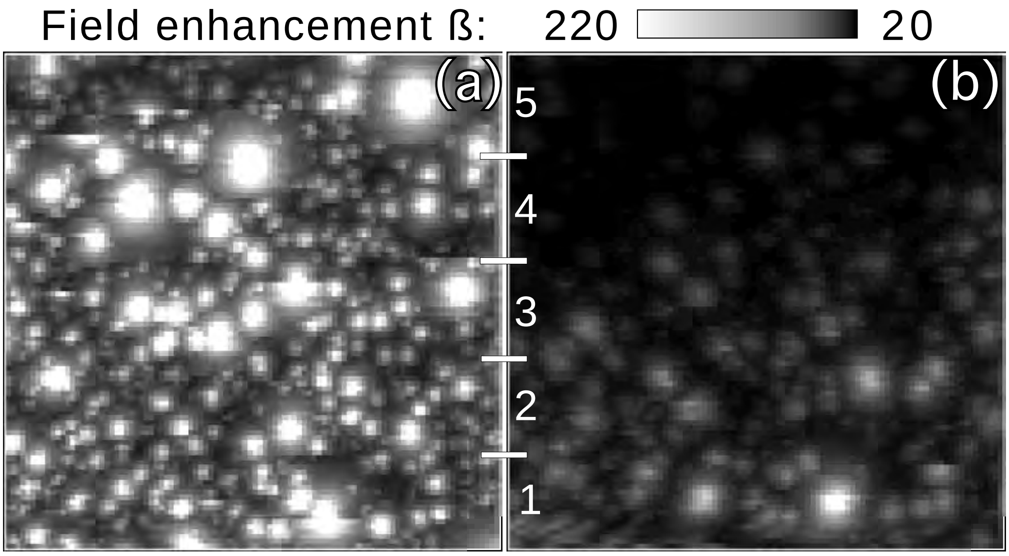

Figure 2.47: (a) The β(x,y) map derived from V(x,y) of the first scan before high current stress and (b) the β(x,y) map derived from the third V(x,y) map after high current stress, calculated according equation (1) for I= 10 nA. The emission current of sub-region 1 to 5 was raised to 0.1, 0.5, 1.0, 5.0 and 10.0 μA respectively during the second scan (not shown). Size of the β(x,y) maps is 200×200 μm^2.

---

measured in parallel.

Therefore we have adopted the following measurement scheme to investigate the single site degradation current level. The FE properties are first characterized by scanning a sample area of 200×200 μm^2 in the constant current mode (CCM) with an emission current of 10 nA. At this current level no current induced degradation can be observed. The same area is then subdivided in five equal regions of 40×200 μm^2. Each of these regions is then scanned with a constant current of 0.1, 0.5, 1.0, 5.0 to 10 μA respectively. After this step the total area is again scanned in CCM with 10 nA and compared with the initial situation before the scans at high emission current levels were performed.

Fig. 2.46(b) displays the first V(x,y) map where high field enhancement emission sites are pin-pointed by low extraction voltage (dark spots). Irregularities in the intensity between two adjacent linescans, where an emitter "disappears" or the emission spot size is reduced (white arrows), are typical for the first FE scan. Such discontinuities seldom appear for subsequent FE scans (at equal current levels), which have smooth and continual variation in the intensity between adjacent lines (round emission spots) and continues minimum values.

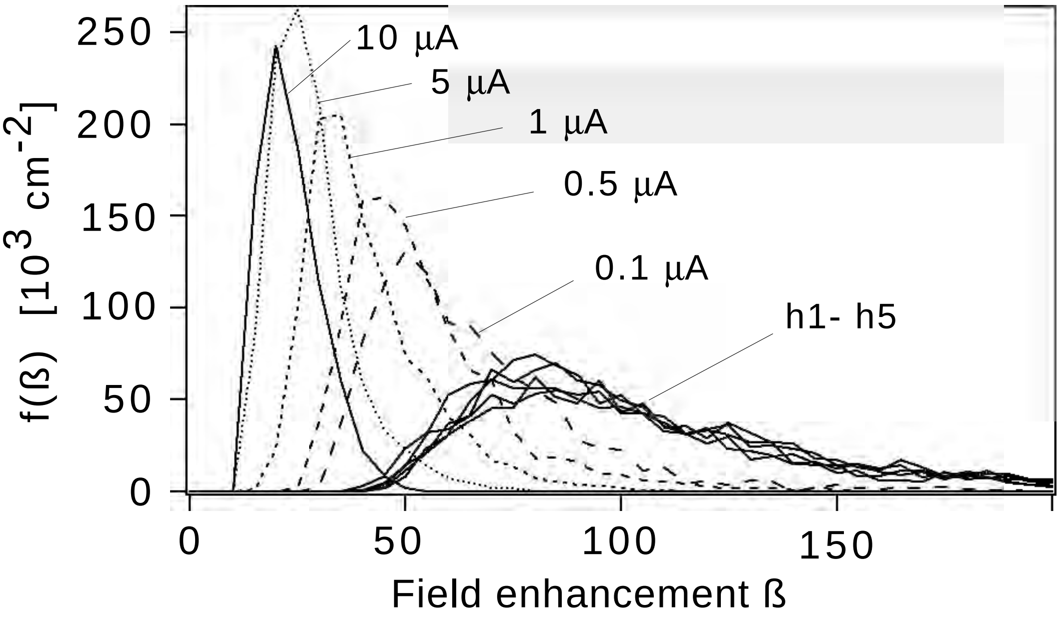

Figure 2.48: The β-distributions of sub-region 1 to 5 in Fig. 2 before (h1-h5) and after (0.1-10 μA) the high current scanning. The shift of f(β) in each sub-region towards lower field enhancement correspond to an irreversible emission degradation. It can be shown that the negative slope of f(β) is exponentially dependent on β and that the low β cut-off is due to a measurement resolution artifact [13].

The β(x,y) maps before (derived from V(x,y) of Fig. 2.46(b)) and after the high emission current scanning are displayed in Fig. 2.47, where the five horizontally arranged sub-regions are indicated by numbers 1-5. For each area 1-5 the field enhancement distribution can be derived as histograms from the corresponding β(x,y) map. In Fig. 2.48, f(β) from area 1-5 is plotted before (denoted by h1-h5) and after (denoted by 0.1-10 μA) high current levels. The intrinsic fluctuations of h_i are caused by variations in the number and intensity of emitting sites between each area.

In Fig. 2.47(b) the emission degradation becomes apparent from the reduction of the field enhancement from region 1 to 5 and as a shift of f(β) in Fig. 2.48. Refined scans up to 500 nA on other sample areas have shown that up to 300 nA/site routinely and repeatedly can be obtained without reduction of β. The initial degradation below 100 nA is a field- and not current-driven effect, associated with detachment of whole or parts of CNTs during the first scan and is most clearly seen as irregularities in the intensity of the first V(x,y) map.

On a microscopic level at least four possible explanations to the degraded emission can be given: structural damage to the CNT cap, the shaft or body, the substrate-tube interface or adsorbates at the CNT tip apex. We observe two distinct types of emission degradation behavior. The first occurs even at very low emission currents and seems to be driven rather by the electric field than the emission current. The second is current driven and occurs at emission currents above 300 nA per emitter.

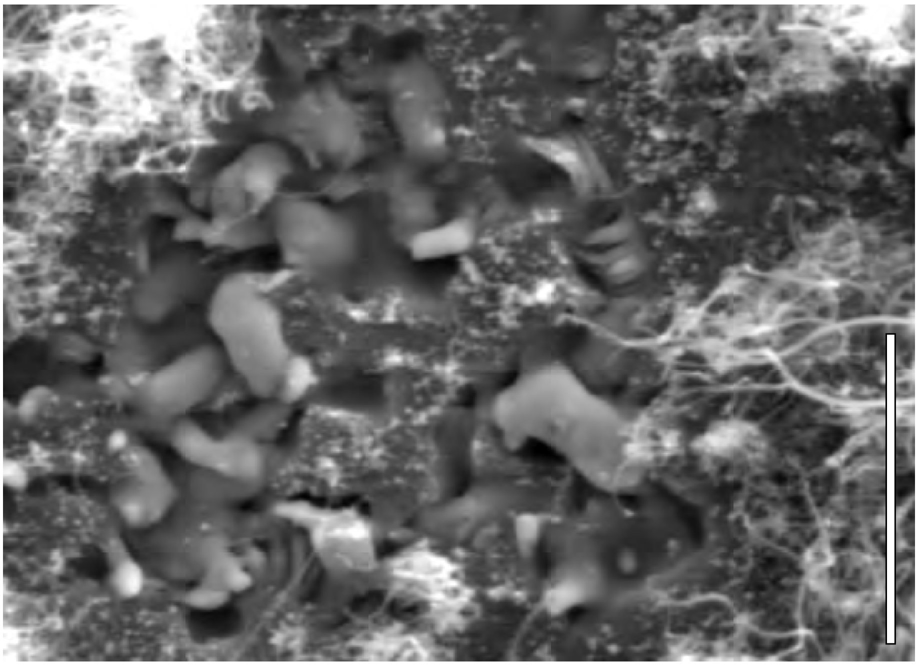

Figure 2.49: Field emission currents in excess of 10 μA per CNT can even cause the temperature at the CNT-silicon interface to reach the melting point 1420 °C of silicon.

The field dependent degradation is typically seen in the first scan (white arrows Fig. 2.46(a)) and can be attributed to field induced removal of CNTs or nm-sized amorphous carbon allotropes from the CNT tip apex as shown by transmission electron microscope (TEM) images of single free standing CNTs [15]. SEM images of the anode reveal that loosely adhered CNT are removed from the substrate due to the electrostatic forces, with instantly terminated FE as a consequence. We note that the field induced degradation also is consistent with the adsorbate induced current saturation mechanism reported by Dean et al. [16], where adsorbates enhance the emission in the low current range up to 300 nA. It is possible that some adsorbates are removed due to the high field conditions at the tip apex during the first scan on the pristine CNT film, and the emission may therefore decrease abruptly at a site between two adjacent linescans.

The current dependent degradation mechanism is active for currents higher than 0.3 μA per emission site and can be attributed to the interaction and energy dissipation during the solid state transport of a high current density through the CNT, at the CNT-substrate contact or at the CNT apex. I-V measurements on two point contacted CNTs have shown that straight and probably defect free CNTs, repeatable can conduct currents up to 3 mA ballistically without heat dissipation [17, 18]. Zettl et al. [19] pealed off outer layers and sharpened arc-grown MWNT by contacting the CNT ends in-situ inside a TEM. The current-induced CNT sharpening took probably place at defect sites (pentagons etc) for 200 mA current. Since the current dependent emission degradation of our CNT films occurred at much lower current levels, we do not believe resistive heating at defect sites in the CNT shaft to be the main cause of emission failure. Scanning electron microscopy (Fig. 2.49) of the emission area on the CNT film after high current (> 10 μA/CNT) FE, indicates that the CNT-substrate interface plays an important role for the energy dissipation. A poor electric contact between the substrate and the CNTs therefore provides the main obstacle in the electron transport from the substrate to the vacuum and can cause heat high enough to even melt the silicon substrate. Bonard et al. managed to repeatable draw a maximum emission current of 0.1 mA from a single MWNT mounted on the tip of an etched gold wire [10]. The discrepancy with our results may be explained by the difference in cathode geometry, since the single tube was well contacted and probably had a lower contact resistance.

On the investigated sample current dependent emission degradation could be observed from 300 nA per emitter. From this value the maximum current density of a thin planar emitting film can be estimated. For an arrangement of one emitting CNT with a tube length of 1 μm per 2×2 μm^2, current densities up to 8 A/cm^2 without screening effects [6] could theoretically be realized. Higher densities could be achieved with shorter tubes and higher CNT density, although at the cost of higher applied fields. By improved adhesion and electric contact between the emitting structures and the substrate even higher current densities should be possible.

The authors gratefully acknowledge financial support from the Swiss National Science Foundation.

References for 2.6

[1] H. Kind, J.-M. Bonard, C. Emmenegger, L.O. Nilsson, K. Hernadi, E. Maillard-Schaller, L. Schlapbach, L. Forró, K. Kern, Adv. Materials **11**, 1285 (1999).

[2] S. Fan, M.G. Chapeline, N.R. Franklin, T.W. Tombler, A.M. Cassell, H. Dai, Science **283**, 512 (1999).

[3] Z.F. Ren, Z.P. Huang, D.Z. Wang, J.G. Wen, J.W. Xu, J.H. Wang, L.E. Calvet, J. Chen J.F. Klemic, M.A. Reed, Appl. Phys. Lett. **75**, 1086 (1999).

[4] J.M. Kim, W.B. Choi, N.S. Lee, J.E. Jung, Diam. and rel. Mater. **9**, 1184 (2000).

[5] H. Murakami, M. Hirakawa, C. Tanaka, H. Yamakawa, Appl. Phys. Lett. **76**, 1776 (2000).

[6] L. Nilsson, O.Groening, C.Emmenegger, O.Kuettel, E.Schaller, L.Schlapbach, Appl. Phys. Lett.**76**, 2071 (2000).

[7] V.V. Zhirnov, A.B. Voronin, E.I. Givargizov, A.L. Meshcheryakova, J. Vac. Sci. Technol. B **14(3)**, 2034 (1996).

[8] F.Lacher, C.Wild, D.Behr, P.Koidl, Diamond and Rel. Mat.**6**, 1111 (1997).

[9] A.M. Rao, D. Jacques, R.C. Haddon, W. Zhu, C. Bower, S. Jin, Appl. Phys. Lett. **76**, 3813 (2000).

[10] J-M. Bonard, J.P. Salvetat, T. Stöckli, L. Forró, A. Châtelain, Appl. Phys. A **69**, 245 (1999).

[11] K.A. Dean, B.R. Chalamala, Appl. Phys. Lett. **75**, 3017 (1999).

[12] L. Nilsson, O. Groening, P. Groening, O. Kuettel, L. Schlapbach, Proc. XIV Inter. Winterschool on Electr. Prop. of Novel Materials, Kirchberg, Tirol, Austria, 499 (2000).

[13] L. Nilsson, O.Groening, P. Groening, O.Kuettel, L.Schlapbach, "To be published", Journ. Appl. Physics. (2001).

[14] O.Gröning, O.M. Küttel, P.Gröning and L.Schlapbach, J. Vac. Sci. Techol. **B17**, 1970 (1999).

[15] Zhong L. Wang, Advanced Materials **12**, 1295 (2000).

[16] K.A. Dean, B.R. Chalamala, Appl. Phys. Lett. **76**, 375 (2000).

[17] P.J. de Pablo, E. Graugnard, B. Walsh, R.P. Andres, S. Datta, R. Reifenberger, Appl. Phys. Lett. **74**, 323 (1999).

[18] S. Frank, P. Poncharal, Z.L. Wang, W.A. de Heer, Science **280**, 1744 (1998).

[19] A. Zettl, J. Cumings, Proc. XIV Inter. Winterschool on Electr. Prop. of Novel Materials, Kirchberg, Tirol, Austria, 526 (2000).

2.7 Optimization of the thin film electron emitter

Simulations of the thin film electron emitter

As we have showed the f(β) of carbon/nanotube thin film emitters exhibit a kind of exponential dependence upon the field enhancement β. It therefore seems plausible to believe that the exponential character of f(β) is a general property of an electron emitting thin film where the geometry of a single emitter is not controlled:

$$f(\beta) = k_1 \cdot exp(k_2\beta) \qquad [cm^{-2}] \tag{2.5}$$

The shape of f(β) is determined by the constants k_1 and k_2 and the ESD and the current density (J) will therefore depend on k_1 and k_2 according to equations 2.3 and 2.4. In the following we like to investigate the influence of the shape of f(β) on the ESD and J.

In general, the high requirements of homogeneous emission on a flat panel display require an ESD on the order of 10^7 emitter per cm^2 for applieds fields on the order of 10 V/μm or less. Accordingly the emitted current density of a cold cathode must be spatially homogeneous on a micrometer scale. Measurements on CNT and CVD diamond thin films with the phosphor screen and the SAFEM have shown however that the spatial homogeneity and the ESD currently does not suffice for high resolution FED applications, see sections 2.4 and 2.5. The highest ESDs recorded for applied fields below 10 V/μm do normally not exceed 10^4-10^5 sites per cm^2. The average thin film current density is therefore on the order of 1 to 100 mA/cm^2 if the average single emitter is assumed to withstand a mean current of about 300 nA without disruption, see section 2.6. Such low densities are insufficient for most device applications.

We therefore like to investigate how the ESD and the current density evolve and depend on the values of k_1 and k_2 of equation 2.5. For this current I(x,y) maps of randomly scattered emitters are simulated, which obey f(β) with different values of k_1 and k_2. Both experimentally obtained β-distributions as well as hypothetical β-distributions which have been "invented" for comparison purpose have been used to generate the randomly scattered emitter ensembles. For all simulations an applied field of 6.2 V/μm is used and the single site current is assumed to follow a resistor-limited Fowler-Nordheim (F-N) behavior. The as-

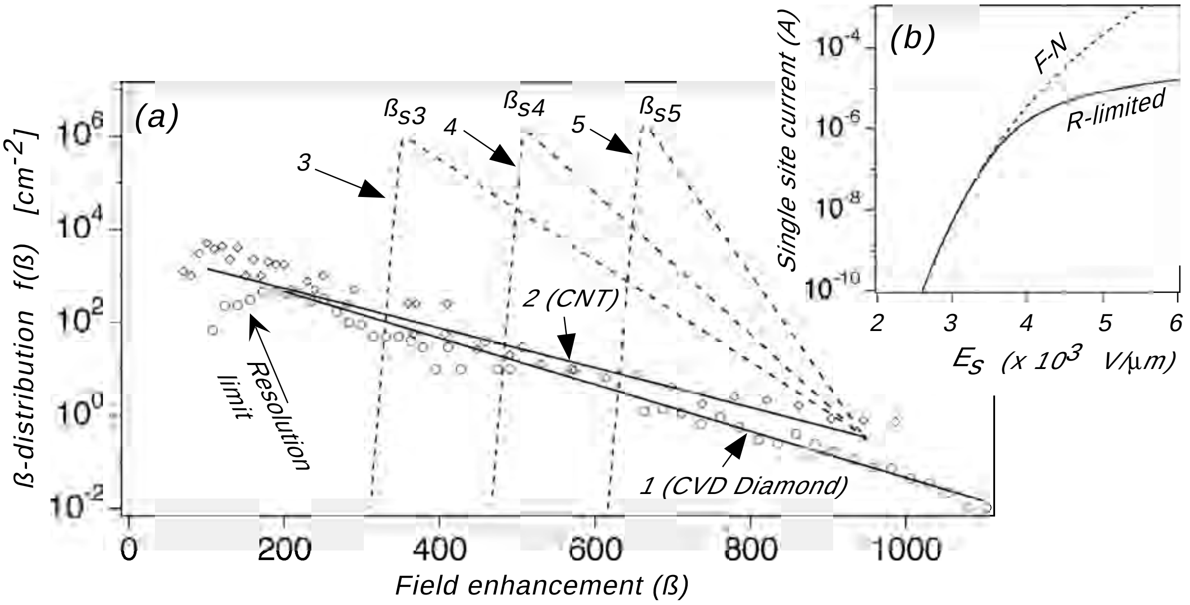

Figure 2.50: The two solid lines (1) and (2) in (a) depict f(β) as determined from two different thin film emitters. The three dashed lines (3)-(5) are hypothetical β-distributions in order to investigate the effects of increased slopes in f(β). The cut-off in f(β) for field enhancement $< \beta_s$ is explained by electrostatic screening effects for emitter densities of the order of 10^7 cm^{-2}. The inset (b) shows the Fowler-Nordheim (F-N) and resistor (R) limited emission current as a function of the local field E$_s$ at the emission site, which has been used in the simulations.

---

sumed R-limited emission current per site is shown in the inset of Fig. 2.50(b). As a first example two experimentally determined β-distributions with different f(β) slopes (1 is a CVD diamond and 2 is a CNT sample) are compared. Fig. 2.50(a) shows f(β) for both samples (solid lines), where the measurement points have been added for comparison. The resulting current maps of 1583 (Sample 1) respectively 2834 (Sample 2) generated emitting sites are shown in Fig. 2.51. The reason for the higher ESD of the carbon nanotube film (2) resides in the larger number of sites in the high field enhancement regime. We point out that the simulated current maps are similar to the emission patterns on phosphor screens during similar conditions and applied fields.

In order to generate emitter ensembles with higher ESD and therefore different variation in the field enhancement three hypothetical f(β) distributions (3)-(5) have been pre-defined, i.e. they have not been experimentally verified. Fig.

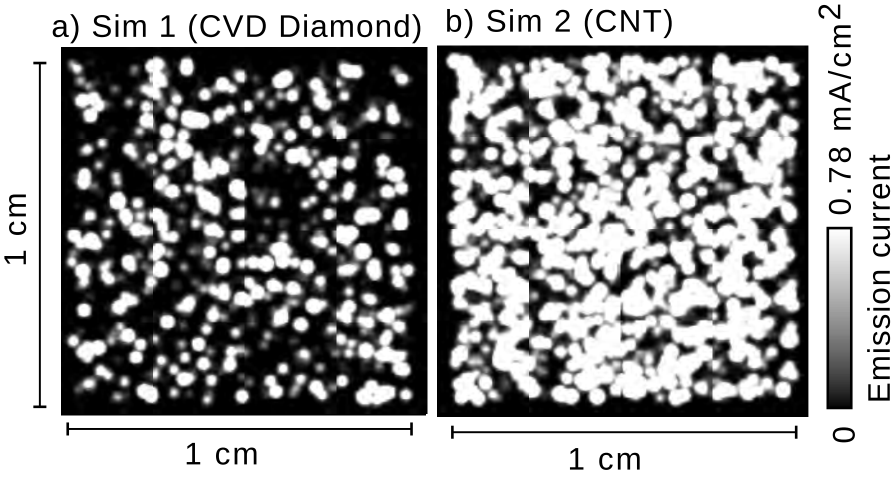

Figure 2.51: Simulation (a) of the current of 1583 emitters according to the β- distribution (1) for an applied field of 6.2 V/μm. Simulation (b) of the current of 2834 emitters according to the β- distribution (2) for an applied field of 6.2 V/μm. The total current is 0.39 mA in (a) and 1.1 mA in (b).

2.50(a) shows the variation of the field enhancement of the three f(β). Due to the increased slopes of the hypothetical distributions (3)-(5) the number of sites per unit area increases very rapidly as we integrate from high to low field enhancement. Contrary to the experimentally obtained f(β), the density therefore rapidly increases going from high to low field enhancement up to a critical density, where electrostatic screening reduces the effective field enhancement. From our early investigations the critical screening density has been calculated to be in the range of 10^7 to 10^8 emitters per cm^2, section 2.3, if the field enhancing structures FES are about one micrometer long. We speculate that this field enhancement reduction has the form of a rapid drop in f(β) below the critical field enhancement screening limit β_s as indicated in Fig. 2.50(a). If the critical screening density is assumed to occur (and we neglect the dependence of the size of the field enhancing structures upon β and assume monodisperisive FES) for about $4.5 \cdot 10^7$ cm^{-2}, then we find for the three hypothetical distributions (3)-(5), β_{s3}= 350, β_{s4}= 507 and β_{s5}= 660.

A surface area on the order of 1 cm^2 seems adequate for investigations and simulations of emitting site densities on the order of 10^4 cm^{-2} or lower. However in the case of a FED where an ESD on the order of 10^7 cm^{-2} is required and where each subpixel is defined on a length scale of typically 100×100 μm^2, 1 cm^2 surface area is too large for investigations of the current spatial distribution. The individual sites cannot be recognized or resolved with 10^7 emitters on 1 cm^2. Instead due to the high density of about $4.5\cdot10^7$ cm^{-2} the simulation of the emission current of about 4500 randomly distributed emitters is done in a 100×100 μm^2 window. These 4500 emitters are generated from the respectively distribution (3) to (5) and the simulations of the I(x,y) maps under the applied field $E_a \sim 6.2$ V/μm are shown in Fig. 2.52.

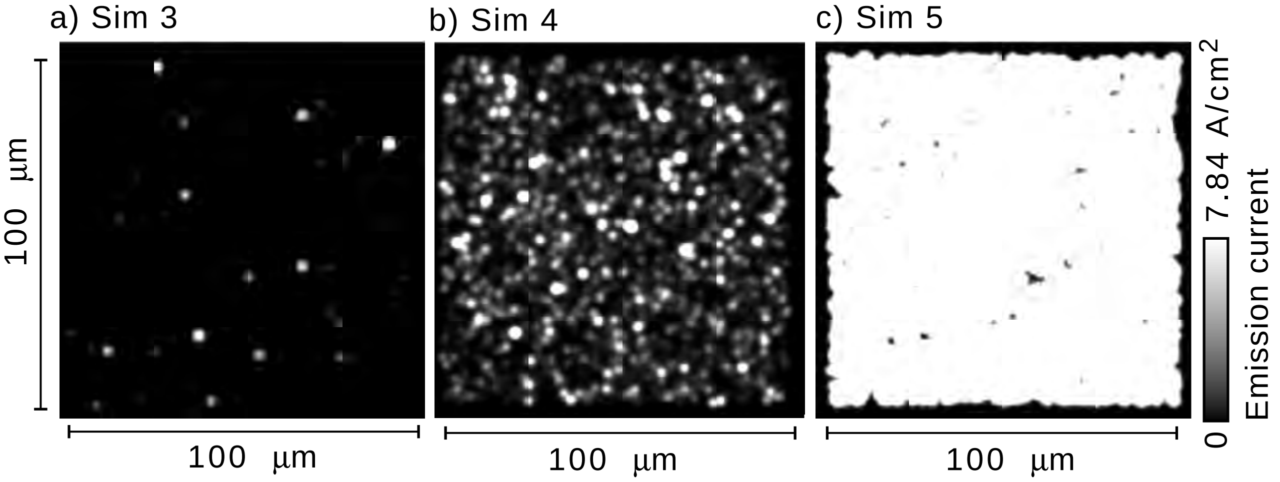

Figure 2.52: Simulations (a)-(c) of the emission current of 4500 emitters according to β-distributions (3)-(5) for a thin film emitter area typical of a pixel in a display. The applied field is 6.2 V/μm and the total current is (a) 7.6 μA, (b) 0.15 mA and (c) 3.2 mA.

We note that the increased slope of distribution (3) has provoked an increased ESD to about $2\cdot10^5$ cm^{-2}. The ESD in the case of distribution (4) is further improved to about $2\cdot10^6$ cm^{-2} due to the increased density of emitters in the field enhancement range $\beta > 507$. The majority of the sites are active emitters in the simulation of Fig. 2.52(b), albeit we note that the variation in intensity between the weak and the strong sites is explained by their relative difference in field enhancement. In order to equalize the intensity per emission site and to make the weaker sites visible, it appears in analogy to the I(x,y) simulations in Fig. 2.52(a) and (b) that an increased mono-dispersivity of the field enhancement values is favorable. Such an increased mono-dispersivity is realized by the β-distribution (5) and the resulting current map from simulation (5) clearly depicts an improved homogeneity in the I(x,y) map. The increased mono-dispersivity in the case of (c) provokes an equalization of the "turn-on" field for the 4500 sites, which effectuate a better homogeneity on the screen.

The here presented simulations therefore show that a β-distribution with a narrow shape and with a high density of emitting FES in a small field enhancement range is the best option in order to achieve a high and homogeneous ESD. The more narrow this distribution is, the more homogeneous the ESD. However as the density of FES approaches the limit where the inter-FES distance becomes comparable with the size of the FES, electrostatic screening will effectively reduce the field enhancement. This reduction is expressed as a drastic cut in the characteristics of f(β) in the low field enhancement regime.

Hence a narrow shaped β-distribution of mono-dispersive field enhancing structures is needed in order to obtain an efficient thin film emitter with a high ESD. In the next section the possibilities to realize such a distribution with carbon/graphite based thin film emitters is discussed.

2.8 Design of carbon-based gated field-emitter arrays

According to the previous section the emitting structures should be deposited in such a way that the field enhancement factors β are as mono-dispersive as possible. The cost and the complexity to do so depends on the degree of orientation, alignment and precision at which the FES (like CNTs) are deposited. *Selective* growth of single FES with well defined aspect ratios and high density requires a high degree of control and is therefore expensive. A *non-selective* growth process of several or many FES arranged in patches requires less control and is therefore less expensive. We here propose two possible cathode designs, see Fig. 2.53, with different degrees of orientation and alignment in order optimize the cathode performance with regard to the cost. The FES must be deposited in the gated structures on a level of one- or tens of micrometers depending on the wanted emission site density.

In the first approach (a) the structures are deposited in a pre-defined gate aperture of typically 10×10 μm^2 area. The exact size of the area is a matter

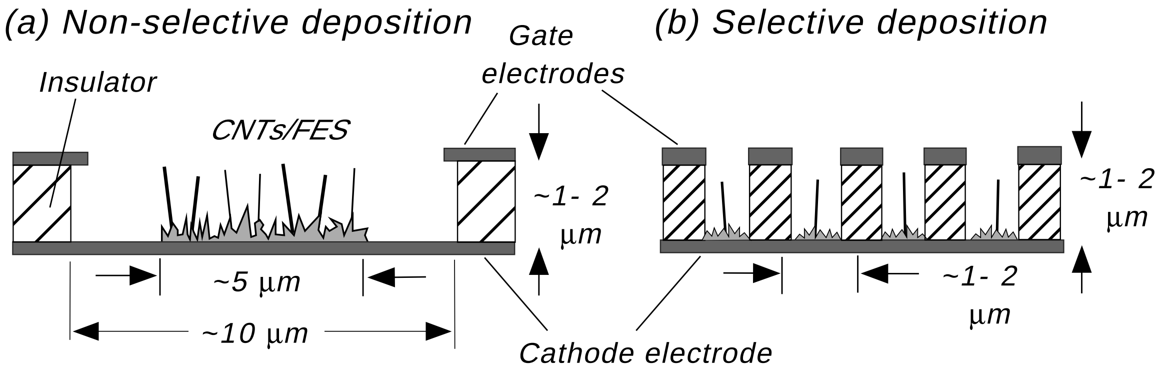

Figure 2.53: The non-selective deposition (a) of field enhancing structures (FES) relies on the self-organized alignment between the FES in each gate aperture, whereas the alignment of the FES in the selective deposition (b) is defined by the confinement of the single FES to the gate aperture.

---

of engineering and depends on the desired ESD of the device. The structures, like CNTs or other FES like graphite fibers, are deposited in such a way that shorting the surrounding gate electrodes is avoided. One possibility to do that is to deposit the FES confined to only the central parts of the gate apertures, as indicated in the figure (a). Contrary to the metal tip FEA, where only one tip is deposited per gate aperture, several FES can be parallel processed during a single deposition step. We like to call this approach *non-selective deposition* since there are no intrinsic constraints like the walls of the aperture, upon which we can relay on for the number and/or alignment of the FES during the deposition process. The method of deposition must therefore itself ensure a certain self-organization of the structures, in order for these to fulfill requirements of density, field enhancement and orientation. The higher the degree of self-organization, the better the quality of the deposit will be. It seems reasonable to think that not all, but primarily those FES close to the borders of the deposit (which are close to the gate) will emit in the first place, presumably only one, two or three emitting FES. For an array of closely packed $10 \times 10\ \mu\text{m}^2$ gate aperture areas, the ESD will be of the order $10^6\ \text{cm}^{-2}$ in the best case provided that the field enhancement values are largely mono-dispersive. The effects of emission inhomogeneities could be controlled to some degree using resistive layers. The tubes or structures which are present adjacent to the emitting structures in each gate but that are in-active (i.e. provides a negligible emission current) partly due to lower field enhancement or screening effects, constitutes an valuable "reserve" of FES. This reserve provides emitter redundancy in the case of disruption of one or more active emitters, which makes the gated structure less sensible to emitter failure.

The second approach (b), using *selective deposition* includes a step up both in cost and complexity since instead of relying on self organized alignment and growth between a group of parallel deposited structures on a relatively large length scale (~ 10 μm), the individual emitting structures must be manipulated or deposited in a single structure manner. In this approach single emitters are deposited in gate apertures on a μm (or possibly even sub-μm) scale provided single FES growth or deposition methods can sustain the stringent requirements of orientation and aspect ratio of the structures. It therefore has to be ascertained that only *one* FES is placed in *exactly* the right position preferably with sub-μm resolution and that absolute control of the aspect ratio is maintained. Control of the aspect ratio is important not only because the ESD should be high but also because short circuit contacts with the gates have to be avoided. Since such a deposition is assumed to take place on a micrometer scale, not unlike the case of the metal tip array, emitting site densities on the order of 10^8 cm^{-2} should theoretically be possible. However since the cost of producing a pre-defined micrometer sized gated structure is approximately inversely proportional to length scale or size of the pattern, the selective approach can be expected to be more expensive than the non-selective approach, as far as standard lithographic patterning techniques are concerned.

State of the art and future directions

Since their discovery 1991 by Iijima [1] carbon nanotubes have been recognized as promising candidates for electronic and specifically electron emission applications. After ten years of extensive research efforts many of the physical properties have been carefully investigated and documented, but still today the exact mechanism(s) under which carbon nanotubes are formed is not clear. It seems plausible to believe that the tubes formed under the high temperature conditions of an arc discharge are created under the influence of other driving forces and other non-equilibrium conditions than tubes grown by the catalytic decomposition of hydrocarbon gases. Even if a number of theories on the growth mechanism(s) of CNTs exists today nobody has been able to experimentally verify and exploit these to fully control the growth regarding density, lengths, diameters, number of shells, etc. of the tubes. Reports of catalytically grown CNTs, similar to the curved, curly and spaghetti like tubes in Fig. 2.54(a) are given on a regular basis in the literature today [2].

The random length and non-aligned orientation of the curved CNTs is a partly unsolved problem. Catalytically grown spaghetti like CNT thin films of this type do therefore in general not exhibit emitting site densities above 10^4 cm^{-2} for applied fields in the range 5 to 10 V/μm. One interesting approach to improve both the density and the alignment (and hence the ESD) of the CNTs is done in a prototype diode structure by Samsung, where purified SWNT are dispersed in isopropyl alcohol and mixed with an organic binder and metal particles [4]. The CNT-epoxy mixture is squeezed onto a metal patterned sodalime glass through a metal mesh of size 20 μm. Subsequent cathode surface rubbing is used to liberate parts of the tubes which are protruding above the surface of the paste of dispersed CNTs in Fig. 2.54(b). This approach is interesting since it does not include any complex stages (and thus is inexpensive) and the density of the tubes can be adjusted by the ratio tubes/organic binder. The disadvantage from a technical point of view is that the alignment, although considerably improved compared to the spaghetti type CNT deposit, only can be manipulated to a limited extent. The method by Ren et al. [5] of growing well-aligned and self-oriented multiwalled CNTs on nickel-coated glass in a plasma-enhanced hot filament CVD process marks an important progress towards large area CNT alignment (see Fig. 2.54(c)). However the relatively large variation in height and aspect ratio of the tubes does not favor mono-dispersive field enhancement. The efforts made by Li et al. [6] to catalytically grow CNTs confined to nanochannels (mean diameter $\sim$ 47 nm) in the self-organized pores of anodic alumina films, has largely improved the mono-dispersivity of the aspect ratios (see Fig. 2.54(d) and inset below). The hexagonally well ordered array of CNTs with lengths of $\sim$ 6 μm has a very high density of approximately 10^{10} cm^{-2}. It seems therefore that both the method of Ren and Li needs improved controle and adjustment of the density, in order to avoid too high CNT densities which leads to electrostatic

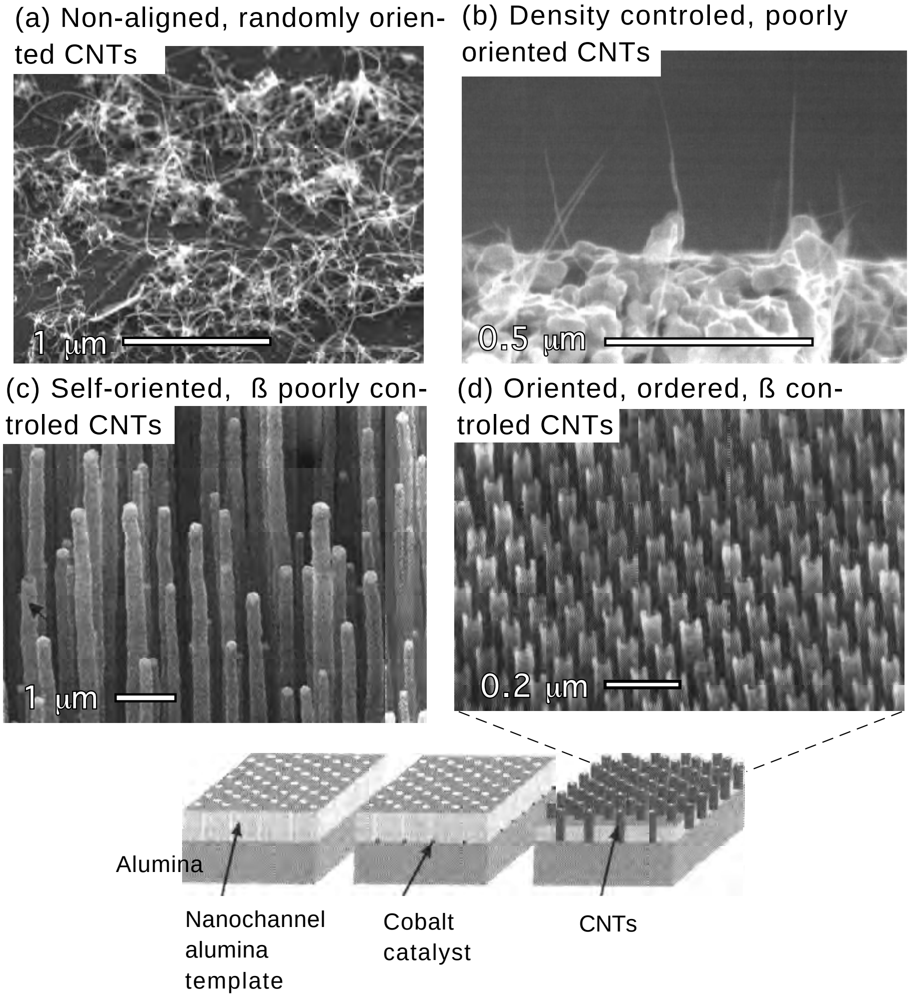
(a) Non-aligned, randomly oriented CNTs
(b) Density controled, poorly oriented CNTs
(c) Self-oriented, ß poorly controled CNTs
(d) Oriented, ordered, ß controled CNTs

Figure 2.54: Illustrations of different degrees of organization and alignment of the field enhancing structures (a)-(d). The catalytically grown CNTs [3] in (a) exhibit typically a random, non-aligned orientation with respect to the substrate. The arc discharge produced SWNT [4] of (b) have been mechanically post- deposited. The catalytically grown CNTs in (c) are self-oriented but lack a precise controle of density and aspect ratio [5]. The CNTs/graphite rods in (d) have improved mono-dispersivity and alignment but still lacks a variable density of structures [6].

screening effects and reduced effective field enhancement β.

This section has so far focused much on the cathode design and not on other technical or economical aspects of VMED design and development. There is no guarantee that the carbon emitter will prevail since the original technological incentive to produce a carbon based FED was due to the vision of cold cathodes without tips.

In order to commercialize a FED the criteria listed in paragraph 1.5 must be fulfilled. The scalability of the deposition and the number of critical steps in the manufacturing of the cathode largely affects the production cost. The complexity and price of the cold cathode has therefore to be weighted with the expected performance and device quality, e.g. measured as in the form of the ESD, see Fig. 2.55. As a comparison with existing and non-existing fabrication technologies the "ideal" CVD flat thin film [7] emitter has been inserted in Fig. 2.55.

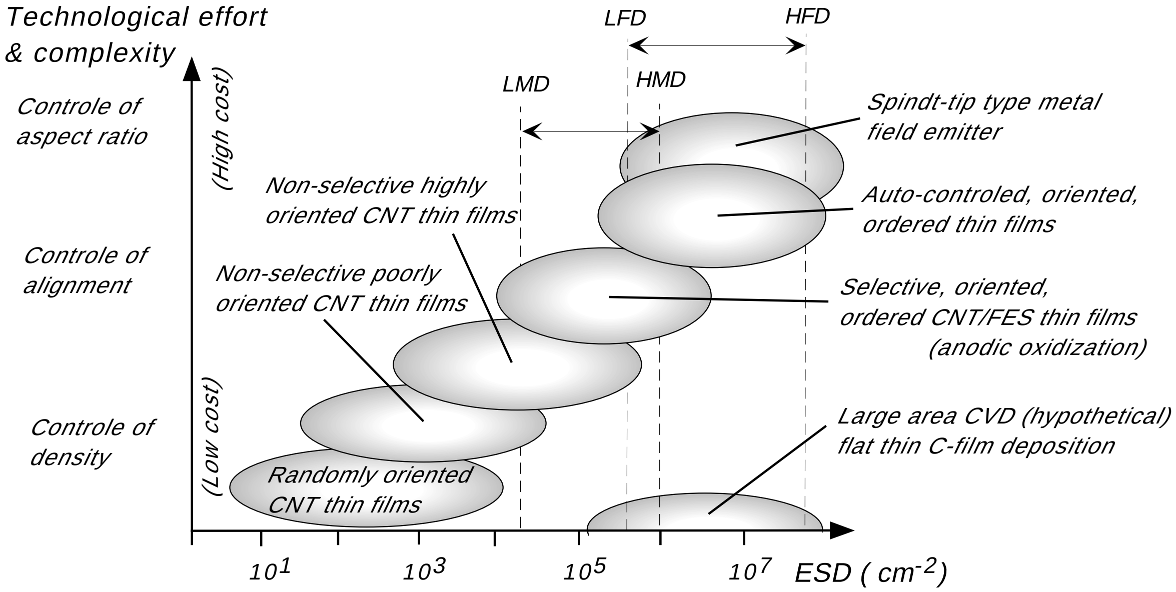

Figure 2.55: The technological complexity and cost can be said to be a monotonic increasing function (here assumed linear) of the wanted device performance. The device performance is here measured as the emitting site density (ESD) of the thin film emitter. LMD= Low Resolution Mono-crome Display, HMD= High Resolution Mono-crome Display, LFD= Low Resolution Full color Display and HFD= High Resolution Full color Display.

Whereas films of the types in Fig. 2.54(a) and (b) are relatively easy and thus not to expensive to manufacture today, they do not match the high requirements of quality (here measured as high ESD). The films which Samsung produced may be characterized as non-selective poorly oriented CNT thin films and may therefore fit in the lower left part of the diagram in Fig. 2.55. Despite the clever and easy way of manufacturing of these films, the lack of precise controle of alignment and field enhancement, make the CNT epoxy technique insufficient for device applications where high resolution is wanted. However the quality may be suffice for a low resolution mono-crome display (LMD) or for electronic billboard applications. Since the price is considered lower than for a Spindt-tip array of similar quality, the CNT epoxy mixture is very competitive for large scale production of an device where less performance is expected. The trade-off between quality and cost is here the driving force of commercialization. Films of same quality as the Spindt emitter must be called auto-controlled, fully oriented and ordered thin film emitters. Such films are expected to have an ESD in the range 10^6 to 10^8 cm^{-2} and are found in the upper right part of the diagram in Fig. 2.55. Films with an inter-mediate degree of alignment and orientation between the Samsung films and the Spindt-type emitters are situated on a straight line in Fig. 2.55. The slope of this line and the intersection of the auto-controlled thin film emitter with the Spindt-tip type emitter in Fig. 2.55, determines the competitiveness of the carbon films with regard to the ESD. We speculate that the slope is such that the degree of complexity of the auto-controlled thin film emitter is slightly lower than for the Spindt-type emitter. It seems however probable that the complexity will be of the same order as for the Spindt emitter.

The future progress in the field of controlled growth or deposition of carbon FES like carbon nanotubes will determine the slope in Fig. 2.55. It thereby seems that a major breakthrough in the understanding of the complex non-equilibrium processes leading to the formation of carbon nanotubes in a cathodic arc or during catalytic decomposition of carbon containing gases, is very important. The full control of density, aspect ratio and alignment can only be reproduced on a large scale if full understanding of the growth parameters has been achieved. The time to that breakthrough is controversial and therefore it is very difficult to foresee the time of introduction of a high resolution carbon based field emission display on the market. Meanwhile other devices like electronic billboards or hybrid field emission displays/CRTs [8] with lower requirements on the emitting site density, may be developed and commercialized.

References for 2.7 and 2.8

[1] S. Iijima, Nature **354**, 56 (1991).

[2] C. Emmenegger, P. Mauron, A. Züttel, C. Nützenadel, A. Schneuwly, R. Gallay, L. Schlapbach, Appl. Surf. Sci, **162-163**, 452 (2000).

[3] H. Kind, J.-M. Bonard, C. Emmenegger, L.O. Nilsson, K. Hernadi, E. Maillard-Schaller, L. Schlapbach, L. Forró, K. Kern, Adv. Materials **11**, 1285 (1999).

[4] J.M. Kim, W.B. Choi, N.S. Lee, J.E. Jung, Diam. and rel. Mater. **9**, 1184 (2000).

[5] Z.F. Ren, Z.P. Huang, J.W. Xu, J.H. Wang, P. Bush, M. Siegal, P.N. Provencio, Science **282**, 1105 (1998).

[6] J.Li, C. Papadopoulos, J. M. Xu, M. Moskovits, Appl. Phys. Lett. **75**, 367 (1999).

[7] J.E. Jaskie, MRS Bulletin **21**, 59 (1996).

[8] R.C. Robinder, Z. Yaniv, R.L. Fink, Z. Li Tolt, L. Thuesen, Field Emission Picture Element Technology Inc., Austin, Texas (www.carbontech.net) (2001).

Chapter 3

Electron emission environmental stability

The term *environmental stability* is used to describe the interaction of electron emitters with the gaseous environment in which they are operated. Such interactions typically lead to emission current fluctuations on a time scale of seconds to minutes. If the current fluctuations are large the may negatively affect the device performance. In addition the device long-term stability is dependent on the emitter interactions with its environment, wherefore investigations on environmental stability are important. Such investigations have been done in the past on etched metal tips using field emission microscopy (FEM).

3.1 Field Emission Microscopy on CNT emitters

The Field Emission Microscope (FEM) invented by Dr. Müller [1] in 1937 has for a long time been the state of the art to investigate adsorption and diffusion phenomena at surfaces with almost atomic resolution. At the time etched tungsten tips of high aspect ratio were used as cathodes. Observations of the field emitted electrons from the emitter apex region on phosphor screens at high spatial magnification ($\sim 10^7$ times) yielded better insight into diffusion, ad- and de-sorption rates and workfunction dependence upon crystallographic planes and coverage of adsorbates [2]. In particular alkali and alkaline earth adsorption has been studied in this way [3]. The FEM gave qualitative evidence of surface segregation in form of bright rings about various crytallographic planes long before the advent of Auger spectroscopy. As a matter of fact the FEM was one of only very few existing techniques for such investigations until the discovery of the scanning tunneling microscope (STM) in the mid eighties. Much of the analytical work in this field has since then been taken over by the STM due to its versatility under a wide range of experimental conditions. The discovery of the carbon nanotubes and their use as field emitters has however lead to the revival of the experimental technique of the FEM. Mostly because of the nanotube geometry with high aspect ratio which is well suited for investigations in a FEM and thus for investigations of the charge distribution and its time dependence on carbon nanotube caps.

The principle of such measurements is indicated in Fig. 3.1(a), where different CNT electronic cap states are reproduced on a phosphor screen.

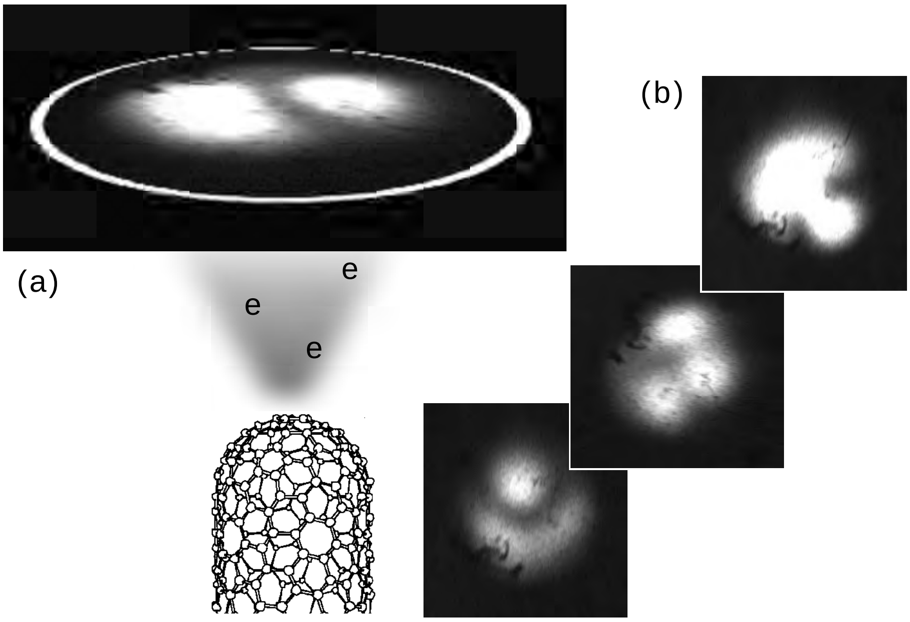

Figure 3.1: The lobed FEM pattern of a multiwalled CNTs at 300 K in (a) has been observed for adsorbates on metal tip emitters. Some examples of a large variety of such patterns commonly observed from both single walled and multi walled CNT are shown in (b).

It is recognized that the FEM pattern on the screen reflects the electronic structure, the anisotropy of the workfunction, local variation of the microscopic field and transmission probability of a single CNT cap. This means that atomically sized areas on the CNT cap, where the workfunction is low or the local field is higher than on surrounding regions, are reproduced with a higher intensity on the phosphor screen. Analytical investigation of such patterns would ideally yield better insight into the CNT cap electronic structure. Unfortunately, the state and the structure of the individual CNT is cap very often not known during the typical experimental conditions in a FEM. Contrary to the etched metal tips it is difficult to align the CNTs towards the screen. The termination of the individual tubes, e.g. if they are capped or not or if they have metallic inclusions, is often difficult to predict. The probably most important factor of experimental uncertainty comes from residual gas particles, molecules or atoms that are present at very low concentrations in the vacuum chamber background, see section 3.2. During the high field conditions around the emitter tip such species can be polarized at large distances from the emitter compared to the Langmuir mean free path. They are therefore accelerated in the high field and strike the emitter tip at very high energies and impact rates as compared to field-free gas kinetics. Due to the large distance at which the polarization can take place, the impact rates can be several orders higher than for ordinary field-free Langmuir gas kinetics at comparable temperatures and ambient gas pressures [4]. At present it is not exactly clear which effect this bombardment has and in which way the FEM pattern are changed due to adsorption of species onto the emitter tip.

Probable origin of the FEM pattern

With FEM investigations it has become clear that the spatial charge distribution on the CNT tip apex is time dependent. Some typical examples of time dependent FEM patterns from the same MWNT emitter are depicted in Fig. 3.1(b), but a rich variety of these can be found. The time dependence and the anisotropy over the CNT cap of the field emitted electrons can be understood in terms of switching between different states with relatively small energy difference in levels which are close to the Fermi energy. These states can be seen upon as "electron clouds" above the sp^2 bonded carbon atoms which can change their shape as a function of the state energy. Ideally, for a "clean" CNT cap without adsorbed molecules, the FEM pattern represents an image or a finger-print of these electron clouds or states.

In order to illustrate how the states are formed and may look like one can take the π-states of a benzene molecule (C_6H_6) as an example, see Fig. 3.2. The hexagonal sp^2 bonded network of carbon atoms (C) form a ringstructure with 120 ° angles in benzene [5]. Of the three sp^2 hybrid orbitals per C atom one forms a binding σ orbital with the 1s orbital of an hydrogen (H) atom and the two others form binding σ orbitals with the corresponding sp^2 orbitals of the C atoms on each side, Fig. 3.2(a). The remaining $2p_x$ electron forms maces protruding perpendicular above the plane of the six C atoms. The totally six $2p_x$ electrons can form six types of electron clouds (π-states) where 3 are binding and 3 are anti-binding π-orbitals (i.e. above zero energy), see Fig. 3.2(b). The six electrons belong to the entire C_6H_6 molecule and not to individual C atoms wherefore they are said to be delocalized.

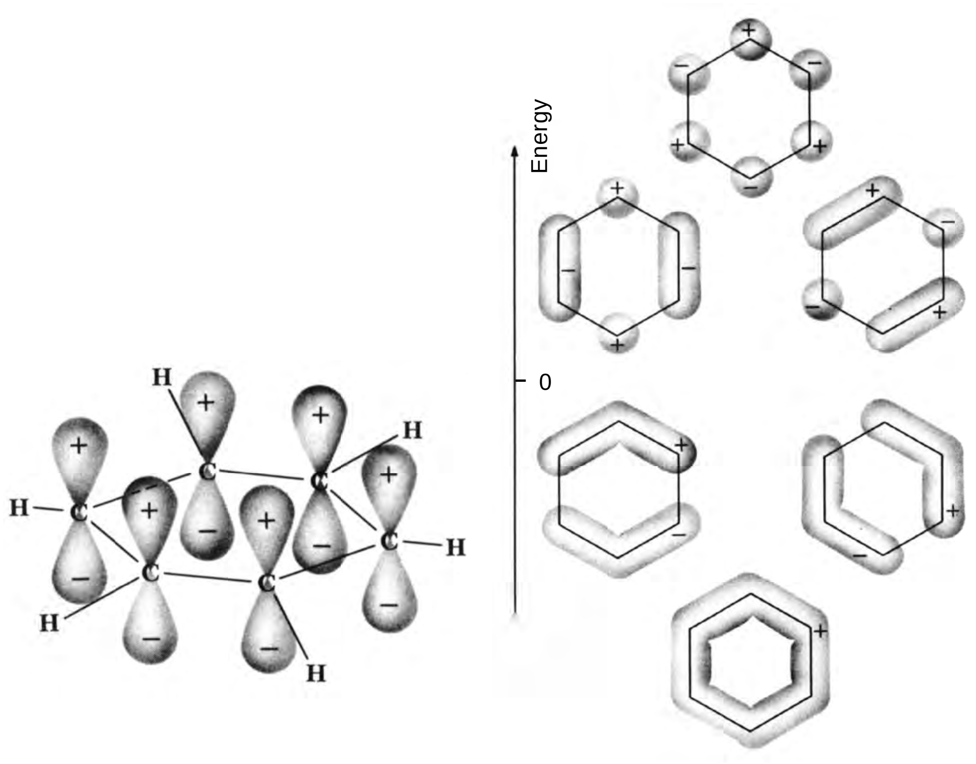

(a) p_X orbitals in C_6H_6

(b) π hybrid orbitals (top view) in C_6H_6

Figure 3.2: The p_x orbitals (a) of benzene C_6H_6 can form six π hybrid orbitals of delocalized electrons (b), whereof 3 are in a binding stabilized state (i.e. below zero energy) and 3 are in a anti-binding state [5].

In analogy to the C_6H_6 molecule the π-states of a "clean" CNT cap can be thought of as linear combinations of p_x orbitals which are protruding out perpendicular to the carbon lattice on the tube apex. The limited variety in shape, style and energy of such π-states can only partly explain the large number of FEM patterns from CNT emitters at 300 Kelvin. It therefore seems plausible to think that the energy levels of the clean CNT caps are modified through adsorbed species coming from the gas phase during field emission. It seems probable that some of the species stick (chemisorption) to the CNT emitter. Sometimes the sticking is very firm and may result in a resonant tunneling state which can lead to increased tunneling probability and anisotropy in the FE current on the CNT cap [6]. It also seems as if the adsorbed molecules are "shuffled" around the tip apex due to the bombardment on a time scale of seconds to minutes. Our investigations indicate that the rate of change of the FEM pattern is only a weak function of the ambient gas pressure in the FEM vacuum system. Instead the state of the phosphor screen seems to play a more important role for the FEM pattern rate of change at 300 K. This would in turn indicate that alien gas species and molecules, liberated through electron scrubbing of the phosphor screen, in fact are responsible for the enhanced resonant tunneling states and changes in the FEM pattern. One possibility to investigate the CNT electronic cap states without superimposed electronic states coming from adsorbed molecules is by short term in-situ heating. Such a procedure cause the adsorbed species to receive thermal energy high enough for them to desorb from the surface, leaving the bare CNT cap free. Unfortunately re-adsorption takes place on a time scale of minutes depending on how well the screen was electron scrubbed before heating the CNTs.

The experiments in this chapter have been designed to elucidate the origin of the alien gas species and their possible effect(s) upon the FEM patterns from the CNT emitters. It has to be stressed that the term *environmental stability* here is used to describe the above related phenomena at the CNT cap during field emission at a time scale of seconds to minutes, whereas the term *emission stability* normally is used to describe the degradation of the emission current (e.g. due to disruption or burn-out) at longer periods of time of hours or weeks.

References for 3.1

[1] Z. Phys. **106**, 541 (1937).

[2] J.A. Becker, "Advances in Catalysis", edited by W.G. Frankenburg, E.K. Rideal and V.I. Komarewsky (Academic, New York), Vol **VII**, 184 (1955).

[3] R. Gomer, Solid State Phys. **30**, 93 (1975).

[4] A. Zangwill, "Physics at Surfaces" (Cambridge), 20 (1992).

[5] A. Beiser, "Atome, Moleküle, Festkörper" (Vieweg), 139 (1982).

[6] Dean K , Chalamala B.R., Journ. Appl. Phys., vol 85, no 7, p.3832-3836 (1999).

3.2 Environmental stability of carbon nanotube field emitters

L. Nilsson, O. Groening, P. Groening, O. Kuettel, L. Schlapbach
Institute of Physics, University of Fribourg, Pérolles, CH-1700 Fribourg, Switzerland

Published in Electronic Properties of Novel Materials - Molecular Nanostructures, XIV International Winterschool, Kirchberg, Tirol, Austria, 499 (2000).

Abstract

Investigations of the current-time (I-t) characteristics of field emission (FE) from single-walled carbon nanotubes (SWNT), does not show any significant dependence on ambient partial pressures to 10^{-5} mbar of hydrogen or water. It is however shown that oxygen causes substantial reduction of the FE current and this is believed to be related to reactive etching/ oxidation of the nanotubes. By heating the tubes up to 1100 Kelvin an increased instability in the FE current as well as on the field emission microscopy (FEM) screen can be observed. These instabilities become less and less pronounced after repeated annealing steps. FEM during short-time heating reveals dim five-fold as well as six-fold feinstructures. These feinstructure FEM patterns are not stable and have a short lifetime. Resonant tunnelling states as well as FE from nanotube cap states might explain these observations.

3.2.1 Introduction

World wide efforts to produce stable carbon nanotube (CNT) field emission sources are underway since the middle of the last decade [1-4] and at the IWEPNM 2000 in Kirchberg, Samsung presented a 9-inch full colour field emission display (FED) based on CNT emitters. CNTs have proven to be more robust than comparable unballasted metal field emitters [5], however the inherent short-term emission instability has not yet been understood. From field emission microscope (FEM) investigations it is recognised that emission does not occur homogeneously all over the CNT cap, but in a time-variable (sec) lobed pattern, which reflects the electronic structure, local variation of the microscopic field and transmission probability. Explanations to these spatial pattern fluctuations, include FE from non-metallic cap states correlated to the presence of pentagonal defects [6], FE from open/closed tubes with dough-nut pattern [7] and FE through resonant tunnelling states caused by adsorbed gas species [8]. For reasons of long term stability and safe operation of e.g. FEDs, a fundamental understanding of the underlying short-term emission instability mechanism is required.

3.2.2 Pressure and Temperature Dependence on FE (SWNT)

Experiments were carried out in a FEM with different phosphor-coated planar anodes at a typical base pressure of $5{\cdot}10^{-9}$ mbar.

Commercial SWNTs were pasted to a tungsten heating filament with conductive carbon cement. FE currents were recorded on the grounded anode as a function of temperature and partial gas pressures of high purify oxygen, hydrogen and water. Typical potentials of 2000 Volts were applied over a variable 2-cm anode-cathode separation and the filament temperature was determined with a pyrometer. FEM patterns were real time recorded using a charge coupled device camera. As observed from I-t measurements, initial heating increases the noise (sub-sec fluctuations) of the FE current (Fig. 3.3(a), point 1). Analogous to the increased current noise level, the FEM pattern rate of change is increased and the typical one-, two- and four-lobed symmetrical and asymmetrical patterns, fluctuate at a time scale of sub-seconds. Other, more exotic five/six-fold FEM patterns may occasionally be visible during heating, showing a dim structure,

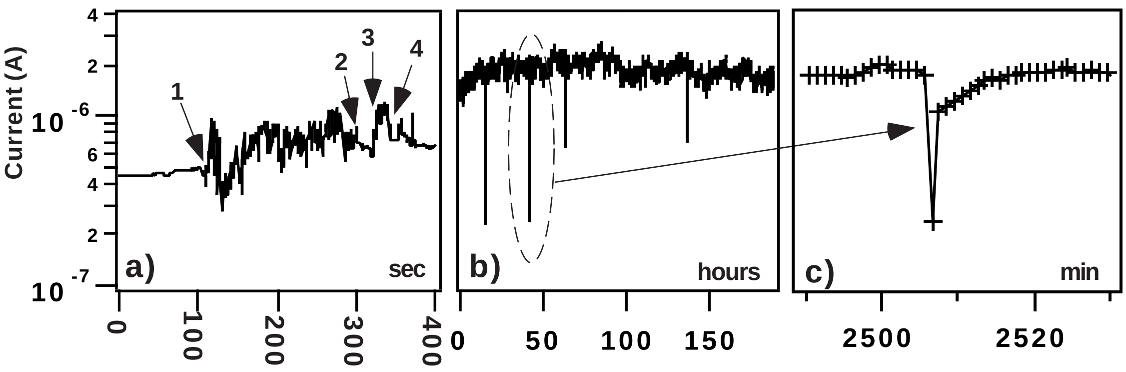

Figure 3.3: (a) FE current vs. time during heating to 900 Kelvin between point 1-2 and 3-4 causes increased noise level. Before point 1, between 2-3 and after point 4 the level of noise is decreased; i.e. at T= 300 Kelvin. This behaviour is typical during first period heating. This sample was not annealed before. P $\sim 1.6 \cdot 10^{-7}$ mbar, 2600 Volts, 22 mm gap. (b) Current dependence during one week (one point/ minute) - stable FE at ~1.5 mA, 4 emitters, FEM pattern unchanged at 1900 Volts, 20 mm, T= 300 Kelvin and P$\sim 5 \cdot 10^{-9}$ mbar. Current decay at four occasions; second event resolved in (c) Possible spontaneous desorption (~1 sec) and current recovery during 15-16 minutes. Same current scale in (a)-(c). Different samples a and b.

Fig. 3.4(c), but do not seem to be long time stable. When the initial heating is turned off, point 2 and 4 in Fig. 3.3(a), the level of noise is drastically reduced to the initial level, and a few minutes after heating the FEM pattern remain quite stable, Fig. 3.4(e).

With repeated annealing steps, the increase of the noise level upon heating, becomes less and less pronounced. Repeated heating over 1000 Kelvin causes in general the overall current level to decrease, sometimes up to a factor of 10, and this current reduction is irreversible, depending mainly on the state of the screen (see below). We further investigated the long-term stability (one week) of four emitters using a thermally outgassed phosphor screen, Fig. 3.3(b) and (c). In contrast to unballasted metal field emitters no current runaway (associated with protrusion growth) is observed and the current level is maintained at approximately 1.5 μA with the exception of spontaneous current reduction about on order of magnitude at four occasions (see Fig. 3.3(b)). It can be speculated that the rapid current decay is associated with the spontaneous desorption of chemisorbed molecules or atoms, and that the current recovery is due

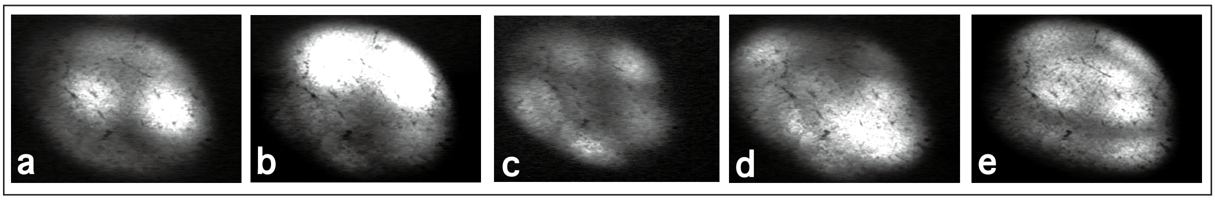

Figure 3.4: FEM time-resolved sequence of single SWNT cap at 2000 volts, d= 21 mm, P ~2^{-7} mbar. Average diameter of spot ~1cm. (a) t=0: Long-term stable pattern at T= 300 Kelvin; possibly representing the surface electronic structure of an adsorbed two-atom configuration on the NT cap. (b) t= 39s: Short-term filament heating (3 sec) to T=1600 Kelvin. The stable atomic configuration in a, is disturbed and possibly a two-atom molecule is formed as the molecule is desorbed from the NT cap surface. (c) t= 42s: Removing the lobed pattern reveals an intensity-weaker five-fold fine structure underneath. This form lasts only for some seconds at T= 300 Kelvin (Intensity magn. ×3). (d) t= 74s: Spatial charge fluctuations. The pattern in c is occasionally spotted. (e) after t=140s is the pattern stable again. T= 300 Kelvin.

to readsorption from the gas phase. However we are not able to assign a certain relation between the current recovery time and the ambient gas pressure up to 10^{-5} mbar. Current recovery times of normally 8-20 minutes are observed independent of the ambient gas pressure. Preliminary investigations show stronger dependence on both current level and type of screen material used in experiment. This would indicate that the source of molecules/ions possibly being readsorbed after heating, is the screen. This dependence can be explained in terms of ion bombardment of the NT cap, where the ions are liberated from the screen due to the impinging electrons. When we used metal plate anodes or well thermally outgassed thin phosphor coatings, that had been electron scrubbed for a long time, we could not restore initial higher current levels after heating to 900, 1000 or 1100 Kelvin. We further investigated the FE instability during high partial pressures (up to 10^{-5} mbar) of hydrogen, water and oxygen, all of them to be expected in our chamber (or FED) background.

The samples were thermally annealed at 900-1500 Kelvin, before any gases were introduced into the ultrahigh vacuum system through a leak vent. Thermal annealing causes a reduction of both current level (up to a factor of 10) as well as of current noise. Hydrogen or water exposure for periods of hours did not degrade or improve the emission, Fig. 3.5(b) and (c). Nor could we secure a relation between the partial pressure and the level of noise in these cases. That is if

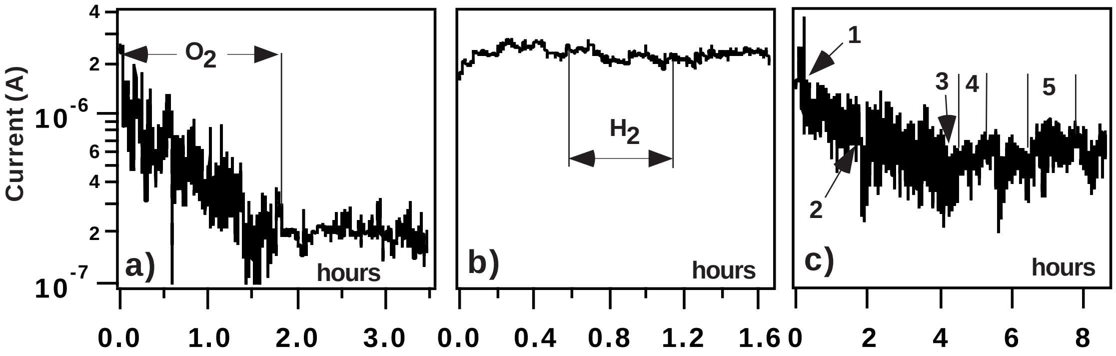

Figure 3.5: FE current vs. time as a function of high partial gas pressure, 10^{-5} mbar, of oxygen, hydrogen and water at T= 300 Kelvin. Current scale 10^{-7} to $4{\cdot}10^{-6}$ Ampere. (a) Oxygen causes an irreversible damage by reactive ion etching. FE current is reduced by a factor 10. (b) Hydrogen does not seem to affect the FE current stability on a time scale of hours. (c) Point 1,2 and 3: heating of filament to 900, 1000 and 1100 Kelvin for 120 sec ⇒ current reduction. H_2O at 10^{-7} mbar (4) and 10^{-6} mbar (5) during ~1 hour does not restore initial current of 2mA.

impinging gas molecules or ions are responsible for chemisorbed states, we should be able to see a dependence on the ambient background pressure. Moreover we were never able to restore the initial current of 2.2 μA after heating to 900, 1000 and 1100 Kelvin, in Fig. 3.5(c), by introducing water vapour. Repeated trials on several sample with shorter and longer (~ hour) exposures of 10^{-7}, 10^{-6} and 10^{-5} mbar left us without success. Operation of nanotubes in 10^{-5} mbar of O_2 causes however a 10-fold irreversible degradation over a time of 1.5 hours. We propose that this decrease be due to a reactive ion etching effect [9], where C-O bonds are formed at the open NT cap.

3.2.3 FEM-Pattern During Short-Term Heating

Traditional one-, two- and four lobed patterns are commonly reported from NTs in the literature [8], and we observe them as well. We will however here not show any of these patterns but patterns of rather rare nature. They are obtained during short periods of filament heating and show five-fold fine structure, Fig. 3.4(c), with lower intensity than before heating. In an adsorbate-tunnelling-state model they could be interpreted as an adsorbate-free NT cap, where the chemisorbed state is removed when given enough heat. We speculate that the remaining fine structure of the five-fold spatial charge distribution, is a result of pentagons introduced into a hexagonal C-bonding network of the NT cap. Such a five-fold fine structure has been theoretically calculated [10] from the NT cap. In conclusion we have shown that the ambient gas phase pressure of both hydrogen and H_2O has a negligible effect on the long-term stability of the FE currents from SWNTs. Increased partial pressure of oxygen causes a degradation of the FE, and this effect is ascribed to reactive ion etching in the vicinity of the open NT cap. The temperature dependence indicates that adsorbates are present on the as-introduced pristine NT cap and that these states can be removed during heating. Re-adsorption does not seem to come from the ambient gas phase but rather from the screen if not well thermally outgassed. The spatial charge fluctuations of the pristine NT cap reflect the ion bombardment coming from the screen, which probably displace adsorbed species around the NT cap. This work was supported by NFP36 ”Nanoscience” and TOP Nano 21 (ETH BoardKTI).

References for 3.2

[1] Gulyaev Yu.V., Chernozatonskii L.A, Kosakovskaya Z.Ya., Sinitzyn N.I., Torgashov G.V., Zakharchenko Yu. F., "Field Emitter Arrays on Nanofilament Carbon Structure Films", Revue Le Vide, les Couches Minces" Supplment au No 271-Mars-Avril (1994).

[2] Heer W.A, Châtelain A., Ugarte D., Science, vol 270, p. 1179 (1995).

[3] Küttel O., Gröning O., Emmenegger C., Schlapbach L., Appl. Phys. Lett., 73, 2113 (1998).

[4] Nilsson L., Gröning O., Emmenegger C., Schlapbach L., Appl. Phys. Lett., 76, 2071 (2000).

[5] Dean K.A., Chalamala B.R., Appl. Phys. Letters, vol 75, no 19, p. 3017-3019 (1999).

[6] Bonard J-M., Salvetat J-P., Stöckli T., de Heer, W.A., Forró L., Châtelain, Appl. Phys. Letters, vol 73, no 7, p.918-920 (1998).

[7] Saito Y., Hamaguchi K., Hata K., Tohji K., Kasuya A., Nishina Y., Uchida K., Tasaka Y., Ikazaki F., Yumura M., Ultramicroscopy 73, p.1-6, (1998).

[8] Dean K , Chalamala B.R., Journ. Appl. Phys., vol 85, no 7, p.3832-3836 (1999).

[9] Mazzoni M.S.C., Chacham H.,Phys. Rev. B, vol 60, no 4, R2208 (1999).

[10] De Vita A., Charlier J-C, Blase X., Car R., Appl. Phys. A 68, p.283-286 (1999).

3.3 Carbon nano-/micro-structures in field emission: Environmental stability and field enhancement distribution

L. Nilsson, O. Groening, P. Groening, O. Kuettel, L. Schlapbach
Institute of Physics, University of Fribourg, Pérolles, CH-1700 Fribourg, Switzerland

Published in Thin Solid Films **383**, 78 (2001)

Abstract

The field emission (FE) properties of carbon films can be understood in terms of local field enhancement β(x,y), which can be determined with x,y-scanning FE. β(x,y)$\Rightarrow$ the spatial distribution of emitting sites, which can be counted as f(β)$\propto$exp(-kβ). f(β) is connected with the presence of sharp protruding objects, whiskers or nanotubes on the surface. Investigations of the current-time (I-t) characteristics of field emission from single-walled carbon nanotubes (SWNT) do not show any significant dependence on ambient partial pressures of hydrogen or water up to 10^{-5} mbar. Oxygen however causes a substantial reduction of the FE current. Field emission microscopy (FEM) during short-time nanotube annealing ($\sim$1000 Kelvin) reveals dim five-fold as well as six-fold feinstructures, which are believed to be nanotube cap states. The nanotube cap states have a short life-time due to impinging atoms/ions, that are adsorbed due to the high local electric field at the cap ($\sim$3000 V/μm), and create resonant tunnelling states. The anode material is believed to be the main source of adsorbed species and not the ambient gas phase.

3.3.1 Introduction

World wide efforts to produce stable carbon based field emission sources are underway since the middle of the last decade [1], and recently Samsung presented a 9-inch full colour field emission display (FED) based on carbon nanotube emitters (CNT). The macroscopic low-field (~ 1 V/μm) emission from carbon thin films like diamond-like carbon, tetrahedral carbon and nanocrystalline diamond is attributed to the presence of micro- and nano-scopic whiskers and field enhancing structures (FES). The FES amplify the applied electric field up to thousand times at the emission site according to $\mathrm{E}_{site} = \beta \cdot E_{applied}$, where β is called the field enhancement factor. The macroscopic emission site density (ESD) and current density (Acm^{-2}), can be controlled by tuning the structural properties (β) and inter-FES distance [2]. The controlled deposition of carbon FES like CNTs, in a gated structure is therefore a problem of uttermost technological importance. From field emission microscope (FEM) investigations it is recognised that emission does not occur homogeneously over the entire CNT cap but in a time-variable ($\sim$s) lobed pattern, which reflects the electronic structure, local variation of the microscopic electric field and transmission probability [3,4]. In order to commercialise a carbon-based cathode it is necessary to master the production of FES in a controlled way, but also to understand the spatial current fluctuations at the emission site, since safe operation and long term stability of a FED is connected to the short-term emission instability.

3.3.2 Scanning FE in constant current mode and the f(β)-distribution

Microscopic (x,y) scanning FE was performed over $\sim 200 \times 200$ $\mu\mathrm{m}^2$ using a Pt-Ir tip of radius ~ 1 μm, at a typical anode-cathode distance of ~ 5 μm.

One can either record FE currents I(x,y) for a fixed voltage or the required voltage V(x,y) for a fixed current, e.g. I_{FE}= 50 nA/pixel (Const Current Mode). V(x,y) is plotted as a function of tip position. It can be shown from electron energy distributions (EED) [5], that the local field at the emission site E_{site} is $\sim$ 4000 V/μm (CNTs) for I_{FE}= 50 nA. Since $\mathrm{E}_{site} = \beta \cdot E_{applied} \approx \beta(V_{tip}/d)$, where V_{tip} is the applied bias and d is the tip-cathode separation, we can estimate the local β(x,y) according to:

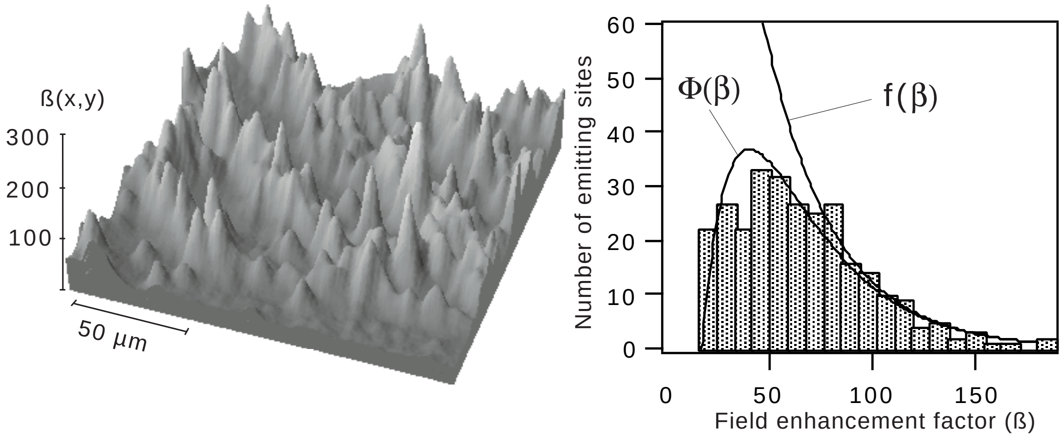

a) ß(x,y) scanning FE-map

b) ß-distributions Φ(β), f(β)

Figure 3.6: (a) The β(x,y) map of a patterned CNT sample according to equation (1). The peaks are correlated to the presence of nanotubes. (b) The peaks have been counted as a function of the β-factor (grey bars) in the FE-map (a) and fitted with the effective β-distribution $\Phi(\beta)$. The effective β-distribution is calculated from the true distribution f(β) according to $\Phi(\beta)$= A$_E(\beta)$·f(β), where A$_E(\beta)$ is the available emitting area corresponding to the probability of detecting FES with $\beta > \beta_0$. The low-β cut-off at $\beta \sim$ 30-50 is due to the screening effect of proximity CNTs.

$$\beta(x,y) = \frac{d \cdot E_{site}}{V(x,y)} \tag{1}$$

The β(x,y) map depicts the field enhancement landscape and is correlated to the surface roughness and the presence of FES. β(x,y) of a patterned CNT sample is shown in Fig. 3.6(a). β values below 50 are "screened" due to neighbouring FES with larger β value. The probability of detecting FES is thus a monotonic increasing function of β according to:

$$A_e(\beta) \propto \{1 - \int_\beta^\infty f(\beta) A_0 \, d\beta\} \rightarrow 1 \qquad when \qquad \beta \rightarrow \infty \tag{2}$$

The integral can be understood as the area occupied by emitters with field enhancement $> \beta$. The effective β-distribution $\Phi(\beta) = A_E(\beta) \cdot f(\beta)$, as calculated from the true β-distribution f(β), can be fitted to the experimental values in Fig. 3.6(b). It can be shown that f(β) can be fitted to experimental values over 5 orders of magnitudes using scanning and integral FE techniques according to:

$$f(\beta) = k_1 \exp\{-k_2\beta\} \tag{3}$$

The functional dependence of f(β) is equivalent to the surface roughness $\propto$ exp(-kβ). This is an indirect proof of the correlation between the low-field electron emission and the surface protrusion effect. k_1 is a measure of the ESD in constant voltage mode and k_2 is connected with the structural order/disorder of the carbon FES. By changing k_1, k_2, the FE properties of any surface can thus be tuned. Engineering technological relevant FE cathodes is thus the story of how to change/manipulate the fundamental equation (3).

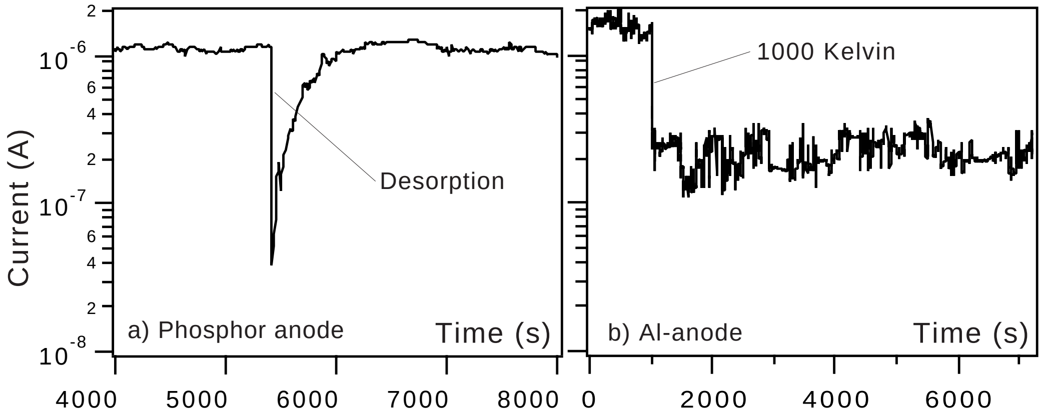

Figure 3.7: (a) Spontaneous desorption of atoms/molecules from the CNT cap causes a significant current reduction. The initial current level is restored as impinging molecules, from the phosphor-screen, are re-adsorbed (~10-20 min). (b) Short thermal annealing (~ 1 min) cleans the CNT cap from adsorbed species. However the thermally cleaned Al-anode does not emit atoms/molecules due to the electron scrubbing and re-adsorption does not take place.

3.3.3 Environmental stability of CNT field emitters

The environmental stability was studied using a FEM with different phosphor-coated planar anodes (~ $5 \cdot 10^{-9}$ mbar). Commercially available single walled CNTs were pasted to a tungsten heating filament.

FE currents were recorded on the grounded anode as a function of temperature and partial gas pressures of high purity oxygen, hydrogen and water. Typical

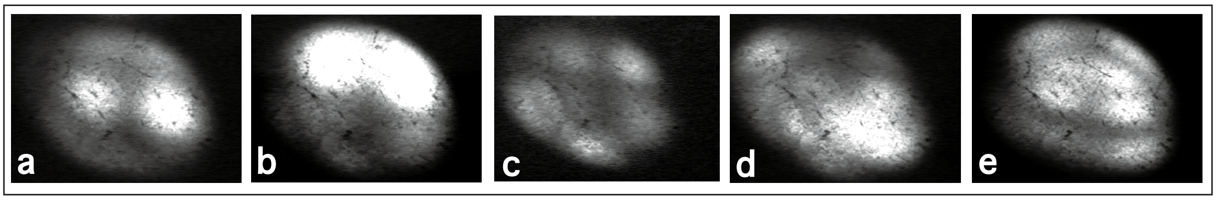

Figure 3.8: FEM time-resolved sequence of CNT; spot-size ~ 1cm. (a) t=0: Long-term stable pattern at T= 300 Kelvin. Possibly the surface electronic structure of an adsorbed two-atom configuration on the NT cap. (b) t=39s: Short-term filament heating (3 sec) at T=1600 Kelvin. The stable atomic configuration is disturbed and a two-atom molecule is formed and desorbed. (c) t=42s: Resonant tunnelling state removed. Five-fold fine structure of the clean CNT cap? Not stable at T= 300 Kelvin (Intensity magn. × 3). (d) t=74s: Spatial charge fluctuations due to sputtering. (e) After t=140s the resonant tunnelling state is re-established and stable (T=300 Kelvin).

potentials of 2000 Volts were applied over the variable 2 cm anode-cathode separation. Thermal annealing of the CNTs to 1000 Kelvin causes a reduction of both current levels (up to a factor of 10) as well as of current noise. This is believed to be connected with desorption of atoms from the CNT caps, where the atoms created resonant tunnelling states and enhanced tunnelling probability. Outgassing phosphor-screens are believed to be the main source of adsorbing molecules/atoms (if not carefully thermally cleaned), and re-adsorption takes place on a time-scale of ~minutes. If however, a carefully cleaned Al anode is used, re-adsorption does not take place, Fig. 3.7. We could not find a relation between the ambient background pressure and re-adsorption from the gas phase. Hydrogen or H_2O exposure for periods of hours (up to 10^{-5} mbar) did not degrade or improve the emission. Operation of nanotubes in 10^{-5} mbar of O_2 causes however a 10-fold irreversible degradation. The adsorbed species and the resonant tunnelling states can be removed by short-term annealing. The clean CNT cap reveals a five- and six-fold fine-structure on the FEM, Fig. 3.8(c). This work was supported by NFP36 "Nanoscience" and TOP Nano 21 (ETH BoardKTI).

References for 3.3

[1] R.L. Fink, Z. Li Tolt,, Z. Yaniv, Surf. Coat. Tech.,108-109, 570 (1998).

[2] Nilsson L.,Gröning O., Emmenegger C., Schlapbach L., Appl.Phys.Lett., 76, 2071 (2000).

[3] Dean K , Chalamala B.R., Jour. of Appl. Phys., 85, 7, 3832 (1999).

[4] Bonard J-M., Salvetat J-P., Stöckli T., de Heer, W.A., Forró L., A. Châtelain, Appl. Phys. Letters, 73,7, 918 (1998).

[5] O. Gröning, O. Küttel, P.Gröning, L.Schlapbach, J. Vac. Sci. Tech. B17, 1970, (1999).

Conclusions and outlook

Significant progress in the understanding of the electron emission has been achieved since the first reports on the low threshold electron field emission from carbon thin films in the beginning of the last decade. It seems certain that the low threshold electron emission from most thin film electron emitters can be explained in terms of field enhancement β from surface protrusions. Contrary to a single emitter, the emission properties of a thin film emitter requires a statistical treatment, since the field enhancing structures exhibit a distribution with regard to the field enhancement. Therefore we introduced the field enhancement distribution f(β) and measured it from the emitter density with a phosphor screen and from field enhancement β(x,y) maps as determined from scanning anode field emission microscopy (SAFEM). In contrast to "threshold" fields, f(β) and β(x,y) can be used to describe the emission properties of most thin film emitters under a wide variety of experimental conditions. f(β) has in general an exponential characteristic wherefore the field enhancing structures of thin film emitters exhibit a low density in the high β regime and a high density in the low β regime. It was shown that the field emitted current is reduced due to electrostatic screening when the inter-emitter distance becomes comparable with the typical size of the emitters. For emitters of one micron length this indicates a maximum theoretical density on the order of 10^7 to 10^8 emitters per cm^2. For f(β) distributions with a steep exponential slope one can therefore expect that the screening will induce a cut-off in the f(β) characteristics for low field enhancement. Theoretically f(β) should therefore take the form of an asymmetrically shaped distribution. The state of the art emitter densities are however too low to experimentally verify the predicted asymmetric shape of f(β), where the effective field enhancement is confined to a narrow β-range. The narrower this range is, the more the structures will be mono-dispersive. It was shown that improved mono-dispersivity will induce an equalization in the electric "turn-on" field and hence a more homogeneous emitting site density for the emitters of the emitter ensemble. It can thus be stated that an efficient thin film emitter should consist of field enhancing structures with mono-dispersive field enhancement factors. The homogeneity of the emission can be further improved by the use of resistive layers. The substrate-emitter resistivity induces deviations from the Fowler-Nordheim behavior and plays an important role for the emitter degradation under high current stress.

Investigations of the *environmental stability* of single carbon nanotubes (CNT) in a field emission microscope (FEM) have indicated resonant tunneling states on the CNT tip apex. It appears that gas species (atoms or molecules) coming from the phosphor screen are responsible for these states. However more work is needed to clarify the origin of the FEM patterns from CNTs.

The hopes for easy fabrication and good emission properties of thin film electron emitters without surface protrusions was a strong incentive for the research in this field. It turns out, however, that stringent, mainly geometrical requirements have to be put upon the carbon cold cathodes. The hereby increased technological complexity will be the next challenge in the vacuum microelectronic design. This challenge depends for sure on the future progress in the field of controlled growth of field enhancing structures such as nanotubes. This challenge is further complicated by the fact that the carbon nanotube emitters will not only have to compete in performance but also in production cost against standard technologies.

In order to engineer new such cold cathodes it will be essential to examine the emission properties as a function of the manufacturing parameters. The SAFEM offers the perfect tool for such investigations.

The here presented measurements with the SAFEM can be improved in several ways:

- The lateral resolution can be enhanced by the use of a micron-sized outer guard ring around the anode. This can serve as a focal lens for the potential distribution between the anode and the cathode if a higher potential is applied to the outer than the inner anode. The current is thereby only measured on the inner anode.

- The SAFEM can be used for automatisized characterization of single emission sites on a thin film emitter in a large number. Statistical evaluation of a large number of sites with regard to single site emission stability and current-voltage characteristics can be advantageous to in order categorize different types of emitters. From these it should be possible to deduce the field enhancement and compare with the β as determined from the V(x,y) maps.

The measurements with the FEM can be extended in several ways as well:

- Theoretical FEM patterns can be simulated and compared to the experimental results. Such comparisons may be used to elucidate the nature of the FEM patterns and the resonant tunneling states in the case of the adsorbed species. In order to find the relationship between the FEM patterns and their energetic levels, FEM can be combined with field emission spectroscopy.

- Complementary field ion measurements on carbon nanotubes can serve as a tool for the characterization of the cap geometry and can be used as input for theoretical models for the simulation of FEM patterns.

Curriculum vitae

Personal details

Family name	Nilsson
First name	Lars-Ola Ingemar
Date of birth	January 12, 1971
Place of birth	Älmhult, Sweden
Nationality	Swedish
Status	Single

Education

1990 - 1996	Technical University Linköping, Sweden: Master of Science in Applied Physics and Electrical Engineering
1994	Göthe-Institute, Göttingen, Germany: German language course from August to October
1994-1995	University of Bayreuth, Germany: Solid state physics, optics and energy physics
1996	University of Uppsala, Sweden: Diploma work for ABB Corporate Reserarch (ABB) at the Institute of High Voltage Research (IfH) “Streamer Discharges in Air and along Insulating Surfaces ” Instructors Dr. Dan Windmar (ABB), Ass. Prof. Dr. Vernon Cooray (IfH), Prof. Dr. Victor Scuka (IfH)
1997-2001	University of Fribourg, Switzerland: Graduate student in the Solid State Physics Group of Prof. Dr. Louis Schlapbach

List of Publications

- **Scanning field emission from patterned carbon nanotube films**
  L. Nilsson, O. Groening, C. Emmenegger, O. Kuettel, E. Schaller and L. Schlapbach, H. Kind, J.-M. Bonard and K. Kern, *Appl. Phys. Lett.* **76**, *2071 (1999).*

- **Environmental stability of carbon nanotube field emitters**
  L. Nilsson, O. Groening, P. Groening, O. Kuettel, L. Schlapbach *Electronic Properties of Novel Materials - Molecular Nanostructures, XIV International Winterschool, Kirchberg, Tirol, Austria, 499 (2000).*

- **Scanning anode field emission microscopy on carbon nanotube thin films**
  L. Nilsson, O. Groening, P. Groening, L. Schlapbach, *The Electrochemical Soc. Proc.,* **2000-28**, *52 (2001).*

- **Carbon nano-/micro-structures in field emission: Environmental stability and field enhancement distribution**
  L. Nilsson, O. Groening, P. Groening, O. Kuettel, L. Schlapbach, *Thin Solid Films* **383**, *78 (2001).*

- **Characterization of thin film electron emitters by scanning anode field emission microscopy**
  L. Nilsson, O. Groening, P. Groening, O. Kuettel and L. Schlapbach, *in press Journ. Appl. Phys. (2001).*

- **Collective emission degradation behavior of carbon nanotube thin film electron emitters**
  L. Nilsson, O. Groening, O. Kuettel P. Groening and L. Schlapbach, *Subm. to Appl. Phys. Lett. (2001)*

- **Microscopic characterization of electron field emission**
  L. Nilsson, O. Groening, P. Groening, O. Kuettel, L. Schlapbach, *Subm. to JVST B (2001).*

- **Electron field emission from carbon films**
  O. Kuettel, O. Groening, L. Nilsson, L. Diedrich, L. Schlapbach, *Proceedings SMAC'97, 338 (1997).*

- **Patterned Films of Nanotubes Using Microcontact Printing of Catalysts**
  H. Kind, J-M. Bonard, C. Emmenegger, L-O. Nilsson, K. Hernadi, E. Maillard-Schaller,L. Schlapbach, L. Forró, K. Kern, *Adv. Mater.* **11***, 1285 (1999).*

- **Field emission from diamond, diamond-like and nanostructured carbon films**
  O. Kuettel, O. Groening, C. Emmenegger, L. Nilsson, E. Maillard, L. Diedrich, L. Schlapbach, *Carbon* **37***, 745 (1999).*

- **Properties and characterization of chemical vapor deposition diamond field emitters**
  O. Gröning, L-O. Nilsson, P. Gröning, L.Schlapbach, *in press Solid-State Electr. (2001).*

- **Field emission from carbon nanotubes: the first five years**
  J-M. Bonard, H. Kind, T. Stöckli, L-O Nilsson, *in press Solid-State Electr. (2001).*

Danksagung

Diese Arbeit wurde in der Festkörperphysikgruppe unter der Leitung von Prof. Dr. Louis Schlapbach, Dr. Oliver Gröning und Dr. Pierangelo Gröning an der Universität Freiburg in der Schweiz ausgeführt. An erster Stelle muss ich mich deshalb bei Louis bedanken, da er mir die Möglichkeit gegeben hat auf einen technologisch als auch als physikalisch sehr interessantem Gebiet zu arbeiten. Obwohl er als grosser Wissenschaftler anerkannt ist, werde ich mich in erster Linie an ihn als Mensch und Humanist erinnern. Seine warme Persönlichkeit hat einen sehr positiven und starke Eindruck hinterlassen.

Bei Oliver höre ich nie auf zu staunen, wie er eine Mischung aus Fachkompetenz, physikalischem Grundwissen und Computerkenntnissen verkörpert. Ich bin ihm sehr dankbar, durch seine Mitarbeit ist die Qualität meiner Arbeit erheblich verbessert worden. Viel Erfolg noch, wünsche ich Dir!

Pierangelo's kritische Haltung und Auge für physikalische und technologische Konzepte hat sich als mehr als wertvoll erwiesen. Seine Kenntnisse auf dem Gebiet der Ultra-Hochvakuumtechnik sind ebenfalls in der Frühphase des Projektes sehr wichtig gewesen. Danke Pierangelo!

Ganz besonders herzlichen Dank muss ich Mechaniker Otto Zosso (alias John Wayne) geben. Seine Anstrengungen sind die Veraussetzung dieser Dissertation. Unglaublich wie er ein Stück rostfreien Stahl in brauchbare experimentelle Ausrüstung umsetzen kann. Seinen Standardsatz *"Made in Nasa"* werde ich nie vergessen. Danke Otto und viel Spass noch auch als Pensionierter!

Dr. Olivier Küttel danke ich für die Führung des Projektes in der Frühphase. Seine Pädagogik und Präsentationstechnik hat mich beeindruckt.

Mein Aufenthalt in Fribourg wäre sicher nicht gelungen ohne die Hilfe von Elisabeth Francois. Ihre stete Bereitschaft, grosse und kleine administrative Angelegenheiten zu erledigen ist eine Voraussetzung dieser Arbeit gewesen. Ein wichtiger Grund, weshalb die administrative Infrastruktur des Physikinstitutes wie geschmiert läuft, ist auf Elisabeths persönliches Engagement zurückzuführen.

Christoph Neururer hat mir sehr viel geholfen wenn es um irgendein technisches Problem ging. Dank ihm sind meine Kenntnisse im Berich Vakuum-Messtechnik und Vakuum Erzeugung viel besser geworden. Danke auch für das gemeinsammes Fischen (nächstes mal besorge ich mir ein Patent).

Dr. Andreas Züttel alias Res bin ich dankbar für seine Hilfe mit einer Menge Informatikprobleme. Seine Expertkenntnisse auf Labview 1.2 (und auch höhere versionen) findet man nicht überall. Ausserdem wenn Res in der Kaffepause dabei ist, muss man keine Angst haben, dass es langweilig wird.

Prof. Dr. Philippe Aebi bin ich dankbar, er hat mir eine Menge Ratschläge im Berich von Ultra-Hoch-Vakuum Technik gegeben. Sein klares und weitgehendes physikalisches Verständnis ist eine grosse Hilfe gewesen.

Für die kompetente technische Unterstützung danke ich folgende Leuten herzlich: Elmar Mooser, Oswald Raetzo und Francis Bourqui. Danke auch an die gesamte Besatzung der Werkstadt für die gemeinsamen Freitag nachmittag Kaffepausen.

Ich danke Pierangelo, Louis, Oliver und Dr. Patrik Schwaller für das Lesen des Manuskriptes dieser Dissertation.

Herzlichen Dank an Dr. Jean-Marc Bonard und Dr. Hannes Kind für eine fruchtbare Zusammenarbeit. Danke auch an Herrn Prof. Dr. André Châtelain, dass er sich zur Verfügung gestellt hat, als externer Experte, die vorliegende Arbeit zu begutachten.

Zudem bin ich folgenden alten Doktoranden-Kollegen und Personen zu Dank verpflichtet: Dr. Daniel Chartouni, Dr. Adrian Schneuwly, Dr. Torsten Pillo, Dr. Joseph Hayoz, Dr. Christoph (Nützi) Nützenadel, Dr. Elmar Boschung, Dr. Leon Diedrich, Dr. Eric Leroy, Dr. Karl Gross, Dr. Eliane Maillard-Schaller. Ihr habt mir viel geholfen als ich in die Schweiz gekommen bin.

Ich danke Michael Bielmann und Carine Galli für das Teilen des Büros und die Hilfe mit den Druckern und Computern. Ohne Euch hätte ich meinen Computer längst aus dem Fenster geworfen.

Herzlichen Dank an Pascal Ruffieux, Dr. Patrick Schwaller, Christian Koitzsch, Christoph Emmenegger, Dr. Martine Collaud-Coen, Marc Bovet, Philippe Mauron, Patrick Sudan, Dusanka Naumović, Marianne Zbinden und allen die zum

Gelingen dieser Arbeit beigetragen haben.

A very special thank go to Motorola Inc. Res., Phoenix, Arizona for its financial and scientific support. Thank you Dr. Jim Jaskie and Dr. Ken Dean.

Many thanks go also to Dr. L. "Chip" Thuesen and Dr. Richard Fink of Field Emission Picture Element Technology, Inc., Austin, Texas.

Mina föräldrar tackar jag för att alltid ha gett mig sitt stöd och alltid givit mig tillräckligt med frihet att göra vad jag vill.